Continuous Basalt Fiber as Reinforcement Material in Polyester Resin

by

Jón Ólafur Erlendsson

Master of Science
in Civil Engineering with
Specialization in Structural Design

August 2012

Continuous Basalt Fiber as Reinforcement Material in Polyester Resin

Jón Ólafur Erlendsson

Thesis (30 ECTS) submitted to
the School of Science and Engineering
at Reykjavík University in partial fulfillment
of the requirements for the degree of
Master of Science in Civil Engineering with Specialization in Structural Design

August 2012

Supervisor:

Eyþór Rafn Þórhallsson
Associate Professor, Reykjavík University, Iceland

Examiner:

Dr. Sigurður Brynjólfsson
Associate Professor, University of Iceland

Abstract

The industry is always striving to find new and better materials to manufacture new or improved products. Within this context, energy conservation, corrosion, sustainability and other environmental issues are important factors in product development. Basalt fibers are a natural material, produced from igneous rock which can provide high strength relative to weight. Research has also shown that basalt fibers have many other advantageous qualities.

This thesis describes an applied research project, investigating the material characteristics of a relatively new material, continuous basalt fibers in polyester resin. The objective was to examine whether a composite material made of polyester resin reinforced with basalt fibers, could be used for engineering structures. The project combines two phases. The first phase was a basic research of material properties where specimens made of basalt fibers in polyester resin were constructed and tested according to the ASTM standard. The second phase was the construction and testing of two1200 mm long tubes made of basalt fiber in polyester resin.

The material testing phase included a study of simple state of the art methods used to analyze layered composite materials layer (laminate) by layer. Various standard load tests were then applied to the samples. A uniaxial static tensile test, a uniaxial compression test, an in-plane shear test and a pin bearing test were carried out. The test results were compared with published test results for similar composite materials, such as glass fibers in epoxy and carbon fibers in epoxy.

The results of the material testing indicated that basalt fibers can be used as reinforcement material in polyester resin, to create a composite structural material with acceptable engineering properties. The comparison with other similar results for other composite materials showed that basalt fibers in polyester resin were in fact 19.3% stronger in tension than glass fibers in epoxy resin.

Structural testing of the 1200 mm long tube, built using a composite material of basalt fiber reinforced polyester resin revealed, that the tube was strong enough to meet the standard design criteria’s specified for a regular four-meter high lamppost.

Keywords: Basalt fiber, basalt fabric, continuous basalt fibers, polyester resin, composite material, laminate material, structural testing.

Ágrip - Basaltþræðir sem styrkingarefni í polyester plastefni

Iðnaðurinn er stöðugt að leitast við að finna ný og betri efni til að framleiða nýjar og/eða endurbættar vörur. Orkusparnaður, tæringarhætta, sjálfbærni og aðrir umhverfisþættir hafa mikil áhrif á val á nýjum efnum og tilsvarandi vöruþróun.

Í þessari ritgerð er kynnt hagnýtt rannsóknarverkefni þar sem nýtt efni, polyester plastefni styrkt með basaltþráðum var prófað til að athuga hæfni þess til notkunar í mannvirkjagerð. Basalt trefjar er náttúrulegt efni sem unnið er úr storkuberginu basalt sem getur gefið mikinn styrk í hlutfalli af eiginþyngd. Einnig hefur komið fram í rannsóknum að basalt trefjar hafa marga aðra hagnýta efniseiginleika.

Verkefnið var tvíþætt. Meginmarkmið verkefnisins var að rannsaka hvort hægt væri að nota basaltþræði, sem styrkingarefni í polyester plastefni til að búa til samsett efni með eiginleika sem henta til mannvirkjagerðar. Þessi rannsókn flokkast undir grunnrannsókn í efnisfræði trefjaefna þar sem prófaðir voru efnisbútar, gerðir úr basaltþráðum í polyester fylliefni, í samræmi við viðurkenndan alþjóðlegan staðal (ASTM). Einnig voru búnir til tveir staurar, 1200 mm langir, úr basaltþráðum í polyester fylliefni. Annar staurinn var innspenntur í annan endann og burðarþolsprófaður með því að setja stakan kraft á hinn endann með stefnu þvert á langstefnu bitans. Hinn staurinn var steyptur niður í fjörunni í Keflavík til að langtíma prófunar á áhrifum veðrunar og annarra umhverfisþátta.

Til að kanna brotstyrk samsetta trefjaefnisins voru gerð mismunandi einása, stöðufræðileg álagspróf. Um var að ræða togþolspróf, þrýstiþolspróf, skerþolspróf og prófun á boltaðri skúftengingu. Niðurstöðurnar voru bornar saman innbyrðis milli einstakra sýna sem og við birtar rannsóknarniðurstöður fyrir önnur sambærileg efni eins og glertrefja- og koltrefjastyrkt epoxy efni. Í tengslum við ofangreindar prófanir voru hefðbundnar reikniaðferðir til greiningar á brotþoli lagskiptra efna kannaðar. Niðurstöður rannsóknarinnar á burðargetu efnissýna, gáfu til kynna að hægt er að búa til samsett efni úr basaltþráðum og polyester fylliefni sem hefur nothæfa verkfræðilega eiginleika. Samanburður á niðurstöðum við aðrar rannsóknir leiddi einnig í ljós að samsett efni úr basalttrefjastyrktu polyester gaf 19.3% meiri styrk í togi heldur en samsett efni úr glertrefjastyrktu epoxy. Álagsprófun innspenntrar súlu úr basalttrefjastyrktu polyester leiddi í ljós að staurinn uppfyllir hefðbundnar hönnunarkröfur fyrir fjögurra metra háan ljósastaur.

Lykilorð: Basalttrefjar, basalt mottur, basaltþræðir, polyester plastefni, samsett efni, lagskipt efni, trefjaplast, burðarþolsprófanir.

Continuous Basalt Fiber as Reinforcement Material in Polyester Resin

Jón Ólafur Erlendsson

Thesis (30 ECTS) submitted
to the School of Science and Engineering
at Reykjavík University in partial fulfillment
of the requirements for the degree of
Master of Science in Civil Engineering with Specialization in Structural Design

August 2012

Student: Jón Ólafur Erlendsson

Jón Ólafur Erlendsson

Supervisor: Eyþór Rafn Þórhallsson

Eyþór Rafn Þórhallsson

Examiner:

Sigurður Brynjólfsson

Acknowledgements

First of all I want to thank my lovely family for their grateful support and being patient for the past five years, through my entire B.Sc. and M.Sc. study. Without their support this study would not have been feasible.

I thank my supervisor Eyþór Rafn Þórhallsson, civil engineer, M.Sc. and associate professor at Reykjavik University, for coming up with this applied project. I wish also to thank him for his guidance and inspiration throughout the entire project.

Special thanks go to all the good people and companies who helped me with the experimental work. Andri Thor Gunnarsson, general manager at Infuse, for manufacturing the plates with the Vacuum Infusion process. Trésmiðja Ella Jóns, for the facilities to cut the specimens and create the tubes. Innovation Center Iceland for the facilities to perform the experiment (part 1). Hreinn Jónsson at Innovation Center Iceland for assistance in the experiment (part 1).

Finally I want to thank the staff at Reykjavik University: Gísli Þorsteinsson, technician; Indriði Ríkharðsson, mechanical engineer, M.Sc.; and Hrannar Traustason, electronics engineer, for assistance in the experimental work.

Table of Contents

List of figures

List of Tables

Notation

S = mirror the layers

$[(0°/90°)_3]_S$ = [0°/ 90°/ 0°/ 90°/ 0°/ 90°/ 90°/ 0°/ 90°/ 0°/ 90°/ 0°]

$[(\pm45°)_3]_S$ = [+45°/-45°/+45°/-45°/+45°/-45°/-45°/+45°/-45°/+45°/-45°/+45°]

$[0°/90°/\pm45°/0°/90°]_S$ = [0°/ 90°/+45°/-45°/ 0° / 90°/ 90°/ 0°/-45°/+45°/ 90°/ 0°]

$[(0°/90°)_2]$ = [0°/ 90°/ 0°/ 90°]

V^f = volume fraction of reinforcing fibers

M^f = mass of reinforcing fibers

M_{total} = total mass (mass of reinforcing fibers plus mass of matrix)

ρ_{total} = total density (density of reinforcing fibers plus density of matrix)

E_1 = elasticity composite modulus in 1 direction (longitudinal)

E_2 = elasticity composite modulus in 2 direction (transverse)

G_{12} = elasticity composite shear modulus in 1-2 plane

E_1^f = elasticity modulus of fiber in 1 direction (longitudinal)

E_2^f = elasticity modulus of fiber in 2 direction (transverse)

E^m = elasticity modulus of matrix

G^m = elasticity shear modulus of matrix

N_x, N_y = normal force in x and y direction (force/width of laminate)

N_{xy} = shear force in x-y plane (force/width of laminate)

M_x, M_y = bending moment in x and y direction (force*length/width of laminate)

M_{xy} = twisting moment in x-y plane (force*length/width of laminate)

F_1^T = Tensile failure strength in the 1 direction (longitudinal)

F_1^C = Compressive failure strength in the 1 direction (longitudinal)

F_2^T = Tensile failure strength in the 2 direction (transverse)

F_2^C = Compressive failure strength in the 2 direction (transverse)

F_{12}^S = Shear failure strength in the 1-2 planes (longitudinal shear failure)

A_f = weight of basalt fabric

N = number of fabrics in a specimen

h = thickness of the specimen

ρ_f = density of the basalt fiber

ρ_m = density of the polyester resin

σ_i = tensile stress at *i*-th data point

P_i = load at *i*-th data point

A = cross-sectional area

ν = Poisson's ratio

P = applied load

ε_l = longitudinal strain

ε_t = transverse strain

τ_{12i} = shear stress at *i*-th data point

γ_{12i} = shear strain at *i*-th data point

σ_i^{br} = bearing stress at *i*-th data point

D = specimen hole diameter

h = specimen thickness

ε_i^{br} = bearing strain at *i*-th data point

δ_i = hole elongation at *i*-th data point

F^{bru} = ultimate bearing strength

F^{bry} = yield bearing strength

ε^{bry} = yield bearing strain

w = specimen width

e = distance, parallel to load, from hole center to end of specimen.

E_1^t = elasticity composite tensile modulus in 1 direction (longitudinal)

E_2^t = elasticity composite tensile modulus in 2 direction (transverse)

E_1^c = elasticity composite compression modulus in 1 direction (longitudinal)

E_2^c = elasticity composite compression modulus in 2 direction (transverse)

F_1^{tu} = tensile ultimate strength in 1 direction (longitudinal)

F_2^{tu} = tensile ultimate strength in 2 direction (transverse)

F_1^{cu} = compression ultimate strength in 1 direction (longitudinal)

F_2^{cu} = compression ultimate strength in 2 direction (transverse)

F_{12}^{su} = shear ultimate strength in 1-2 plane (longitudinal shear failure)

G_{12}^s = elasticity composite shear modulus in 1-2 plane

ν_{12}^t = tensile Poisson's ratio in 1-2 plane

ν_{21}^t = tensile Poisson's ratio in 2-1 plane

ε_1^{tu} = tensile ultimate strain in 1 direction (longitudinal)

ε_2^{tu} = tensile ultimate strain in 2 direction (transverse)

ε_1^{cu} = compression ultimate strain in 1 direction (longitudinal)

ε_2^{cu} = compression ultimate strain in 2 direction (transverse)

t = fabric thickness

Abbreviations

FRP = Fiber Reinforced Polymers

BFRP = Basalt Fiber Reinforced Polymers

CLT = Classical Laminate Theory

ASTM = American Society for Testing and Materials.

UTM = Universal Testing Machine

Introduction

1.1 General

This project was an applied research study where a new material, continuous basalt fibers, was load tested for its suitability for structural design. This study was carried out to determine whether the basalt fiber, as reinforcement material in a polymer matrix, can be used as a composite material. This research focused on basic research and test specimens according to recognized standards and tested regular tubes.

1.2 Problem Overview

Industry is always striving to find new and better materials to manufacture new or improved products. With this in mind energy conservation, the environment, corrosion risk and sustainability are important factors when a product is changed or a new product is manufactured. A few examples of problem overviews that relate to some of these important factors are explained below. High voltage towers have, almost from the beginning, been designed as steel truss towers and in the next few years will need to be replaced. Therefore there is now the opportunity design a new type of tower made of a new material that is strong, light and has minimum risk of corrosion. A large part of lampposts and telephone poles have also been designed as steel and wood for years and there is also a need for new materials which are strong, light and with a minimum risk of corrosion. Structural designers, as for buildings, bridges and windmills, are always looking for new solutions for better and/or bigger structures. One of the solutions could be a new material which is also strong, light and with minimum risk of corrosion. Aircraft, ships and the automobile industries are always trying to develop lighter units without losing material strength to make energy conservation.

Composite materials are composed of two or more elements working together to produce material properties for one composite material (physical, not chemical). The composite material generally consists of a matrix and some type of reinforcement. The reinforcement is usually used in fiber form (for example carbon or glass fibers) and used to increase the strength and stiffness of the matrix (for example epoxy or polyester resins) (SP Systems, n.d.).

Basalt fiber is a natural material which is produced from igneous rock called basalt and can give great strength relative to weight (Ross, A., 2006). As has been shown in some published papers, basalt fiber has versatile material properties (Parnas, R. & Shaw, M., 2007; Van de Velde, K., Kiekens, P., & Van Langenhove, L., n.d.). The aim of this thesis was to examine whether the basalt fiber as reinforcement material in polyester resin can be used as composite material for structural design. Figures 1-1 to 1-4 show a few units which have been produced from similar material as will be investigated in this thesis. Figure 1-1 shows transmission poles made of glass fiber in a polymer matrix which are produced by Shakespeare Composite Structures. They have been producing all kinds of composite poles for years ("Shakespeare composite structures," n.d.). The first plastic bridge in Europe can be seen in figure 1-2. The bridge's carriageway was made of glass fiber in a polymer matrix glued onto two steel bearers ("Europe's first plastic bridge is open," 2010).

Figure 1-1 Transmission poles made of glass fiber in polymer matrix ("Shakespeare composite structures," n.d.).

Figure 1-2 Bridge's carriageway made of glass fiber in polymer matrix ("Europe's first plastic bridge is open," 2010).

Figure 1-3 shows a Swedish warship, 72 m long, made of a composite material. The ship is all carbon fiber/sandwich composite construction (McGeorge, D. & Höyning, B., n.d.).

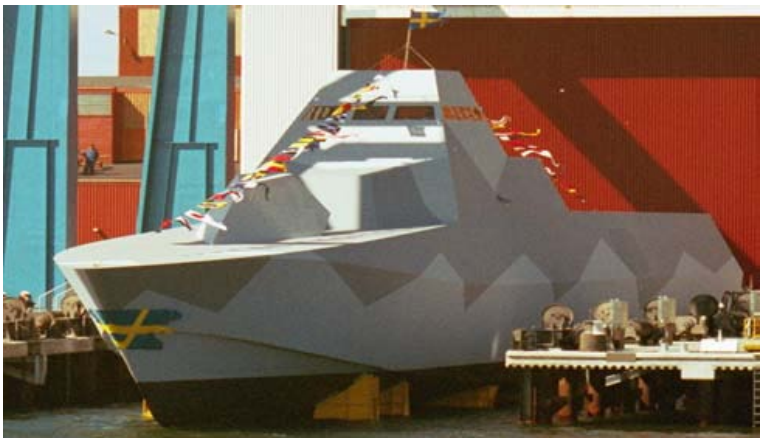

Figure 1-3 Swedish warship, 72 m long, made of carbon fiber in a polymer matrix (McGeorge, D. & Höyning, B., n.d.).

Figure 1-4 shows the composite ratio in the new airplanes, 787 Dreamliner, from Boeing. The composite ratio is 50% of the total materials used in the airplane. The reinforcement in the composite material is carbon fiber or glass fiber. The biggest part of the airplanes is made of carbon fiber (Boeing, n.d.).

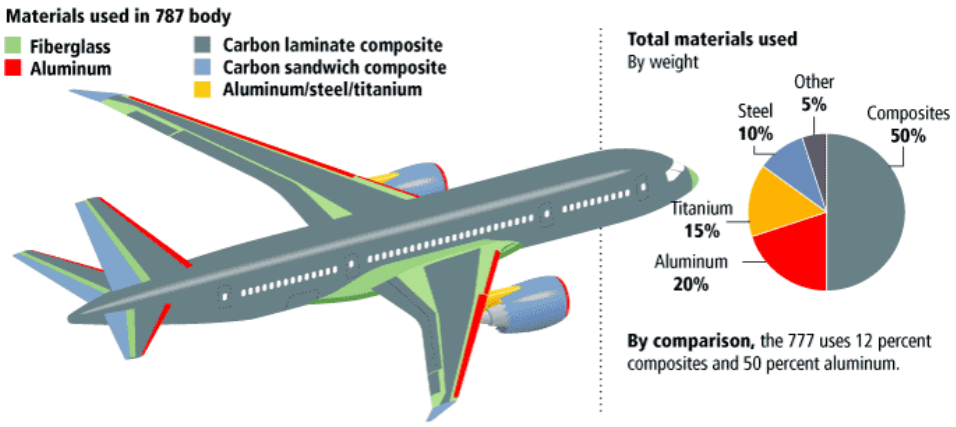

Figure 1-4 Airplane, 787 Dreamliner, made of carbon and glass fiber in polymer matrix (Boeing, n.d.).

As can be seen above, a composite material is used in manufacturing various products, from producing simple poles to complex aircraft.

1.3 Overview of work on basalt fibers

There is a lack of research on basalt fibers; in fact, few studies on basalt fiber as reinforcement material in resin have been published. No published paper has been found about basalt fiber as a reinforcement material in polyester resin, but some in epoxy resin. The papers which were examined for this thesis and used for reference were:

- Static and fatigue characterization of new basalt fiber reinforced composites (Colombo, Vergani, & Burman, 2012).
- The study of AE and ESSPI technique on the CBF composite (Chang, Zou, Chen, & Chen, 2011).
- Investigation on mechanical properties of basalt composite fabrics (Talebi Mazraehshahi & Zamani, 2010).
- Evaluation of basalt continuous filament fibers in composite material (Bruijn, M., 2007).

1.4 Objectives

The main objective was to find out the strength and stiffness of basalt fiber in resin and prove that it can be used as a composite material. The results were then compared with similar material to evaluate the quality of the results. Since no data were found about the strength and stiffness of basalt fibers in polyester resin a few load tests (experiments) were carried out to find out how strong the basalt fiber in polyester

resin can be. To identify the variables; the ultimate strength and strain, the elasticity modulus and Poisson´s ratio, the composite material was measured. The universal testing machine and strain gage were used to measure the stress and strain at a constant speed.

Other objectives of the project were:

- Find calculation methods to analyze a composite material and explore some composite design software.
- Find out the most common calculation methods for laminated material.
- Study a manufacturing processes for laminated material, how the layers can be added together.

1.5 Thesis Overview

This thesis is divided into eight chapters and seven appendixes. The main chapters of this thesis are as follows:

- Chapter one (**Introduction**): Focuses on problem overview, what has been done and objectives of the project.
- Chapter two (**Background**): Discusses composite material in general, what it is, how it works and how it can be analyzed.
- Chapter three (**Material Properties in the Experiment**): Describes the materials which were used in the experiment.
- Chapter four (**Experimental Program and Procedure, Part 1**): Details the experimental work. The first part was carried out as basic research on Basalt Fiber Reinforced Polymers (BFRP) where specimens were tested
- Chapter five (**Experimental Program and Procedure, Part 2**): Details the experimental work. In the second part 1200mm long tubes made of BFRP were tested.
- Chapter six (**Experimental Results**): The results of the experimental tests, from the first and second parts, were presented as graphs and tables.
- Chapter seven (**Discussion**): Discusses the results in general and the interpretation of the results.
- Chapter eight (**Summary**): Summary of what was explored in this research and discussion about further research.

Background

2.1 General

Composite materials are those which are composed of two or more elements working together to produce material properties for this one composite material (physical, not chemical). In a most basic and practical way a composite material consists of a matrix and some type of reinforcement. The reinforcement is usually in fiber form and used to increase the strength and stiffness of the matrix (SP Systems, n.d.).

2.2 Composite material

2.2.1 Resin Systems

There are three groups of most common man-made composites: *Polymer Matrix Composites*, *Metal Matrix Composites* and *Ceramic Matrix Composite* (SP Systems, n.d.). This study focuses on polymer matrix composites which are also known as Fiber Reinforced Polymers or FRP where the polymer-based resin is the matrix with a variety of fibers. Figure 2-1 illustrates how the properties for the composite material FRP can be combined with the properties from the resin and the fiber.

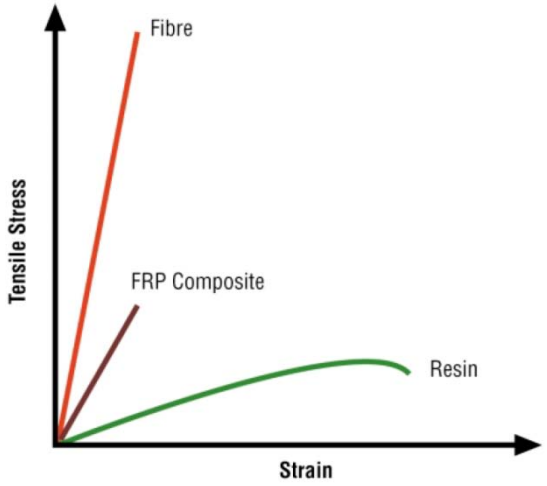

Figure 2-1 Properties of FRP combined with the properties from the resin and fibre (SP Systems, n.d.).

The composite industry uses three main types of resin, namely polyester, vinylester and epoxy, for producing structural parts. This study focused on polyester resins because these are the most generally used resin systems (SP Systems, n.d.).

2.2.2 Reinforcements (fiber)

Fiber reinforcements in composite material are generally used to improve the mechanical properties in an undiluted resin system. The most common fiber reinforcement in resin is glass fiber, accounting for up to 99% of world production (Árnason, P., 2007, p. 143). There are other types of fibers for reinforcement such as carbon fiber, other plastic fibers and the newest, basalt fiber, which is examined in this research. For this reason the study focused on basalt fiber and below the basalt fiber is described roughly.

Basalt is an igneous rock (volcanic rock) formed in volcanic eruptions and found in almost all countries around the world (Ross, A., 2006). The bulk of Iceland's bedrock is basalt, which is widely used as building material in the country. Basalt is a building material that could effectively find wider application since it is so abundant worldwide. One suggested use would be as fiber reinforcement of resin.

The production of basalt fibers is similar to the production of glass fibers. Basalt is quarried, crushed and washed and then melted at 1500° C (Ross, A., 2006). Next, the molten basalt is drawn into filaments. When the filaments cool down it is transformed into fibers (Ross, A., 2006).

Manufacturers of basalt fibers (e.g. Kamenny Vek in Russia) say that basalt fibers have preferable mechanical properties, such as higher tensile strength, as well as a lower manufacturing cost than glass fibers (Kamenny Vek, 2009). Kamenny Vek also says recycling of basalt fibers is much more efficient than glass fibers and therefore basalt fibers can be environmentally friendly (Kamenny Vek, 2009). Basalt fiber can be classified as a sustainable material because basalt fibers are made of natural material and when the basalt fibers in resin are recycled the same material is obtained again as natural basalt powder (Kamenny Vek, 2009).

2.2.3 Manufacturing Processes for laminate material

A composite laminate is generally made of several composite material layers with different fiber orientations; thus some manufacturing process is needed to add the layers together. This section focuses on three common types of manufacturing processes which are Hand Lay-up, Vacuum Bagging and Vacuum Infusion. All these methods can work with various types of fiber fabrics and general resin. The fabrics are generally made of continuous fibers which are in the form of woven or stitched fabrics (SP Systems, n.d.).

In the Hand Lay-up process the resins are impregnated by hand into fiber fabrics and usually done by rollers or brushes, as illustrated in figure 2-2. The Vacuum Bagging uses the Hand Lay-up process where pressure is applied to the laminate with vacuum bagging as illustrated in figure 2-3. In the Vacuum Infusion process the fabrics are dried in the mold, under the vacuum bagging, before the resin is drawn through the fabrics by vacuum, as illustrated in figure 2-4. These manufacturing processes were used in the research directly or indirectly and the process is described in more detail in the experimental procedures in this thesis.

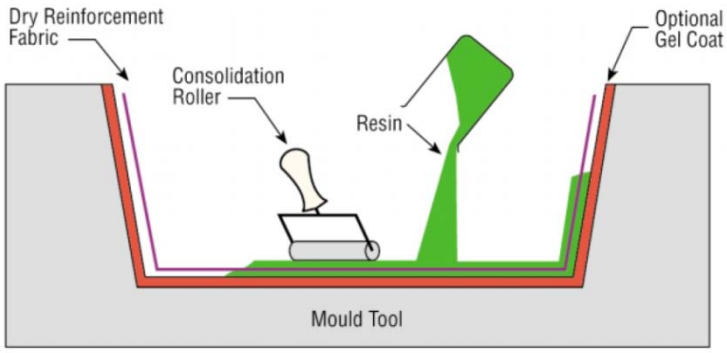

Figure 2-2 Hand Lay-up manufacturing processes for laminate material (SP Systems, n.d., p. 51).

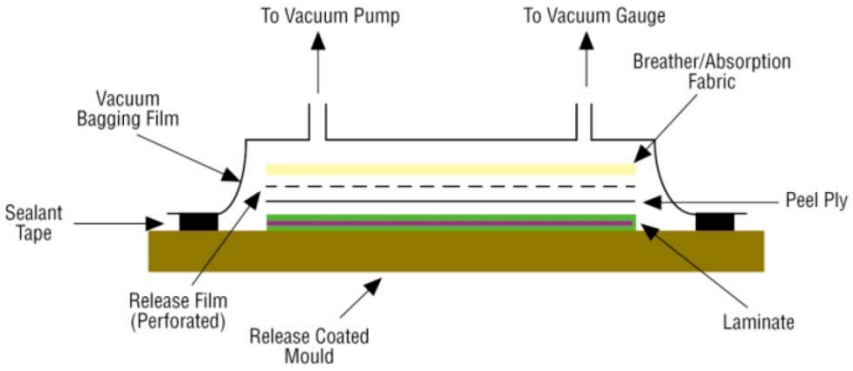

Figure 2-3 Vacuum Bagging manufacturing processes for laminate material (SP Systems, n.d., p. 53).

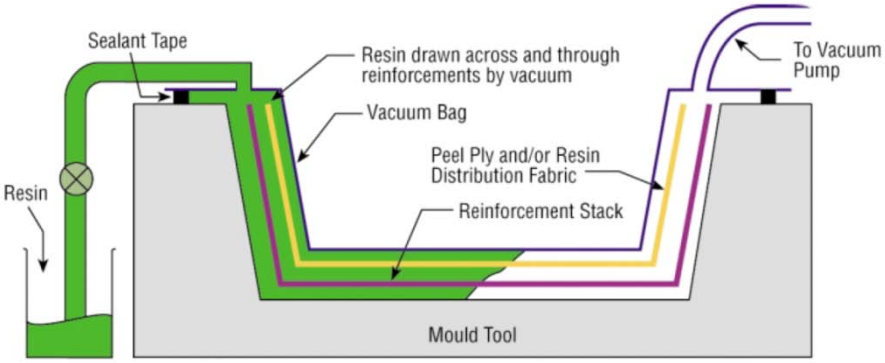

Figure 2-4 Vacuum Infusion manufacturing processes for laminate material (SP Systems, n.d., p. 57).

2.3 Analytical Modeling (analysis of composite materials)

The physical behavior of composite laminate can be more complicated than other engineering materials. The most common engineering materials are assumed to be isotropic and homogeneous (Greene, E., n.d., p. 99). That kind of materials are assumed to be constant throughout and the elastic properties are the same in all direction (Staab, 1999, p. 13).

Most composite materials are nonhomogeneous and behave as anisotropic or orthotropic materials, which means the elastic properties can be different in all directions. For that reason it can be more complex to analyze and make a design method for composite structures. Composite material will hereafter stand for fiber-reinforced material in a matrix and this study focuses always on a continuous fiber composite.

The figure 2-5 describes in three steps or stages involved in the design and analyze a composite material: micromechanics-ply calculation, macromechanics-laminate design and laminate evaluation (Meunier, M. & Knibbs, S., 2007). These steps will be described separately in sections 2.3.1, 2.3.2 and 2.3.3.

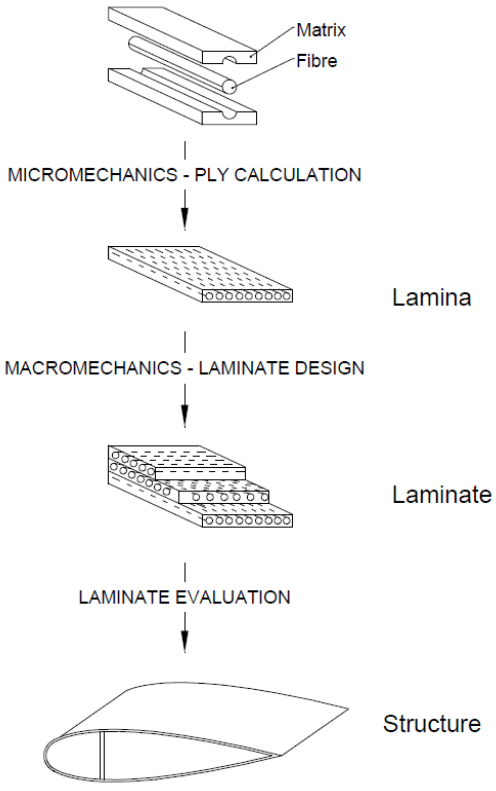

Figure 2-5 Three steps to design and analyze composite materials (Meunier, M. & Knibbs, S., 2007).

2.3.1 Micromechanics of a unidirectional ply

Micromechanics-ply calculation is the first step to design and analyze composite materials. In order to predict the composite properties it is useful to set up a model where the model will let the composite materials behave like a homogeneous material. The model which will be described here and will be used in further calculations in this research is such a model and called the strength-of-materials model, or the *rule-of-mixtures model* (Hyer, 2008, p. 140).

Figure 2-6 shows how the fiber and matrix are arranged parallel side-by-side depending on the widths of each material in the model (denoted by W^f for width of fiber and W^m for width of matrix). The principal material direction is denoted by 1 and 2 (as in figure 2-6). Direction 1 stands for longitudinal direction (often called fiber direction) and direction 2 stands for transverse direction (often called matrix direction).

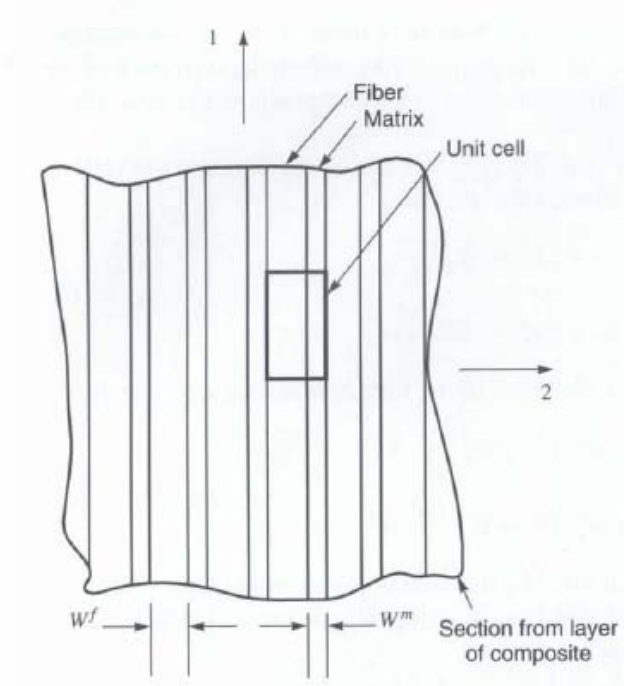

Figure 2-6 Section cut from a fiber-reinforced composite material and a unit cell (Hyer, 2008, p. 141).

When the composite properties like Young's modulus of elasticity E, Poisson's ratio ν and shear modulus of elasticity G are calculated with *rule-of-mixtures models*, selection of the fiber and matrix type and volume fraction of the reinforcing fibers is needed. The volume fraction of reinforcing fibers can be calculated by equation (2.1).

$$V^f = \frac{M^f / \rho^f}{M_{total} / \rho_{total}} \quad (2.1)$$

where V^f = volume fraction of reinforcing fibers

M^f = mass of reinforcing fibers

ρ^f = density of reinforcing fibers

M_{total} = total mass (mass of reinforcing fibers plus mass of matrix)

ρ_{total} = total density (density of reinforcing fibers plus density of matrix)

The model of Rule-of-mixtures when stress (σ_1) is acting in a longitudinal direction is illustrated in figure 2-7. Equation (2.2) shows how the modulus of elasticity (E_1) can be calculated by using this arrangement of the mode and equation (2.3) shows how the Poisson's ratio (ν_{12}), in 1-2 plan, can also be calculated.

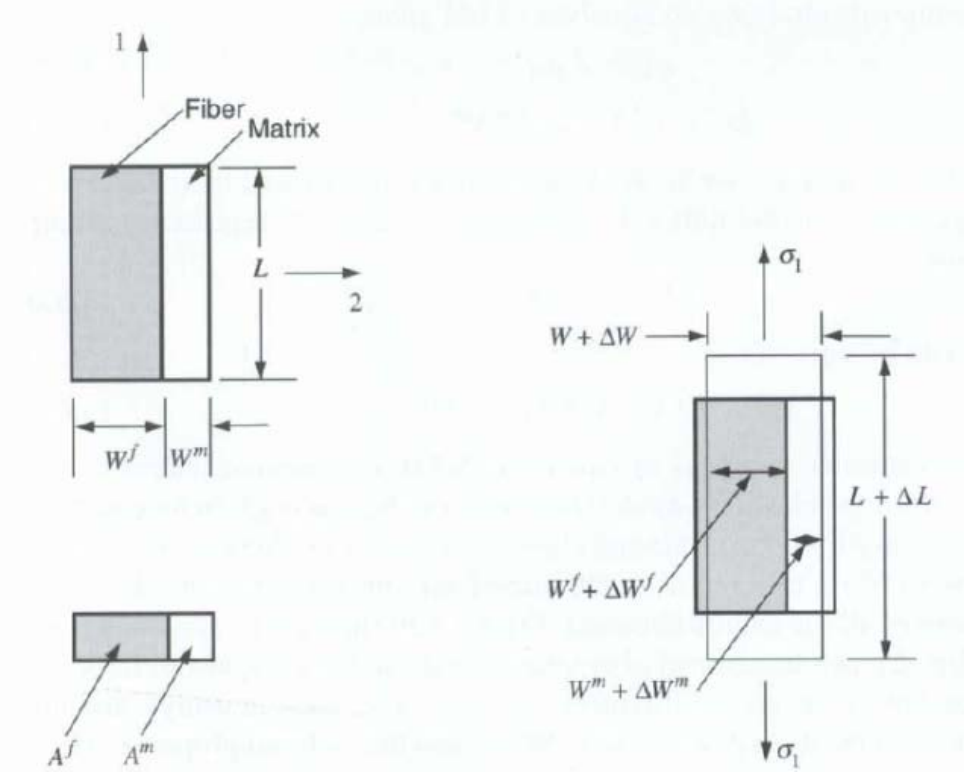

Figure 2-7 Rule-of-mixtures model for composite modulus of elasticity E_1 and Poisson's ratio ν_{12} (Hyer, 2008, p. 142).

$$E_1 = E_1^f V^f + E^m(1 - V^f) \quad (2.2)$$

$$\nu_{12} = \nu_{12}^f V^f + \nu^m(1 - V^f) \quad (2.3)$$

The model of Rule-of-mixtures when stress (σ_2) is acting in a transverse direction is illustrated in figure 2-8. Equation (2.4) shows how the modulus of elasticity (E_2) can be calculated by using this arrangement of the mode.

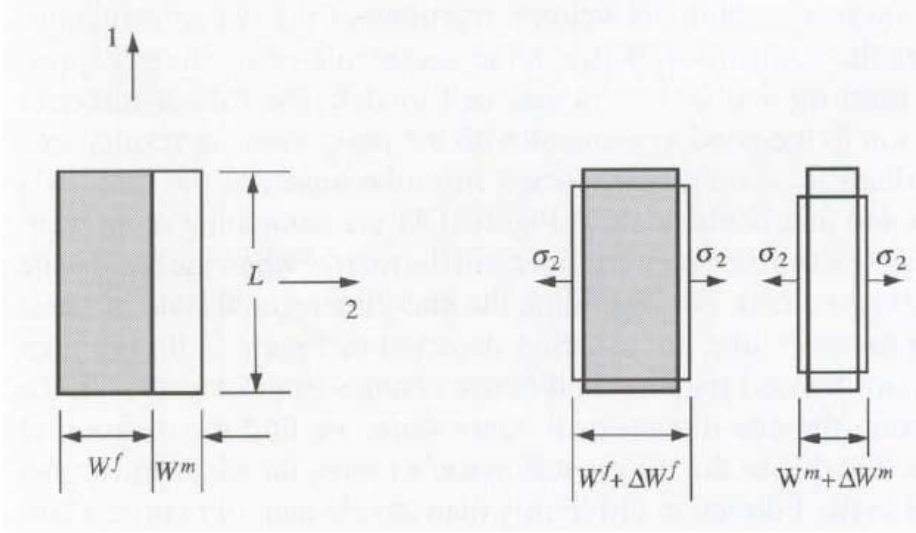

Figure 2-8 Rule-of-mixtures model for composite modulus of elasticity E_2 (Hyer, 2008, p. 146).

$$\frac{1}{E_2} = \frac{V^f}{E_2^f} + \frac{(1 - V^f)}{E^m} \tag{2.4}$$

The model of Rule-of-mixtures when shear stress (τ_{12}) is acting in a longitudinal direction is illustrated in figure 2-9. Equation (2.5) shows how the shear modulus of elasticity (G_{12}) can be calculated by using this arrangement of the mode.

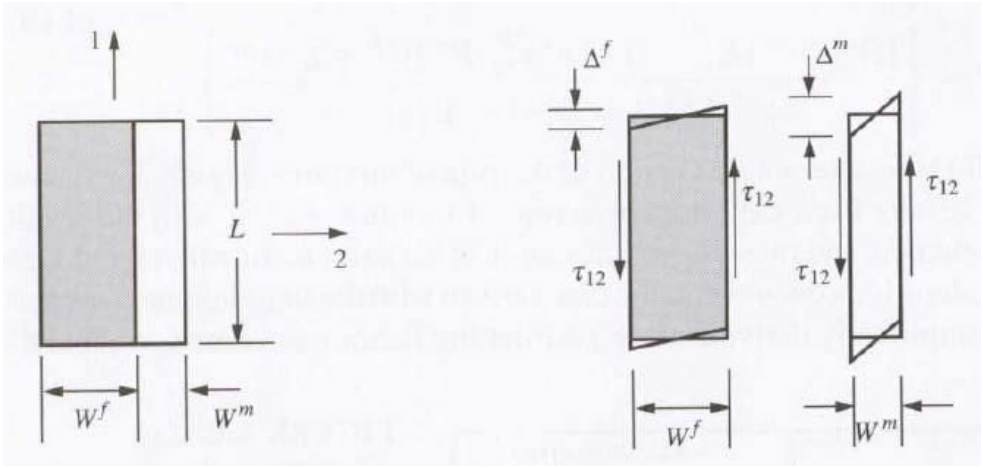

Figure 2-9 Rule-of-mixtures model for composite shear modulus of elasticity G_{12} (Hyer, 2008, p. 154).

$$\frac{1}{G_{12}} = \frac{V^f}{G_{12}^f} + \frac{(1 - V^f)}{G^m} \tag{2.5}$$

where: E_1 = elasticity composite modulus in1 direction (longitudinal)

E_2 = elasticity composite modulus in 2 direction (transverse)

G_{12} = elasticity composite shear modulus in 1-2 plane

E_1^f = elasticity modulus of fiber in 1 direction (longitudinal)

E_2^f = elasticity modulus of fiber in 2 direction (transverse)

E^m = elasticity modulus of matrix

G^m = elasticity shear modulus of matrix

If a small element is considered to be removed from a composite material plate, then the stresses on its six bounding surfaces on the element can be investigated in a 1-2-3 coordinate system. Figure 2-10 illustrates how the stresses act on the element surfaces and there are six stress components, as can be seen. So to describe the linear behavior of a composite material nine independent composite properties are needed, such as Young's modulus of elasticity, Poisson's ratio and shear modulus of elasticity.

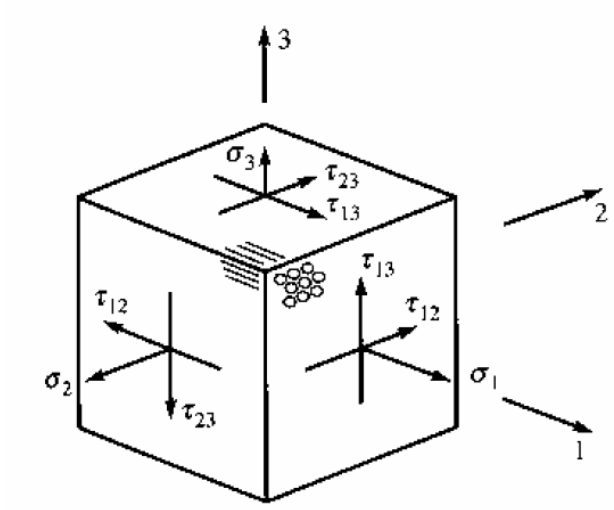

Figure 2-10 Six stress components acting on the element surfaces (Hyer, 2008, p. 46).

In a thin plate (ply) stress analysis, three of the six stress components are generally much smaller than the other three. So the thin plate analysis is calculated in a 1-2 plane and for that reason the stress components σ_3, τ_{23} and τ_{13} are set to zero. Figure 2-11 illustrates how the other three stress components act on the element in the 1-2 plane.

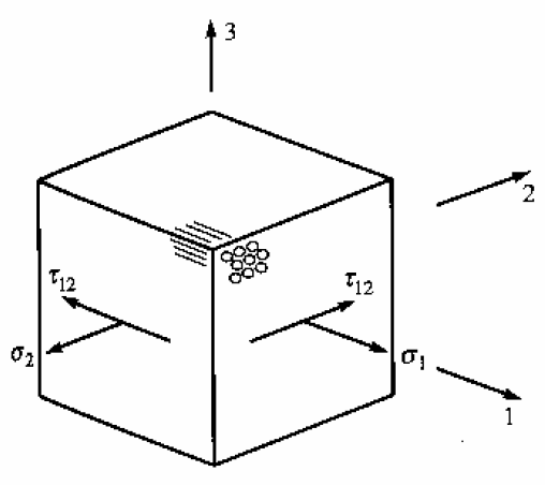

Figure 2-11 Three stress components acting on the composite material element surfaces in the 1-2 plane (Hyer, 2008, p. 166).

A thin plate in the 1-2 plane behaving linearly in a composite material reduces the independent composite properties from nine to four, namely E_1, E_2, ν_{12} and G_{12}. These properties of a thin plate can be calculated with the *Rule-of-mixtures model*, as described above. These composite properties can also be found with mechanical testing as tensile test and in-plane shear test.

From the thin plate in the 1-2 plane, a single thin, unidirectional lamina in plane stress can be analyzed in a stress-strain relationship in a 1-2 plane, as can be seen in equation (2.6).

$$\begin{Bmatrix} \sigma_1 \\ \sigma_2 \\ \tau_{12} \end{Bmatrix} = \begin{bmatrix} Q_{11} & Q_{12} & 0 \\ Q_{12} & Q_{22} & 0 \\ 0 & 0 & Q_{66} \end{bmatrix} \begin{Bmatrix} \varepsilon_1 \\ \varepsilon_2 \\ \gamma_{12} \end{Bmatrix} \tag{2.6}$$

where the elastic properties Q_{ij} of the composite material (based on Young's modulus of elasticity E, Poisson´s ratioν and shear modulus of elasticity G) are defined by equations (2.7).

$$\begin{aligned} Q_{11} &= \frac{E_1}{1-\nu_{12}\nu_{21}} \qquad & Q_{22} &= \frac{E_2}{1-\nu_{12}\nu_{21}} \\ Q_{12} &= \frac{\nu_{12}E_1}{1-\nu_{12}\nu_{21}} \qquad & Q_{11} &= G_{12} \end{aligned} \tag{2.7}$$

The stress is denoted with σ_i and the strain is denoted with ε_i. If the Poisson's ratio ν_{21} is unknown then this ratio $\frac{\nu_{12}}{E_1} = \frac{\nu_{21}}{E_2}$ may be set to equal. This is based on the Maxwell-Betti Reciprocal Theorem (Hyer, 2008, p. 59).

Structural laminates are normally made of multiple layers (several laminas) of composite material, every layer with its own local coordinate system or fiber orientation. From this point, in this study, the composite material has been analyzed in its own local coordinate system. To analyze a structural laminates made of several layers, with different fiber orientations, is needed to set up a global or structural coordinate system. Figure 2-12 illustrates how the local 1-2 coordinate system is dependent on θ-angle to the global x-y coordinate system.

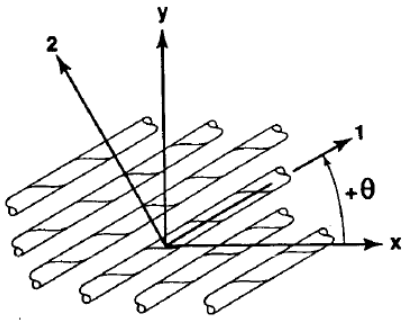

Figure 2-12 x-y axes are global coordinate system, 1-2 axes are local coordinate system and θ is the angle between these two coordinate systems (Jones, 1998, p. 75).

To transform the stress-strain relationship in the local 1-2 coordinate system into the global x-y coordinate system a rotation transformation matrix is used [T] and the matrix is shown in equations (2.8).

$$[T] = \begin{bmatrix} cos^2\theta & sin^2\theta & 2sin\theta\, cos\theta \\ sin^2\theta & cos^2\theta & -2sin\theta\, cos\theta \\ -sin\theta\, cos\theta & sin\theta\, cos\theta & cos^2\theta - sin^2\theta \end{bmatrix} \qquad (2.8)$$

The elastic properties Q_{ij} of the composite material can be transformed from a local to a global coordinate system and that can be done with a transformation matrix [T] as shown in equations (2.9).

$$\left[\bar{Q}_{ij}\right] = [T]^{-1}\left[Q_{ij}\right][T] \qquad (2.9)$$

The stress-strain relationship can now be found in the global coordinate system for each layer in the structural laminates as shown in equation (2.10).

$$\begin{Bmatrix} \sigma_x \\ \sigma_y \\ \tau_{xy} \end{Bmatrix} = \begin{bmatrix} \bar{Q}_{11} & \bar{Q}_{12} & \bar{Q}_{16} \\ \bar{Q}_{12} & \bar{Q}_{22} & \bar{Q}_{26} \\ \bar{Q}_{16} & \bar{Q}_{26} & \bar{Q}_{66} \end{bmatrix} \begin{Bmatrix} \varepsilon_x \\ \varepsilon_x \\ \gamma_{xy} \end{Bmatrix} \qquad (2.10)$$

2.3.2 Classical Laminate Theory

Macromechanics-laminate design is the second step to design and analyze composite materials. There are many macromechanical theories that have been presented in recent years to analyze a composite laminate. A few of them are shown here below.

Two-dimensional theory (Manjunatha & Kant, 1992)

- Classical Laminate theory (CLT)
- Higher-order shear deformation theory (HOST)

Three-dimensional theory (Kant, T., 2010)

- Finite element model

One of the most prevalent models to analyze a composite laminate is the Classical Laminate Theory, or CLT. The theory is explained here below and used for further calculations in this study.

CLT is a first-order shear deformation theory and based on the Kirchhoff hypothesis. It was in the 1800s when the Kirchhoff hypothesis was originally introduced (Hyer, 2008, p. 302). The first paper about CLT was published by Reissner 1961 (Reissner & Stavsky, 1961). The layers in the laminate do not have to be made of the same composite materials. The layers can be from one up to several hundred layers in each laminate and have different fiber orientations. Figure 2-13 illustrates how the CLT is set up in the z-axis in the global coordinate system. There is k number of layers with N layers. The layer thickness is denoted by t_k and the laminate thickness is denoted by t. The middle surface is in the middle of the laminate where the z-axis is zeros and the positive axis downward. The z-axis will describe where each layer located in the system and all layers are perfectly bonded together.

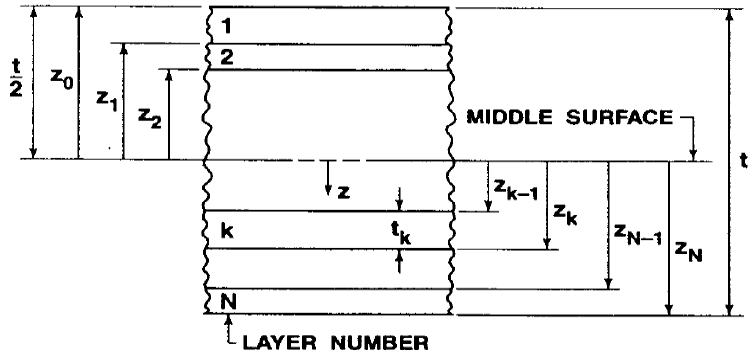

Figure 2-13 The model setup for the z-axis in the Classical Laminate theory (Jones, 1998, p. 196).

Figure 2-14 shows how the Kirchhoff hypothesis works with deformation on a thin plate element where tangential displacement is linear through the thickness of the plate or the laminate.

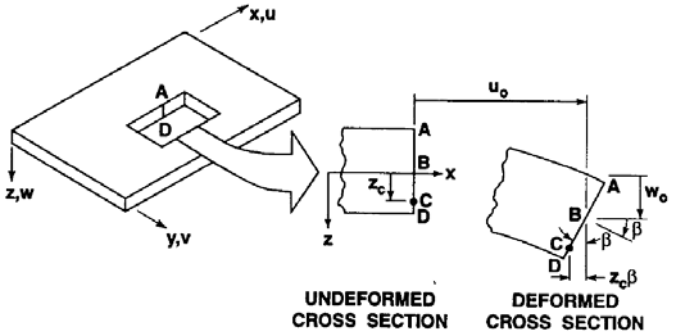

Figure 2-14 Consequences of Kirchhoff hypothesis, geometry of deformation in the x-y plane (Jones, 1998, p. 193).

To find the total displacement of the deformation as shown in figure 2-14 it is necessary to add the displacement which is dependent on the rotation and the length of z_c to the axial displacement. That is done for the x and y directions and for the z direction only the axial displacement is used. Thus in-plane displacements in directions x, y and z are shown in equations (2.11).

$$\begin{aligned} u(x,y,z) &= u^0(x,y) - z_c \frac{\partial w^0(x,y)}{\partial x} \\ v(x,y,z) &= v^0(x,y) - z_c \frac{\partial w^0(x,y)}{\partial y} \\ w(x,y,z) &= w^0(x,y) \end{aligned} \tag{2.11}$$

Given the definition of the displacement according to the Kirchhoff hypothesis the next step is to find the strains that result from the displacement. Kinematics or strain-displacement relations in an elastic body can be used to find the total strain in the plate element as shown in equations (2.12) and (2.13).

$$\begin{aligned} \varepsilon_x(x,y,z) &= \varepsilon_x^0(x,y) + z_c \kappa_x^0(x,y) \\ \varepsilon_y(x,y,z) &= \varepsilon_y^0(x,y) + z_c \kappa_y^0(x,y) \\ \gamma_{xy}(x,y,z) &= \gamma_{xy}^0(x,y) + z_c \kappa_{xy}^0(x,y) \end{aligned} \tag{2.12}$$

with:

$$\varepsilon_x^0(x,y) = \frac{\partial u^0(x,y)}{\partial x} \quad \text{and} \quad \kappa_x^0(x,y) = -\frac{\partial^2 w^0(x,y)}{\partial x^2}$$
$$\varepsilon_y^0(x,y) = \frac{\partial v^0(x,y)}{\partial y} \quad \text{and} \quad \kappa_y^0(x,y) = -\frac{\partial^2 w^0(x,y)}{\partial y^2} \qquad (2.13)$$
$$\gamma_{xy}^0(x,y) = \frac{\partial v^0(x,y)}{\partial x} + \frac{\partial u^0(x,y)}{\partial y} \quad \text{and} \quad \kappa_{xy}^0(x,y) = -2\frac{\partial^2 w^0(x,y)}{\partial x \partial y}$$

Now the stress σ_i can be calculated anywhere on the z-axis for each layer if the mid-plane strain ε_i^0 and curvature κ_i^0 are defined for both the x and y directions. The shear stress τ_{xy} works in a similar way. It is very important to analyze the stress-strain relationship in this way in order to analyze the bending and twisting moment in the plate element. The stress-strain relationship is shown in equation (2.14) in the global x-y-z coordinate system where k is the number of layers and z_k is the distance to layer-k.

$$\begin{Bmatrix} \sigma_x \\ \sigma_y \\ \tau_{xy} \end{Bmatrix}_k = \begin{bmatrix} \bar{Q}_{11} & \bar{Q}_{12} & \bar{Q}_{16} \\ \bar{Q}_{12} & \bar{Q}_{22} & \bar{Q}_{26} \\ \bar{Q}_{16} & \bar{Q}_{26} & \bar{Q}_{66} \end{bmatrix}_k \begin{Bmatrix} \varepsilon_x^0 + z_k \kappa_x^0 \\ \varepsilon_y^0 + z_k \kappa_y^0 \\ \gamma_{xy}^0 + z_k \kappa_{xy}^0 \end{Bmatrix} \qquad (2.14)$$

To design or analyze a structural laminate it is usually more convenient to work with obtained forces and moments (applied loads) in per unit width.

The exact solution for forces and moments are integrals through the laminate thickness of the stresses where t denotes the laminate thickness. Equations (2.15) show the exact solutions for an applied load in the global x-y-z coordinate system for all directions.

$$N_x \equiv \int_{\frac{-t}{2}}^{\frac{t}{2}} \sigma_x dz \qquad M_x \equiv \int_{\frac{-t}{2}}^{\frac{t}{2}} \sigma_x z dz$$
$$N_y \equiv \int_{\frac{-t}{2}}^{\frac{t}{2}} \sigma_y dz \qquad M_y \equiv \int_{\frac{-t}{2}}^{\frac{t}{2}} \sigma_y z dz \qquad (2.15)$$
$$N_{xy} \equiv \int_{\frac{-t}{2}}^{\frac{t}{2}} \tau_{xy} dz \qquad M_{xy} \equiv \int_{\frac{-t}{2}}^{\frac{t}{2}} \tau_{xy} z dz$$

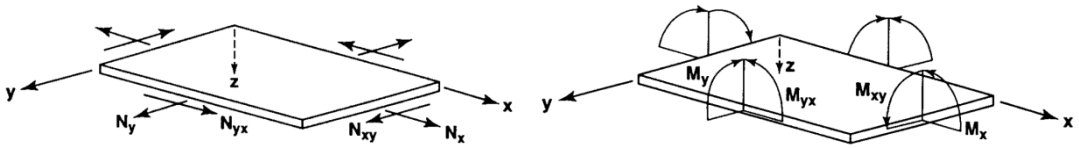

Figure 2-15 In plane forces and moments on a flat laminate (Jones, 1998, p. 196).

N_x, N_y = normal force in x and y direction (force/width of laminate)

N_{xy} = shear force in x-y plane (force/width of laminate)

M_x, M_y = bending moment in x and y direction (force*length/width of laminate)

M_{xy} = twisting moment in x-y plane (force*length/width of laminate)

The locations and directions for the force and the moment are shown in figure 2-15. To calculate the force N_i and the moment M_i for a composite laminate with integrals through the laminate thickness of the stresses as described in equations (2.15) can be complicated or impossible in some cases. To solve this problem it is necessary to use numerical solutions. This can be done by summing the stiffness in a stiffness matrix and multiplying the stiffness matrix by the deformations matrix. Equation (2.16) shows how the applied loads are found by using the stiffness matrix, generally called the ABD matrix, multiplied by the deformations matrix.

$$\begin{Bmatrix} N_x \\ N_y \\ N_{xy} \\ M_x \\ M_y \\ M_{xy} \end{Bmatrix} = \begin{bmatrix} A_{11} & A_{12} & A_{16} & B_{11} & B_{12} & B_{16} \\ A_{12} & A_{22} & A_{26} & B_{12} & B_{22} & B_{26} \\ A_{16} & A_{26} & A_{66} & B_{16} & B_{26} & B_{66} \\ B_{11} & B_{12} & B_{16} & D_{11} & D_{12} & D_{16} \\ B_{12} & B_{22} & B_{26} & D_{12} & D_{22} & D_{26} \\ B_{16} & B_{26} & B_{66} & D_{16} & D_{26} & D_{66} \end{bmatrix} \begin{Bmatrix} \varepsilon_x^0 \\ \varepsilon_y^0 \\ \gamma_{xy}^0 \\ \kappa_x^0 \\ \kappa_y^0 \\ \kappa_{xy}^0 \end{Bmatrix} \qquad (2.16)$$

where the stiffness coefficients are defined by equations (2.17).

$$A_{ij} = \sum_{k=1}^{N} \bar{Q}_{ij\,k}(z_k - z_{k-1})$$

$$B_{ij} = \frac{1}{2}\sum_{k=1}^{N} \bar{Q}_{ij\,k}(z_k^2 - z_{k-1}^2) \qquad (2.17)$$

$$D_{ij} = \frac{1}{3}\sum_{k=1}^{N} \bar{Q}_{ij\,k}(z_k^3 - z_{k-1}^3)$$

The A_{ij} are extensional stiffnesses, the B_{ij} bending-extension coupling stiffnesses and D_{ij} are bending stiffnesses (Jones, 1998, p. 198).

"The ABD matrix defines a relationship between the stress resultants (i.e. loads) applied to a laminate, and the reference surface strains and curvatures (i.e., deformations). This form is a direct result of the Kirchhoff hypothesis, the plane-stress assumption, and the definition of the stress resultants. The laminate stiffness matrix involves everything that is used to define the laminate-layer material properties, fiber orientation, thickness, and location." (Hyer, 2008, p. 323).

2.3.3 Failure theories

The third step is to evaluate the laminate by using the macromechanical failure theories. The failure theories always examine one layer in the laminate so failure theories have to look at all layers one by one. This section will introduce three types of failure theories and they will be the maximum stress theory, the maximum strain theory and the interactive failure theories.

All composite materials have a certain strength, expressed as stress or strain. When the applied load is larger than the ultimate strength of the composite material the material will fail. This can be avoided by using the failure theories to find out if the composite material will fail or not.

To use these failure theories it is necessary to find the ultimate strength from uniaxial tension and compression tests and these values can be:

F_1^T: Tensile failure strength in the 1 direction (longitudinal)

F_1^C: Compressive failure strength in the 1 direction (longitudinal)

F_2^T: Tensile failure strength in the 2 direction (transverse)

F_2^C: Compressive failure strength in the 2 direction (transverse)

F_{12}^S: Shear failure strength in the 1-2 plane (longitudinal shear failure)

Maximum Stress Theory

Maximum stress theory was first suggested by C. F. Jenkins in 1920 and that was for a failure of orthotropic materials (Staab, 1999, p. 144).

There are three models of failure in the maximum stress theory and they are longitudinal failure, transverse failure and shear failure.

Longitudinal failure occurs when $\sigma_1 \geq F_1^T$ (fiber break) or $\sigma_1 \leq F_1^C$ (fiber crushing or kinking).

Transverse failure occurs when $\sigma_2 \geq F_2^T$ (matrix crack) or $\sigma_2 \leq F_2^C$ (fiber and matrix crushing or matrix yielding).

Shear failure occurs when $|\tau_{12}| \geq |F_{12}^S|$ (matrix shear crack).

Maximum Strain Theory

Maximum strain theory is similar to maximum stress theory and the only difference between these two theories is the impact from the Poisson's ratio part of the calculations.

Ultimate strains are calculated with the strength failure divided by Young's modulus, as illustrated in equations (2.18).

$$\varepsilon_1^{Tmax} = \frac{F_1^T}{E_1} \qquad \varepsilon_1^{Cmax} = \frac{F_1^C}{E_1}$$
$$\varepsilon_2^{Tmax} = \frac{F_2^T}{E_2} \qquad \varepsilon_2^{Cmax} = \frac{F_2^C}{E_2} \qquad \gamma_{12}^{Smax} = \frac{F_{12}^S}{G_{12}} \tag{2.18}$$

The strains are calculated for the composite material in the local coordinate system as illustrated in equations (2.19).

$$\varepsilon_1 = \frac{\sigma_1 - \nu_{12}\sigma_2}{E_1} \qquad \varepsilon_2 = \frac{\sigma_2 - \nu_{21}\sigma_1}{E_2}$$
$$\gamma_{12} = \frac{\tau_{12}}{G_{12}} \tag{2.19}$$

There are also three models of failure in the maximum strain theory as in the maximum stress theory, longitudinal failure, transverse failure and shear failure.

Longitudinal failure occurs when $\varepsilon_1 \geq \varepsilon_1^{Tmax}$ or $\varepsilon_1 \leq \varepsilon_1^{Cmax}$

Transverse failure occurs when $\varepsilon_2 \geq \varepsilon_2^{Tmax}$ or $\varepsilon_2 \leq \varepsilon_2^{Cmax}$

Shear failure occurs when $|\gamma_{12}| \geq |\gamma_{12}^{Smax}|$

Interactive failure theories

The interactive failure criterion was introduced, in 1950, by Hill for the first time and since then others have modified his theory (Staab, 1999, pp. 152–153). These theories may be classified into two categories and some of them are listed below (Staab, 1999, p. 153).

1) Criterion: $F_{ij}\sigma_i\sigma_j = 1$ Theory: Ashkenazi, Chamis, Fischer, **Tsai-Hill** and Norris.
2) Criterion: $F_{ij}\sigma_i\sigma_j + F_i\sigma_i = 1$ Theory: Cowin, Hoffman, Malmeister, Marin, **Tsai-Wu** and Gol'denblat-Kopnov.

This section describes one theory from each category, Tsai-Hill and Tsai-Wu, with a rough description of how they work.

Tsai-Hill Theory

The Tsai-Hill theory is an extension of the von Mises theories and is an interactive stress-based criterion and indicates whether or not there is failure (Staab, 1999, p. 155).

The criterion for the Tsai- Hill theory is $F_{ij}\sigma_i\sigma_j = 1$ and for plane stress the failure theory is written as:

Failure occurs when $\frac{\sigma_1^2}{S_1^2} - \frac{\sigma_1\sigma_2}{S_1^2} + \frac{\sigma_2^2}{S_2^2} + \frac{\tau_{12}^2}{F_{12}^{S\ 2}} \geq 1.0$

The following condition has to be satisfied: if $\sigma_1 \geq 0$ then $S_1 = F_1^T$
if $\sigma_1 < 0$ then $S_1 = F_1^C$
if $\sigma_2 \geq 0$ then $S_2 = F_2^T$
if $\sigma_2 < 0$ then $S_2 = F_2^C$

Tsai-Wu Theory

The Tsai-Wu theory is an interactive stress-based criterion and indicates whether or not there is failure. In this theory there is only one model of failure and the criterion for the Tsai-Wu theory is $F_i\sigma_i + F_{ij}\sigma_i\sigma_j = 1 \quad i,j = 1,2,\ldots,6$. For plane stress the failure theory is written as:

Failure occurs when $F_{11}\sigma_1^2 + 2F_{12}\sigma_1\sigma_2 + F_{22}\sigma_2^2 + F_{66}\tau_{12}^2 + F_1\sigma_1 + F_2\sigma_2 \geq 1.0$

F_1, F_{11}, F_2 and F_{22} are determine by using uniaxial tension and compressions tests and the results from that calculation can be seen in equations (2.20).

$$F_{11} = \frac{1}{F_1^T F_1^C} \qquad F_1 = \frac{1}{F_1^T} - \frac{1}{F_1^C}$$
$$F_{22} = \frac{1}{F_2^T F_2^C} \qquad F_2 = \frac{1}{F_2^T} - \frac{1}{F_2^C} \qquad F_{66} = \frac{1}{F_2^T F_2^C} \tag{2.20}$$

To determine the F_{12} a biaxial tension test is used, but it can be difficult to perform a biaxial tension test and it will not give an exact solution. So there is another solution that can be used and that is $F_{12} = F_{12}^* \sqrt{F_{11} F_{22}}$ where F_{12}^* is user-specified constant and this constant is best defined as $F_{12}^* = -1/2$ (Staab, 1999, p. 162).

Comparison of the failure theories

When these three theories: maximum stress theory, maximum strain theory and interactive failure theories, are compared, the differences between them can be large in a particular places.

As shown in figure 2-16, the difference can be largest next to the corners on the stress theory borderline, where the most impact from the Poisson's ratio in the strain theory is. The conservative design should be the gray area in figure 2-16 and that area will have no failure for the all failure theories.

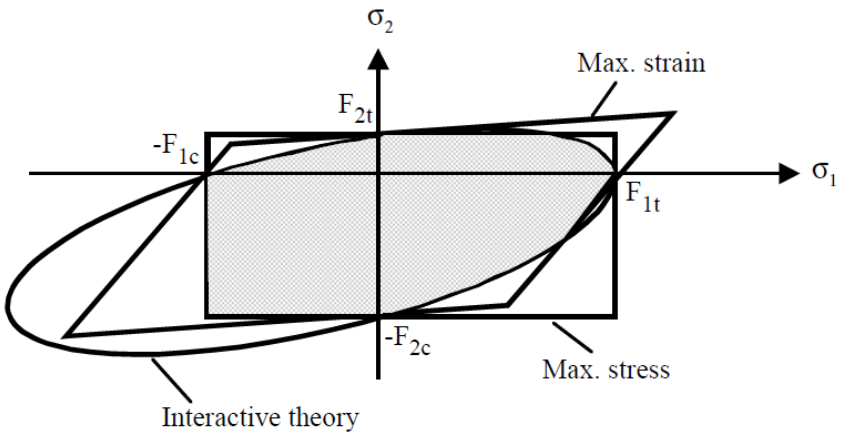

Figure 2-16 Comparison between maximum stress theory, maximum strain theory and interactive failure theories ("Failure Theories," n.d.).

2.3.4 Laminate Design Software

There are a number of software programs which are used to analyze and design a composite material. The National Composites Network published in 2006 a report, named *Design Tools for Fibre Reinforced Polymer Structures* (Meunier, M. & Knibbs, S., 2007). The purpose of the report was to help composite design engineers to select and identify the best design tool for their need.

Nine laminate design tools were compared and they were The Laminator Versions 3.6, ESDU Composites Series, LAP Version 4.0, CoDA Version 3.3, Kolibri Version 3, ESAComp Version 3.5, Composite Star Version 2.0, Composite Pro Version 3.0 and Think Composites. All the software programs used micromechanics-ply calculations and several of them used the rule-of-mixtures model. All the software programs used Classical Laminate Theory in the macromechanics-laminate design. All the software programs used a failure theories maximum stress, maximum strain, Tsai-Hill, Tsai-Wu, and several others in some cases. The summary from the report *Design Tools for Fibre Reinforced Polymer Structures* shows that the theories which have been described in this thesis are commonly used in laminate design tools.

2.4 Test Methods

In basic research where material properties are tested for a new material it is necessary to use recognized standards, such as ASTM, to compare other material properties on same basis. This study performed basic research on material properties and ASTM standards are used. ASTM are international standards and stands for the American Society for Testing and Materials. In 1898 ASTM was created by chemists and engineers and in 2001, the Society became known as ASTM (ASTM International, 2012).

The standard test methods that used in this research were:

1) To find the volume fraction of reinforcing fibers in the composite material using: *ASTM D3171 Constituent Content of Composite Materials* (*ASTM D3171*, 2000).
2) To perform a uniaxial tension tests using: *ASTM D3039 Tensile Properties of Polymer Matrix Composite Materials* (*ASTM D3039*, 2000).
3) To perform a uniaxial compression tests using a combination of two methods: *ASTM D695 Compressive Properties of Rigid Plastics* (ASTM D695, 2002) and *ASTM D3410 Compressive Properties of Polymer Matrix Composite*

Materials with Unsupported Gage Section by Shear Loading (ASTM D3410, 2003).

4) To perform a uniaxial in-plane shear test using: *ASTM D3518 In-plane Shear Response of Polymer Matrix Composite Materials by Tensile Test of a ±45° Laminate* (ASTM D3518, 1994).
5) To perform a pin bearing test using: *ASTM D5961 Bering Response of Polymer Matrix Composite Laminates* (*ASTM D5961*, 2001).
6) To perform the Young's Modulus in the uniaxial test using: *ASTM E111 Young's Modulus, Tangent Modulus, and Chord Modulus* (ASTM E111, 1997).
7) To perform the Poisson's Ratio using: *ASTM E132 Poisson's Ratio at Room Temperature* (ASTM E132, 2004).

2.5 Summary

- A composite material is composed of at two or more elements working together.
- Composite material consists of a matrix and some type of reinforcement.
- The matrix can be a polymer-based resin and this study focused on polyester.
- The reinforcement can be continuous fibers which are in the form of woven or stitched fabrics and this study will focused on basalt fibers.
- Manufacturing processes for laminate material can be Hand Lay-up, Vacuum Bagging and Vacuum Infusion.
- The rule-of-mixtures model can be used to calculate the properties for a composite material.
- Classical Laminate Theory can be used to calculate a laminate material.
- The failure theories can be used to evaluate the laminate and the theories can be maximum stress theory, maximum strain theory, Tsai-Hill and Tsai-Wu.
- The theories which have been described in this section are commonly used in laminate design tools.
- ASTM standards can be used for basic research, such as uniaxial tension and compression tests for composite material.

Material Properties in the Experiment

3.1 General

The experimental programs were divided into two parts. The first part was carried out as basic research on Basalt Fiber Reinforced Polymers (BFRP) where specimens were tested and in the second part tubes made of BFRP were tested. The BRFP were made of continuous fibers which were in the form of stitched fabrics and the polymers were made of polyester resin.

3.2 Basalt Fiber

Two types of basalt fabrics were used in the experiment and both were supplied by Basaltex, Belgium (http://www.basaltex.com). The fabrics were made of basalt continuous fibers which were in the form of stitched fabrics. The basic research (the first part) used biaxial fabric type BAS BI 600, with an areal weight of 605 g/m^2, to produce the specimens as shown in figure 3-1 on the left side. To produce the tubes (the second part) unidirectional fabric BAS UNI 600 was used, with an areal weight of 657 g/m^2, as shown in figure 3-1 on the right side. Table 3-1 shows all the material properties for the basalt fabrics which were used in this thesis. All information on technical data about these two fabrics can also be found in Appendix A.

Figure 3-1 Basalt fabrics from Basaltex, the left side is BAS BI 600 and the right side is BAS UNI 600.

Table 3-1 Material properties of basalt fabrics.

Material Type	Density of basalt [g/cm^3]	Thickness of fabrics [mm]	Surface weight [g/m^2]	Tensile strength [MPa]	Tensile strain [%]	Elastic modulus [GPa]
BAS BI 600	2.67	0.5	605	2410	3.15	86.5
BAS UNI 600	2.67	0.65	657	2410	3.15	86.5

3.3 Polyester resin

Two types of polyester resin were used in the experiment and both were supplied by Reichhold (http://www.reichhold.com). The experiment used two types of manufacturing processes to create the BFRP in composite laminate; for that reason it was not possible to use the same type of polyester resin. The Hand Lay-up process used POLYLITE 440-M850 (standard polyester resin) and the Vacuum Infusion process used POLYLITE 506-647 (designed for vacuum infusion processes). Table 3-2 shows all the material properties for the polyester resins which were used in this study. All information on the technical data about these two polyester resins from Reichhold can also be found in Appendix B.

Table 3-2 Material properties of polyester resin.

Material type	Density of resin [g/cm^3]	Tensile strength [MPa]	Tensile strain [%]	Elastic modulus [GPa]
POLYLITE 506-647	1.11	50	2.1	3.1
POLYLITE 440-M850	1.10	50	1.6	4.6

3.4 Summary

- Two types of basalt fabrics were used made of basalt continuous fibers which were in the form of stitched fabrics.
- Two types of polyester resin were used, for the Hand Lay-up process and the Vacuum Infusion process.

Experimental Program and Procedures, Part 1

4.1 General

In the first part of the experiment two thin plates made of BFRP laminate were made by using the Vacuum Infusion process. The plates were made in the structural laboratory at Reykjavík University. The plats were cut down with a saw into rectangular specimens. The specimens were tested for uniaxial tension, compression, in-plane shear and pin bearing.

4.2 Fabrication Procedure of the Fiber plates

Two types of thin plates were made, using the same reinforcement biaxial fabric type BAS BI 600 and the same matrix polyester resins POLYLITE 506-647. The plates were made of six pieces of fabric where each fabric was 0.5 mm thick and covered two layers with an areal weight of each layer 298.5 g/m^2. The lamination sequences for these two plates with twelve layers were:

$$\text{Plate no.1} = [(\pm 45°)_3]_S \qquad \text{Plate no.2} = [0°/90°/\pm 45°/0°/90°]_S$$

This symmetrical lamination sequence was selected to prevent problems of strain coupling between the layers. Figure 4-1 illustrates, to the left, these six fabrics which were placed on the mold in two different directions, i.e. 0° and 45°. First the fabrics were placed in the mold and then the peel ply, distribution media and vacuum bag were placed on in this order, as shown in figure 4-1 to the right. The peel ply was used to prevent the distribution media from sticking to the laminate plates. The distribution media was used to distribute the resin equally and easily around the plates. The vacuum bag was sealed to the mold with sealant tape (color yellow) as shown in figure 4-1 to the right.

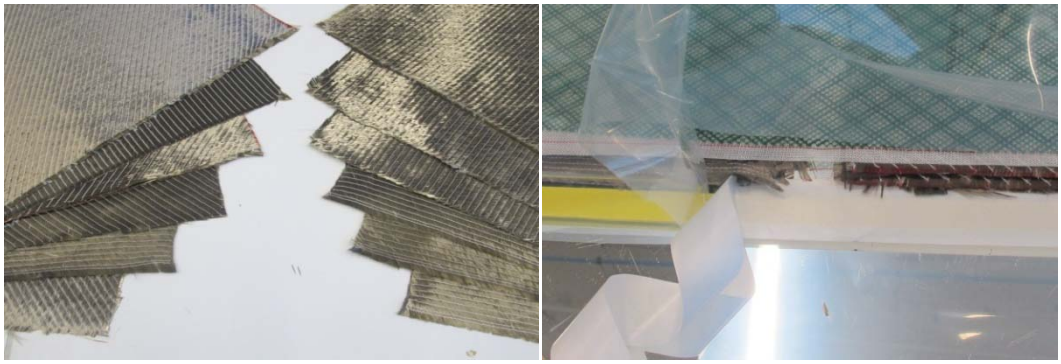

Figure 4-1 Basalt fabrics type BAS BI 600 (to the left) and vacuum infusion process (to the right).

The vacuum pump was used to vacuum out the air from the system and checked for leaking before the polyester resin was infused into the system. When the polyester resin was infused through the fabrics, as shown in figure 4-2 to the left, the system had attained a 90% vacuum. When the fabrics were saturated by polyester resin the vacuum was reduced to 50% for four hours during which time the resin was to harden. Figure 4-2 to the right shows the laminate plates after the vacuum infusion process and the thickness of the plates measured 2.7mm (on average). The width and length of plate no.1 ($[(\pm 45°)_3]_S$) was 900 x 450 mm and the width and length of plate no.2 ($[0°/90°/\pm 45°/0°/90°]_S$) was 450 x 450 mm.

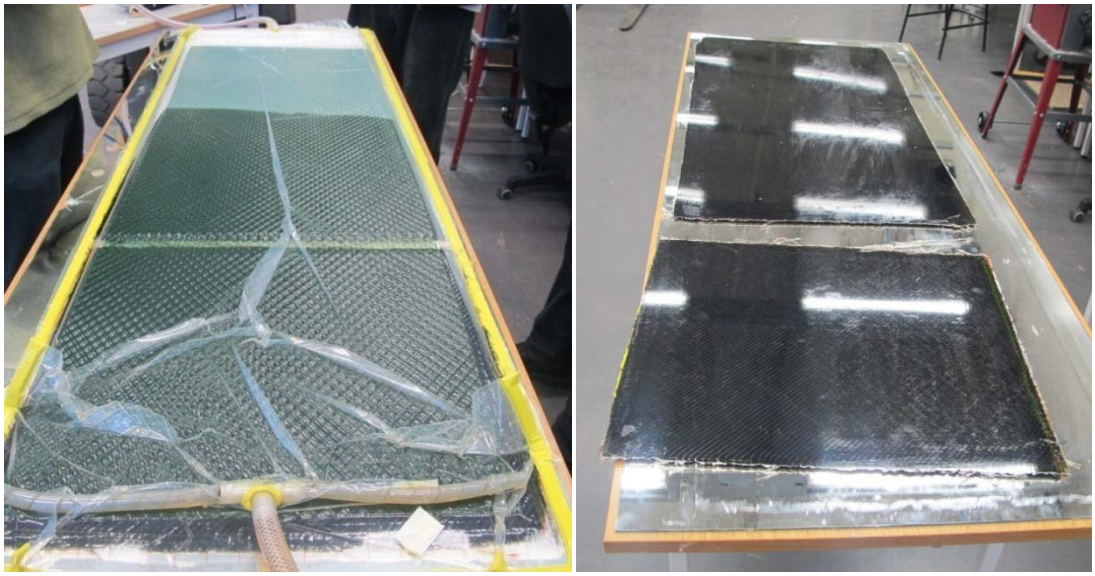

Figure 4-2 The polyester resin was infused through the basalt fabrics (to the left). The laminate plates completed after the vacuum infusion process (to the right).

4.2 Constituent Content Determination of the Fiber plates

The standard ASTM D3171*"Constituent Content of Composite Materials"* (*ASTM D3171*, 2000) was used to ascertain the composite density, the weight and volume ratio for the reinforcement and the matrix for each specimen. Method II in the standard was used because the basalt fabric areal weight was known. Equation (4.1) demonstrates how the specimen density (composite density) was found.

$$\rho_c = \frac{mass\ of\ the\ specimen}{volume\ of\ the\ specimen} \qquad (4.1)$$

The basalt fiber weight percent W_f was calculated for all specimens, as expressed in equation (4.2).

$$W_f = 100 * \frac{A_f * N}{\rho_c * h} \tag{4.2}$$

The basalt fiber volume percent V_f was calculated for all specimens, as expressed in equation (4.3).

$$V_f = W_f * \frac{\rho_c}{\rho_f} \tag{4.3}$$

The polyester resin weight percent W_m was calculated for all specimens, as expressed in equation (4.4).

$$W_m = 100 - W_f \tag{4.4}$$

The polyester resin volume percent V_m was calculated for all specimens, as expressed in equation (4.5).

$$V_m = W_m * \frac{\rho_c}{\rho_m} \tag{4.5}$$

where: A_f = 605 g/m^{2}weight of basalt fabric BAS BI 600 (Appendix A)

N = 6 fabrics, number of fabrics in the specimen

h = average 2.7 mm thickness of the specimen (Appendix C)

ρ_f = 2.67 g/cm^3 density of the basalt fiber Basaltex (Appendix A)

ρ_m = 1.1 g/cm^{3}density of the polyester resin POLYLITE 506-647 (Appendix B)

All measurements for the specimens, such as the mass, thickness and volume, can be found in Appendix C.

4.3 Tensile Test Procedure

4.3.1 Fabrication Procedure of Specimens A and C

Uniaxial static tensile tests were carried out according to ASTM D3039 "*Tensile Properties of Polymer Matrix Composite Materials*" (*ASTM D3039*, 2000). Two types, A and C, of composite material with different fiber orientation were tested. Six specimens of type A were cut out of plate no.1 with a lamination sequence of $[(0°/90°)_3]_S$ and six specimens of type C were cut out of plate no.2 with a lamination sequence of $[0°/90°/\pm45°/0°/90°]_S$. The dimensions of the specimens are illustrated in figure 4-3 and these dimensions are recommended by the standard ASTM D3039.

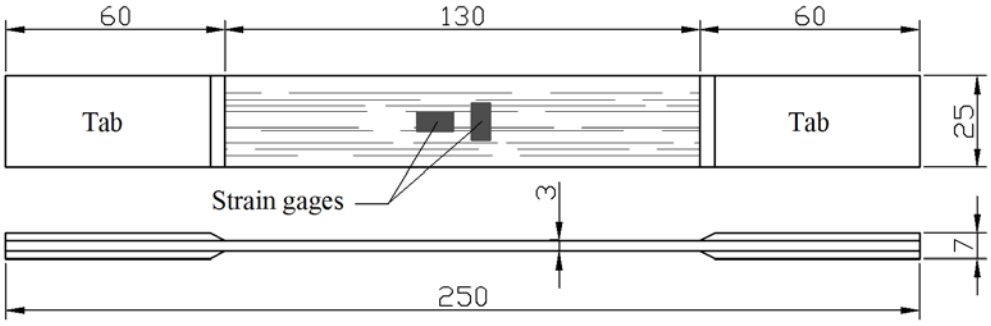

Figure 4-3 Dimensions of the tensile specimen, types A and C.

All the specimens were provided with tabs made of 2 mm thick glass fiber/polyester laminate. This was done to prevent a failure of the specimens at the grips in the testing machine. Two linear strain gages SGD-6/120-LY11 (http://www.omega.com) were glued on each specimen in longitudinal and transverse directions, as shown in figure 4-3. Figure 4-4 shows the specimens ready to be tensile tested, six specimens of type A and six specimens of type C.

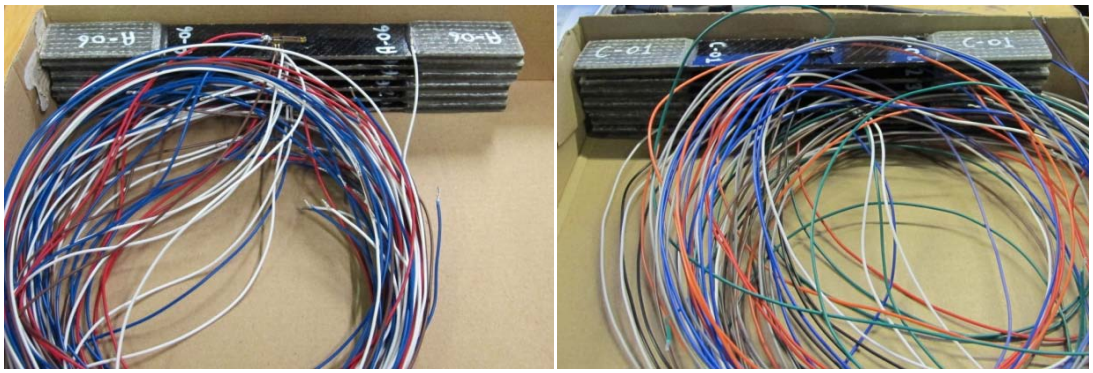

Figure 4-4 Six specimens of type A ready to be tensile tested (to the left) and six specimens of type C ready to be tensile tested (to the right).

4.3.2 Test Procedure of Specimens A and C

The tensile tests were performed at room temperature under standard humidity conditions. The specimens were tested in the Tinius Olsen universal testing machine at the Innovation Center Iceland with a standard head displacement rate of 2 mm/min (speed of testing) according to ASTM D3039. Two computers were used for data collection and both collected data were time-dependent. One computer was connected to a Tinius Olsen machine and collected data about the load carried by test specimens. The other computer was connected to the strain gages and collected strain data in longitudinal and transverse directions from the specimens. The load and the strain from both computers were composed with time. Figure 4-5 illustrates the tools and machine which were used in the tensile test.

Figure 4-5 To the left is the computer which collected data from the strain gages, in the middle is the Tinius Olsen universal testing machine and to the right the computer which collected data from the Tinius Olsen universal testing machine.

The red circle in figure 4-5 is presented as a close-up in figure 4-6 where specimen C-04 was tensile tested. In the tensile tests the specimens were stretched at a constant speed (2 mm/min) until they failed.

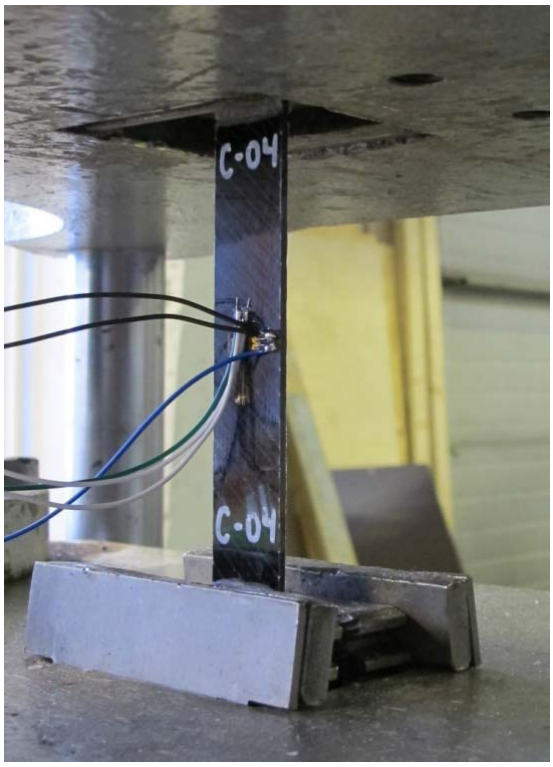

Figure 4-6 Tensile test performed on specimen C-04.

The following composite material properties for each specimen, effects of the tensile tests, were calculated based on the measurements (data from the tests and dimensions of the specimens): maximum load before failure, ultimate tensile strength, ultimate tensile strain, Poisson's ratio, Young's modulus and stress-strain curves. In all calculation the standards of ASTM D3039 were used as well as ASTM E111 for Young's modulus and ASTM E132 for Poisson's ratio.

All the basic results from the tensile test can be found in Appendix D.

4.4 Compression Test Procedure

4.4.1 Fabrication Procedure of Specimens D and E

Uniaxial static compression tests were carried out according to a combination of ASTM D695*"Compressive Properties of Rigid Plastics"* (ASTM D695, 2002) and ASTM D3410*"Compressive Properties of Polymer Matrix Composite Materials with Unsupported Gage Section by Shear Loading"* (ASTM D3410, 2003). Two types, D and E, of composite material with different fiber orientations were tested. Six specimens of type D were cut out of plate no.1 with a lamination sequence of $[(0°/90°)_3]_S$ and six specimens of type E were also cut out of plate no.1 with a lamination sequence of $[(\pm 45°)_3]_S$. The dimensions of the specimens are illustrated in figure 4-7 and these dimensions are recommended by ASTM D3410 standards.

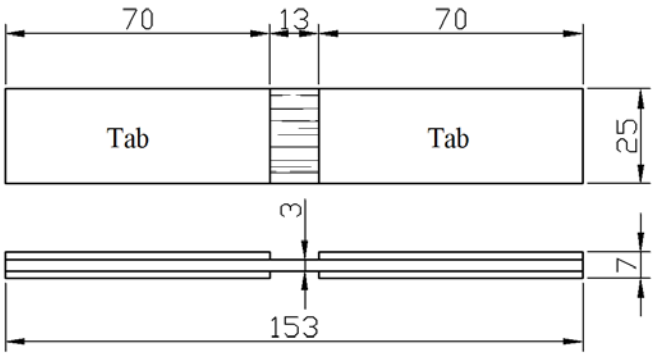

Figure 4-7 Dimensions of the compressive specimen with the gage length 13 mm.

All the specimens were provided with tabs made of 2 mm thick glass fiber/polyester laminate. This was done to make the weakest point be in the middle of the specimens (in the compression test it was meant to fail there). For the compression test an aluminum duct was made to put the specimens in when the specimens were compressed. This was done to avoid global buckling in the specimens. Figure 4-8, to the left, illustrates how the aluminum duct looks with the specimens inside. Figure 4-8, to the right, show the specimens ready to be compression tested, six specimens of type D and six specimens of type E. It was not possible in this experiment to put strain gages on the specimens because of the aluminum duct and the gage length was only 13 mm for all the specimens. Instead a gap was created where the specimens were meant to fail (as seen in figure 4-8 to the left) to make a video and photo of the most critical zone of the specimens in the compression tests.

Figure 4-8 The aluminum duct with the specimens inside (to the left) and specimens of types D and E ready to be compression tested (to the right).

4.4.2 Test Procedure of Specimens D and E

The compression tests were performed at room temperature under standard humidity conditions. The specimens were tested in the Tinius Olsen universal testing machine at the Innovation Center Iceland with a standard head displacement rate of 1 mm/min (speed of testing) according to ASTM D695. One computer was used for data collection which was connected to the Tinius Olsen machine. The data collected were applied load versus displacement as time-dependent. Figure 4-9 shows the Tinius Olsen universal testing machine which was used in the compression tests.

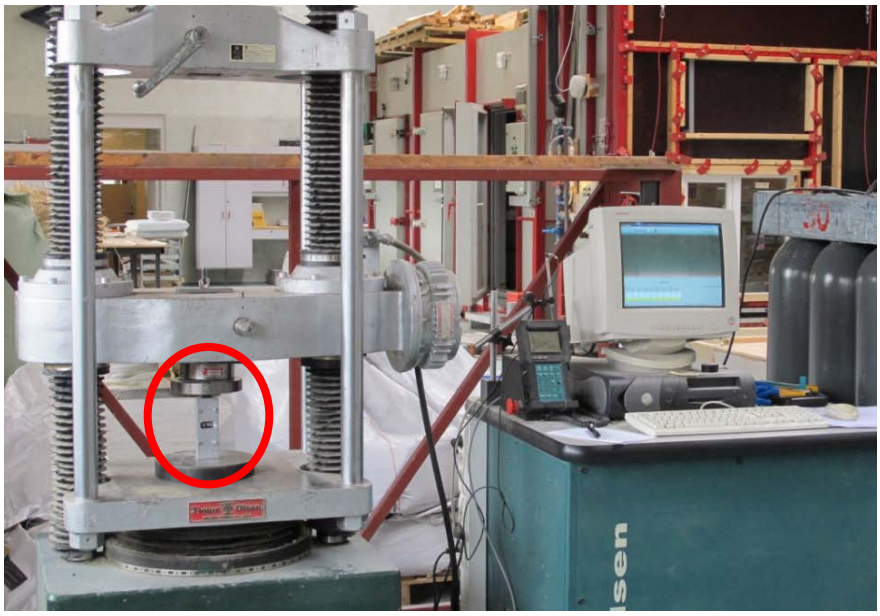

Figure 4-9 Tinius Olsen machine which was used in the compression tests.

The area in the red circle in figure 4-9 appears as a close-up in figure 4-10 where the specimen D-04 was compression tested. In the compression tests the specimens were compressed at a constant speed (1 mm/min) until the specimen failed.

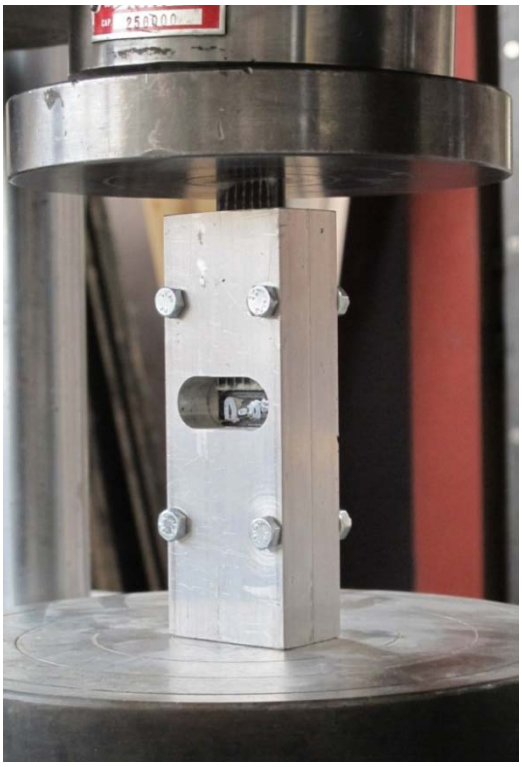

Figure 4-10 Compression test performed on specimen D-04.

The following composite material properties for each specimen, effects of compression tests, were calculated based on the measurements (data from the tests and dimensions of the specimens): maximum load before failure, ultimate compressive strength and deformation at break.

As has been mentioned before strain gages were not available and it was difficult or almost impossible to measure the deformation with a traditional extensometer. For this reason one specimen, D-05, was measured with a Tinius Olsen Video Extensometer (http://www.tiniusolsen.com) in the compression test. Only one test was available because it was done during the promotion meeting on the Video Extensometer in Iceland. The video camera was connected to a computer which collected the data about strain in longitudinal and transverse directions of the specimen and was time-dependent. The video was taken in the gap of the aluminum duct where the specimen had been sprayed black and white to make marks for the strain results. Figure 4-11 illustrates the Video Extensometers set up in the compression test on specimen D-05.

Figure 4-11 Tinius Olsen Video Extensometers set up in the compression test.

The load and the strain data from both computers were composed with time-dependency from the test of specimen D-05 and the ultimate compressive strain, Poisson's ratio, Young's modulus and stress-strain curves were calculated. This information shows roughly the properties for the composite material.

All calculations were according to ASTM D3410 as well as ASTM E111 for Young's modulus and ASTM E132 for Poisson's ratio.

All the basic results from the compression test can be found in Appendix D.

4.5 In-Plane Shear Test ± 45° Procedure

4.5.1 Fabrication Procedure of Specimens B

Uniaxial in-plane shear tests were carried out according to ASTM D3518 *"In-plane Shear Response of Polymer Matrix Composite Materials by Tensile Test of a ±45° Laminate"*(ASTM D3518, 1994). One type (type B) of composite material with fiber orientation $[(\pm 45°)_3]_S$ was tested. Six specimens of type B were cut out of plate no.1 and the dimensions of the specimens are illustrated in figure 4-12.

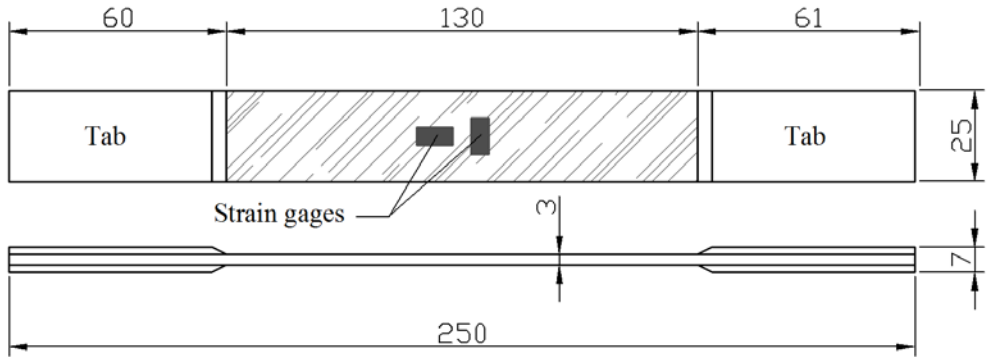

Figure 4-12 Dimension of the in-plane shear specimen type B.

All the specimens were provided with tabs made of 2 mm thick glass fiber/polyester laminate. This was done to prevent a failure of the specimens at the grips in the testing machine. Two linear strain gages SGD-6/120-LY11 (http://www.omega.com) were glued on the specimens in longitudinal and transverse directions as shown in figure 4-12. Figures 4-13 shows six specimens of type B before the strain gages were put on.

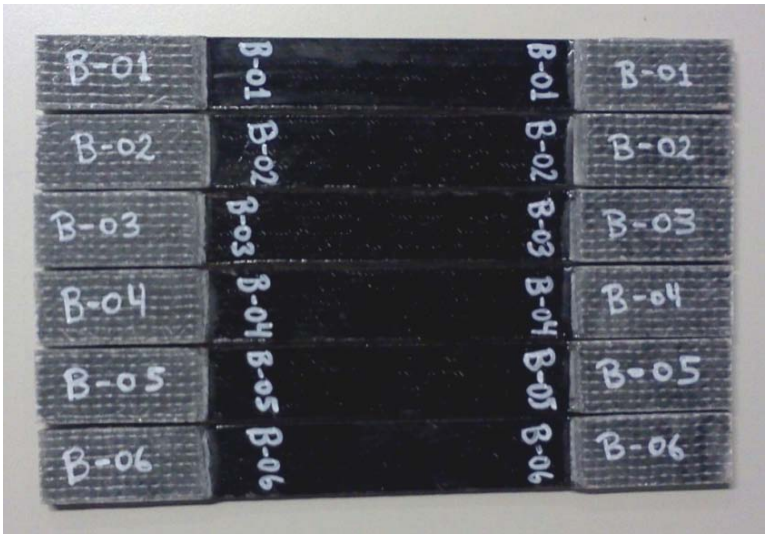

Figure 4-13 Six specimens of type B before the strain gages were put on.

4.5.2 Test Procedure of Specimens B

The test procedure for the specimens, type B, was exactly the same as for specimens of types A and C. All information about the test procedure for type B can be found in section 4.3.2. Figure 4-14 shows when specimen B-05 was in-plane shear tested. In the in-plane shear tests the specimens were stretched at a constant speed until the specimen failed.

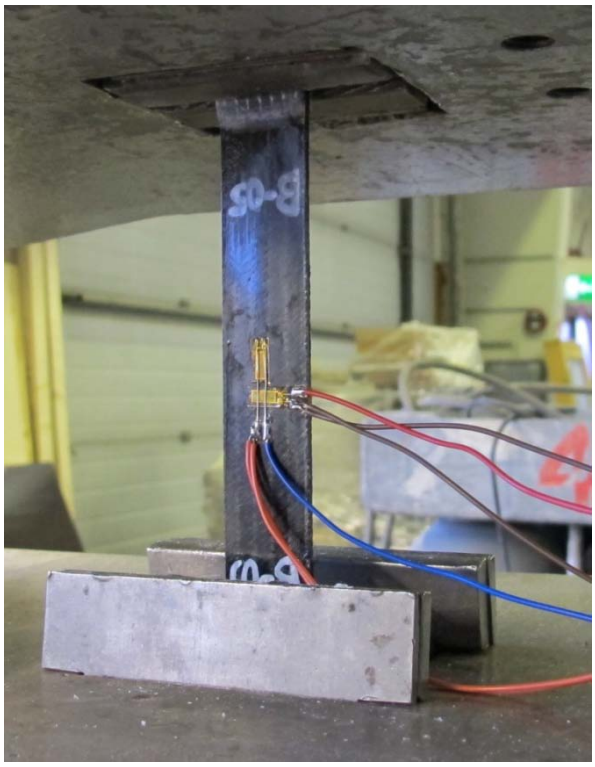

Figure 4-14 In-plane shear test performed on specimen B-05.

The following composite material properties for each specimen, effects of in-plane shear tests, were calculated based on the measurements (data composed from the tests and dimensions of the specimens): maximum load at or below 5% shear strain, maximum in-plane shear stress, maximum tensile strain, Poisson's ratio, shear chord modulus of elasticity and stress-strain curves. In all calculations the standards of ASTM D3518 were used as well as ASTM E132 for Poisson's ratio.

All the basic results from the in-plane shear test can be found in Appendix D.

4.6 Pin Bearing Test Procedure

4.6.1 Fabrication Procedure of Specimens G, H and I

Uniaxial pin bearing tests were carried out according to ASTM D5961 "*Bearing Response of Polymer Matrix Composite Laminates"* (*ASTM D5961*, 2001). Three types, G, H and I, of composite material with different fiber orientations were tested. Six specimens of type G were cut out of plate no.1 with a lamination sequence of $[(0°/90°)_3]_S$. Six specimens of type H were cut out of plate no.1 with a lamination sequence of $[(\pm 45°)_3]_S$ and six specimens of type I were cut out of plate no.2 with a lamination sequence of $[0°/90°/\pm 45°/0°/90°]_S$. The dimensions of the specimens and size and location of the holes are illustrated in figure 4-15.

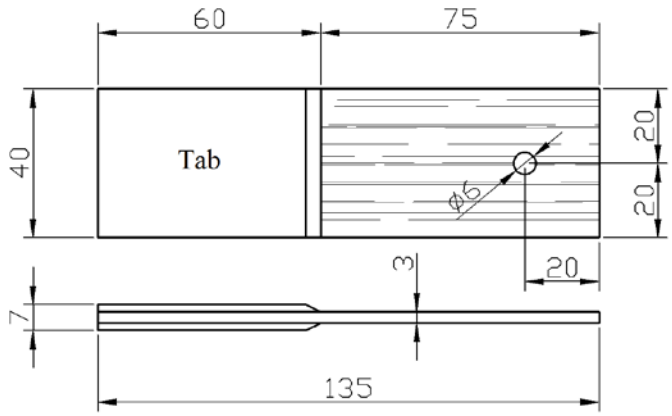

Figure 4-15 Dimensions of the pin bearing specimen types G, H and I.

All the specimens were provided with tabs made of 2 mm thick glass fiber/polyester laminate. This was done to prevent failure of the specimens at the grip in the testing machine. To measure the hole deformation, lines were drawn on the specimens (see figure 4-16) so it was possible to measure the deformation roughly with a Canon G12 video camera. This type of measurement was not equivalent to ASTM 5961. A fixture made of steel was produced similar to procedure A in the ASTM 5961 standard in order to perform the *single-pin double shear tensile tests*. The specimens were connected to the fixture with a pin. Figure 4-16 shows the specimens, types G, H and I, ready for the pin bearing test to the left and the steel fixture which was used in the pin bearing tests to the right.

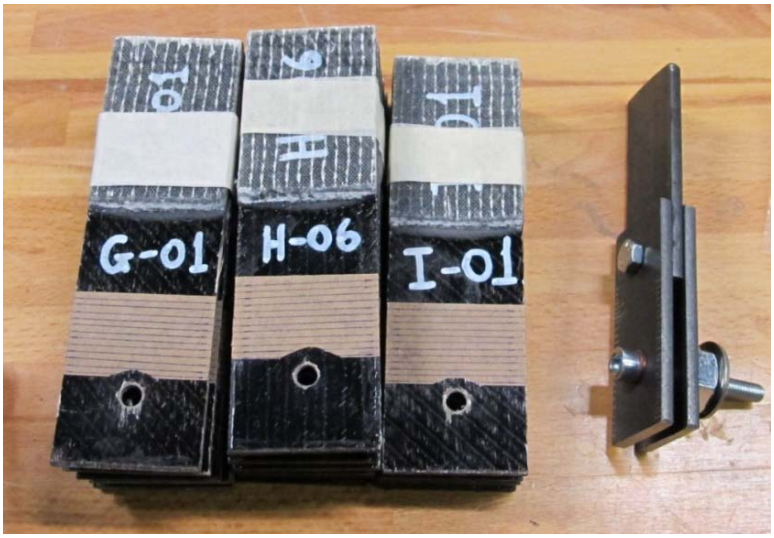

Figure 4-16 The specimens in types G,H and I with the steel fixture.

4.6.2 Test Procedure of Specimens G, H and I

The tensile tests were performed at room temperature under standard humidity conditions. The specimens were tested in the Tinius Olsen universal testing machine at the Innovation Center Iceland with a standard head displacement rate of 2 mm/min (speed of testing) according to ASTM D5961. One computer was used for data collection and it was connected to the Tinius Olsen machine. The data collected were applied load versus displacement as time-dependent. Figure 4-17 illustrates the Tinius Olsen universal testing machine which was used in the pin bearing tests.

Figure 4-17 Tinius Olsen machine which was used in the pin bearing tests.

The area in the red circle in figure 4-17 is shown in close-up in figure 4-18 where specimen G-06 was pin bearing tested. In the pin bearing tests the specimens were stretched at a constant speed (2 mm/min) until the bearing joint failed.

Figure 4-18 Pin bearing test performed on specimen G-06.

The pin bearing tests were filmed with a Canon G12 video camera to measure the hole deformation in the specimens manually. It was measured between the lines on the specimens and the fixture (see figure 4-18) in all the pin bearing tests. With this measured displacement the bearing strain could be calculated. The following composite material properties for each specimen, the effects of the pin bearing tests, were calculated based on the measurements (data from the load tests, measurement from camera and dimensions of the specimens): maximum load prior to failure, ultimate bearing strength, ultimate bearing strain, yield bearing strength, yield bearing strain and stress-strain curves. All calculations were based on ASTM D5961. When the maximum load had clearly been reached in the test, the load was removed so the failure modes in the specimens would not be damaged for further examination.
All the basic results from the pin bearing test can be found in Appendix D.

4.7 Summary

- Composite laminate plates where made with a Vacuum Infusion process.
- The composite density, the weight and volume ratio for the reinforcement and the matrix for each specimen were calculated.
- A tensile test was performed on twelve specimens, types A and C.
- A compression test was performed on twelve specimens, types D and E.
- An in-plane shear test was performed on six specimens, type B.
- A pin bearing test was performed on eighteen specimens, types G, H and I.

Experimental Program and Procedures, Part 2

5.1 General

In the second part of the experiment two tubes made of BFRP laminate were made by using the Hand Lay-up process. One tube was tested in natural weather and the other tube was load tested.

5.2 Fabrication Procedure of the Tubes

The tubes were constructed of matrix polyester resin POLYLITE 440-M850 with reinforcement unidirectional fabric type BAS UNI 600. The basalt fabrics were used to form the tubes and were wrapped in four layers around the mold that shaped the tubes. The polyester resin was always put on by rolling on both sides of the basalt fabric and then the fabric was wrapped around the mold. The basalt fabrics were always crossed to achieve strength and stiffness in both directions on the tubes. The tubes were made of four fabrics where each fabric was 0.65 mm thick and covered by one layer with an areal weight of 657 g/m^2. The laminations was unsymmetrical and the lamination sequences were [(0°/90°)$_2$]. A pipe with a diameter of 110 mm and 1200 mm long was used as a mold for shaping the tubes. Figure 5-1 shows the fabrics and the mold which was used to shape the tubes.

Figure 5-1 Four layers of basalt fabric and the mold for the 1200 mm long tubes. A polyethylene plastic film has been put around the mold to prevent the tube from becoming stuck in the mold.

After the basalt fabrics had been wound around the mold in four layers with wet polyester resin, a plastic film (polyethylene) was then tightened around the outer layers to press the basalt fabrics closer together, as shown in figure 5-2. This was also done to squeeze most of the air out of the layers. The effects were similar to those obtained from the Vacuum bagging process.

Figure 5-2 The tube has been formed and a polyethylene plastic film was then put around the tube to push the layers together.

5.3 Constituent Content Determination of the Tubes

The constituent content determination for the tubes was exactly the same as for the plates in the first part. All information about the constituent content determination for the tubes can be found in section 4.2.

The basalt fabrics in the tube were weighed before they were formatted and the tube was weighed after it was removed from the mold. This was done to determine the ratio between the mass of the resin and fibers.

These values were used in the calculation for the tubes.

A_f = 657 g/m^2 weight of basalt fabric BAS UNI 600 (Appendix A)

N = 4 fabrics number of fabrics in the tubes

h = average 3.0 mm thickness of the tubes (Appendix C)

ρ_f = 2.67 g/cm^3 density of the basalt fiber Basaltex (Appendix A)

ρ_m = 1.1 g/cm^3 density of the polyester resin POLYLITE 440-M850 (Appendix B)

All measurements for the tubes, such as the mass, thickness and volume can be found in Appendix C.

5.4 Weathering test of the Tube

One of the tubes was placed outdoors for natural weather testing. The tube was fixed on an old dock where the tube is in the sea when the tide is high and not in the sea when the tide is low. When tube is going through this tidal range the tube will be exposed to a great deal of salt from the sea and UV (ultraviolet light) rays from the sunlight.The tube was fixed to the dock on February 11, 2012, and will be there for several years. The tube is checked regularly for damage. Figures 5-3 and 5-4 show the tube fixed to the dock when it was low tide and high tide.

Figure 5-3 The 1200mm long tube on the dock when it was low tide.

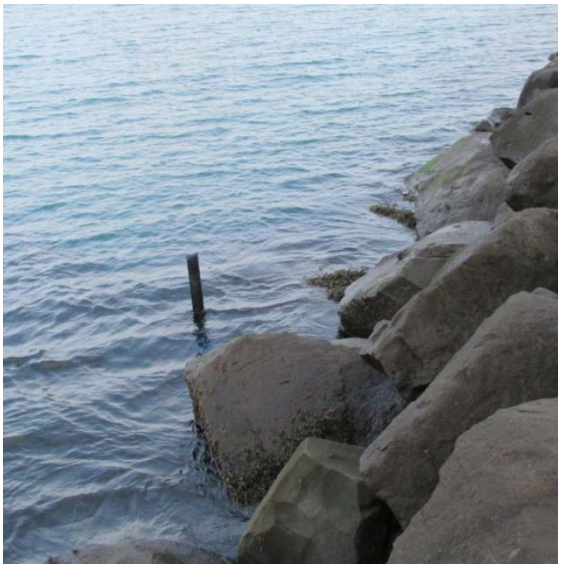

Figure 5-4 The 1200mm long tube on the dock when it was high tide.

5.5 Load Test Procedure of the Tube

When the polyester resin was hardened and reached full strength on the tube, the tube was taken out of the mold (pipe) and load tested. A Universal Testing Machine (UTM) performed the load test and applied tension and compression on the tube. The load test was performed in the structural laboratory of Reykjavík University. The end of the tube was fixed to the UTM. The other end was free where the amplified load was put on the tube.

The UTM performed a wind load at a constant speed where the UTM pushed and pulled alternately, as a swinging load. The speed of the jack load in the UTM was 2.7 mm/sec and the displacement was 60 mm from the vertical tube. A piece of pipe made of iron was glued for 15 cm into each end of the tube. The iron pipe in the lower end of the tube was welded to the UTM to achieve a full moment and the end had no rotation capacity. The jack load pushed and pulled next to the top of the tube where no moment was allowed. The iron pipe, at the top, was pinched between their on pin that kept the tube fixed to the jack load.

In the load test, the UTM transfers data to the computer which draws a graph with load (kN) versus displacement (mm). In the load test, the tube went through four cycles, i.e. one cycle went from zero back to 60 mm and forward to 120 mm and then back again to the starting position of 60 mm. Figure5-5 shows the placement of the tube in the UTM.

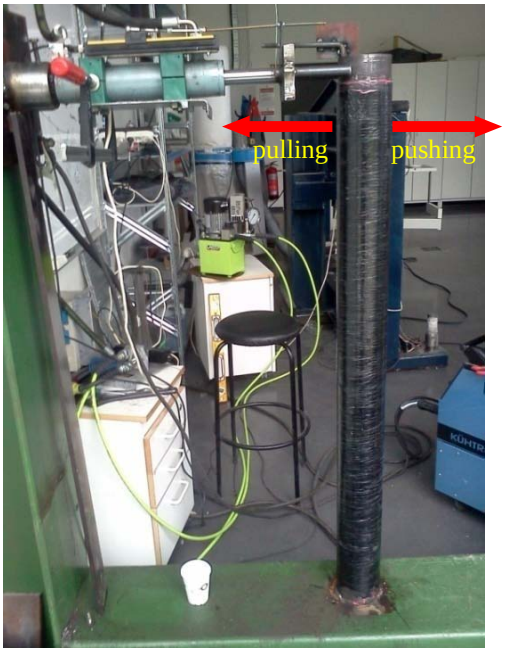

Figure 5-5 The jack-load moves back and forth by the tube in the testing machine (UTM). At the same time it creates tension and compression in the tube.

5.6 Summary

- Two tubes were made of BFRP laminate by using the Hand Lay-up.
- One of the tubes was placed outdoors for natural weather testing.
- The second tube was load tested, where the UTM pushed and pulled alternately, as a swinging load.

Experimental Results

6.1 General

In this section the results of the experimental tests from the first and second parts are presented. Section 6.2 shows the results of the weight and volume for the fiber and resin separated. All sections starting with the caption *General Behavior and Mode of Failure* will describe in text and pictures how the specimens failed. In the standards ASTM D3039, ASTM D3410 and ASTM D5961 are published failure codes with typical or common modes, as can be seen in Appendix E. These standards were used to analyze the specimens' failure. All sections labeled *Test Results* in this chapter show tables and graphs from the load test and a text description of the results. All load measurements from the Tinius Olsen universal testing machine were given in kilogram [kg], as can be seen in Appendix D. To convert to Newton [N] gravity of $g = 9.81\ m/s^2$ in the whole experiment was used. All the results was reported as kilogram-force as$1.00\ kgf = 9.81N$.

6.2 Constituent Content Determination Results

All the forty-eight specimens and the two tubes in the experiment were measured to find the composite density, the weight and volume ratio for the basalt fiber and the polyester resin. The results from the average of specimens which were made with the Vacuum Infusion process can be found in table 6-1. The results from the two tubes which were made with the Hand Lay-up process can be found in table 6-2. All calculations used equations from section 4.2 and further results can be found in Appendix C.

Table 6-1 Constituent content determination results of the specimens.

Specimens 48 pieces	Composite Density (g/cm3)	Fiber Content (wt %)	Resin Content (wt %)	Fiber Volume (vol %)	Resin Volume (vol %)	Total Volume (vol %)
Avg.	1.841	73.49	26.51	50.68	44.01	94.69
St.Dev.	0.014	0.41	0.41	0.45	0.81	-
c.v. (%)	0.78	0.56	1.56	0.89	1.85	-

Table 6-2 Constituent content determination results of the tubes.

Tubes	Composite Density (g/cm3)	Fiber Content (wt %)	Resin Content (wt %)	Fiber Volume (vol %)	Resin Volume (vol %)	Total Volume (vol %)
Tube no.01	1.636	60.87	39.13	37.29	58.19	95.48
Tube no.02	1.692	62.78	37.22	39.78	57.24	97.01

As shown in tables 6-1 and 6-2, the total volume was not 100%. The difference between the calculated total volume and 100% volume, which is around 5%, can be a void volume and inaccuracies in measurements.

6.3 Tensile Test Results

Twelve specimens were static tensile tested, six from type A and six from type C. All tests were with no errors and the specimens failed according to expectations. The basic results for the tensile test can be found in Appendix D.

6.3.1 General Behavior and Mode Failure of Specimens A and C

Types A and C had the same failure mode in the tensile test. In the test delamination of the specimens occurred and it started from the underlying layers. Just before the specimens failed the continuous basalt fiber tended to separate from the polyester resin. The continuous basalt fiber started to wear down next to the edge and close to the top or bottom on the specimen gage until the specimens suddenly exploded and failed. Figures 6-1 to 6-4 show the broken specimens after the static tensile test and graphically how the specimens failed. The figures show the specimens from the front and side views. In accordance with typical failure modes in ASTM D3039 (see Appendix E) the specimens failed, usually mixed with DGM (edge Delamination Gage Middle) and XGM (eXplosive Gage Middle).

Figure 6-1 Broken specimens, type A $[(0°/90°)_3]_S$, after the tensile tests, front view.

Figure 6-2 Broken specimens, type A $[(0°/90°)_3]_S$, after the tensile tests, side view.

Figure 6-3 Broken specimens, type C $[(0°/90°/\pm45°/0°/90°)]_S$, after the tensile tests, front view.

Figure 6-4 Broken specimens, type C $[(0°/90°/\pm45°/0°/90°)]_S$, after the tensile tests, side view.

6.3.2 Test Results of Specimens A and C

All calculations, based on measured values, for type A and C were done in the same way. The applied load (P_i) was presented in Newton (N). The tensile stress (σ_i) was calculated by using the equation (6-1) and the tensile strain (ε_i) was obtained from the measured strain in the longitudinal direction.

$$\sigma_i = \frac{P_i}{A} \tag{6.1}$$

where: σ_i = tensile stress at *i*-th data point

P_i = load at *i*-th data point

A = cross-sectional area

The stress-strain curves were performed as strength (σ_i) versus strain (ε_i) as illustrated in figures 6-5-a and 6-5-b. The tensile Young's modulus of elasticity (E) was found from the slope of the stress-strain curves on the elastic range. The Poisson's ratio (ν) was found by using slopes from figures 6-6-a and 6-6-b to calculate the equation (6-2).

$$\nu = \frac{{d\varepsilon_t}/_{dP} \;\; (slope\ of\ transverse\ strain)}{{d\varepsilon_l}/_{dP} \;\; (slope\ of\ longitudinal\ strain)} \tag{6.2}$$

where: ν = Poisson's ratio

P = applied load

ε_l = longitudinal strain

ε_t = transverse strain

All the results for the specimens in type A in table 6-3 were based on figures 6-5-a and 6-6-a. In the same way the results for the specimens in type C in table 6-4 were based on figures 6-5-b and 6-6-b.

Table 6-3 Tensile testing results of specimens type A $[(0°/90°)_3]_S$.

Specimens Type A	Maximum load bef. failure P^{max} [kN]	Ultimate tensile strength F^{tu} [MPa]	Ultimate tensile strain ε^{max} [%]	Poisson's ratio ν -	Tensile Young's modulus E-modul [GPa]	Coefficient of variation of E-slope V1 [%]
A-01	30.71	446.6	2.63	0.038	19.08	0.16
A-02	30.41	439.0	3.07	0.050	18.96	0.15
A-03	31.39	457.5	2.82	0.071	20.51	0.13
A-04	31.98	460.0	2.85	0.050	18.87	0.00
A-05	26.98	395.4	3.06	0.063	17.55	0.14
A-06	28.55	419.2	2.02	0.050	23.94	0.12
Avg.	30.00	436.3	2.74	0.054	19.82	-
St.Dev.	1.89	24.9	0.39	0.012	2.23	-
c.v. (%)	6.3	5.7	14.2	22.0	11.2	-

Table 6-4 Tensile testing results of specimens type C $[(0°/90°/\pm45°/0°/90°)]_S$.

Specimens Type C	Maximum load bef. failure P^{max} [kN]	Ultimate tensile strength F^{tu} [MPa]	Ultimate tensile strain ε^{max} [%]	Poisson's ratio ν -	Tensile Young's modulus E-modul [GPa]	Coefficient of variation of E-slope V1 [%]
C-01	24.33	362.2	3.03	0.213	16.24	0.15
C-02	25.21	373.0	3.14	0.233	15.75	0.11
C-03	25.02	366.0	3.05	0.220	15.85	0.12
C-04	25.51	376.7	2.86	0.217	15.70	0.12
C-05	23.84	346.2	2.55	0.225	15.33	0.16
C-06	24.82	364.4	2.86	0.233	15.62	0.23
Avg.	24.79	364.7	2.92	0.224	15.75	-
St.Dev.	0.61	10.6	0.21	0.008	0.30	-
c.v. (%)	2.5	2.9	7.3	3.8	1.9	-

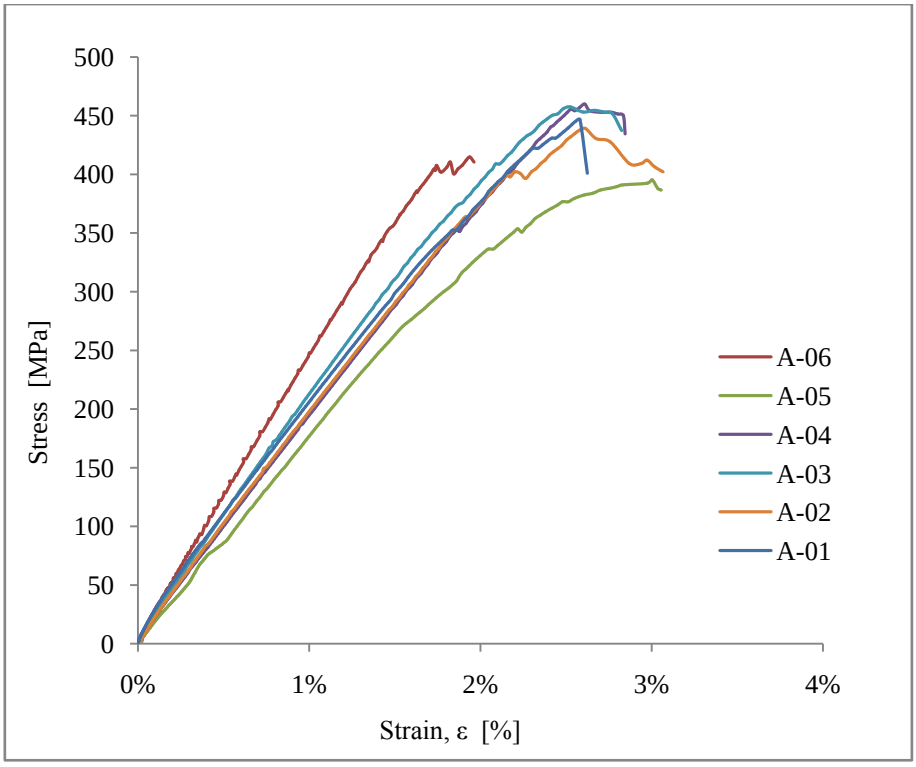

Figure 6-5-a Tensile stress-strain curves of specimens type A $[(0°/90°)_3]_S$.

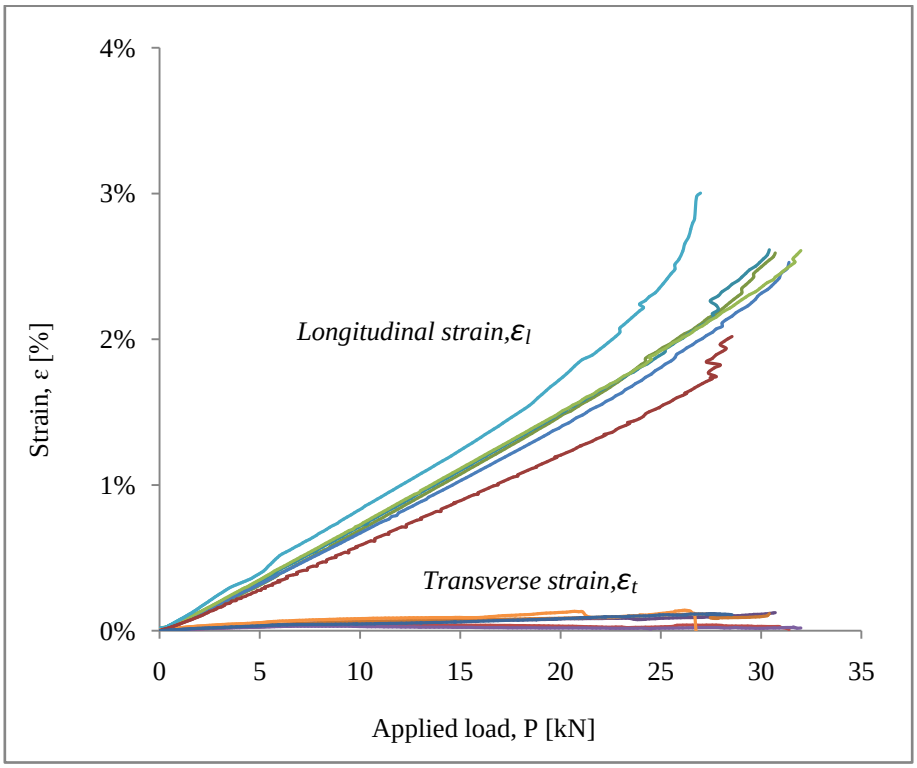

Figure 6-6-a Tensile strain-force curves of specimens type A $[(0°/90°)_3]_S$. The longitudinal strains are with steeper slopes and the transverse strains are with more gentle slopes.

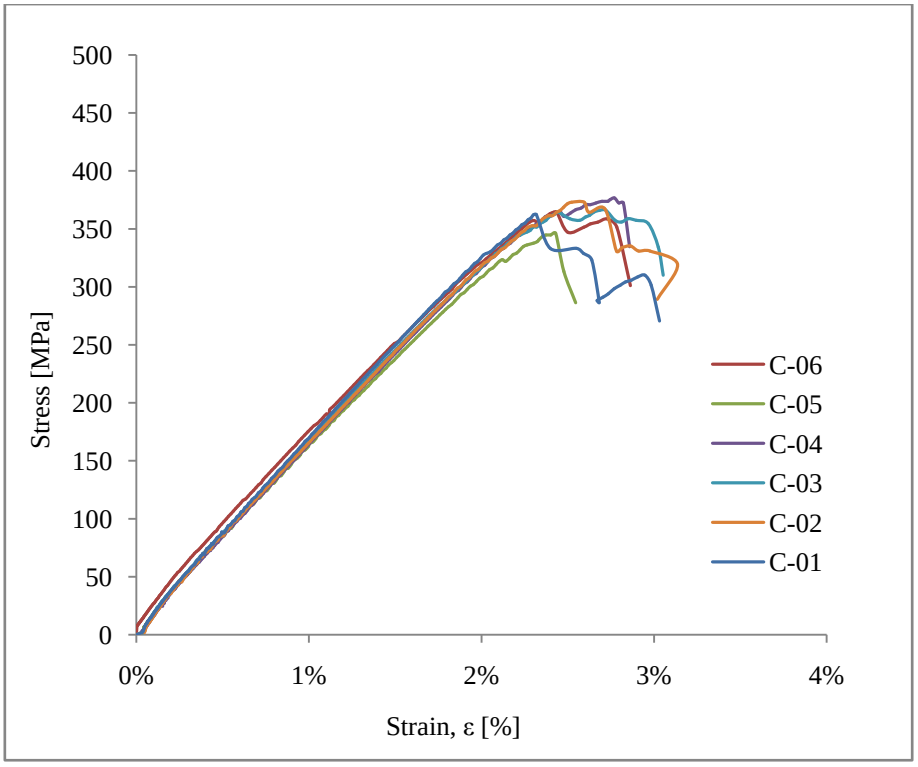

Figure 6-5-b Tensile stress-strain curves of specimens type C $[(0°/90°/\pm45°/0°/90°)]_S$.

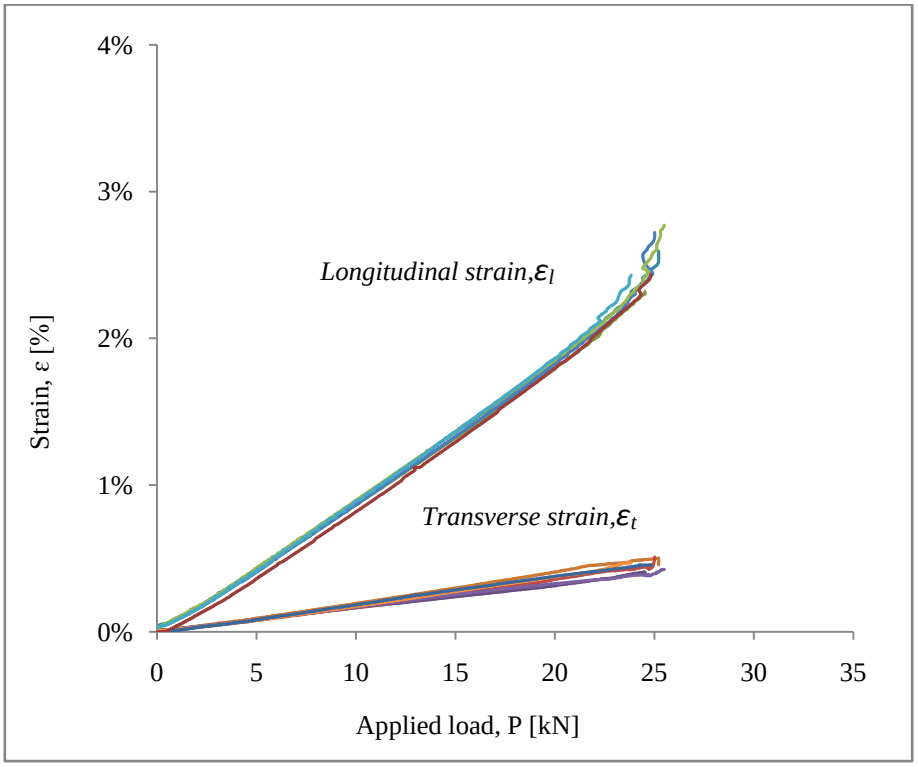

Figure 6-6-b Tensile strain-force curves of specimens type C $[(0°/90°/\pm45°/0°/90°)]_S$. The longitudinal strains are with steeper slopes and the transverse strains are with more gentle slopes.

6.4 Compression Test Results

Twelve specimens were static compression tested, six from type D and six from type E. All tests were with no errors except one and all the acceptable specimens failed according to expectations. Specimen D-06 did not give acceptable results, as can be seen in Appendix D. The specimen D-06 was not included in the reported results in this section. The basic results for the compression tests can be found in Appendix D.

6.4.1 General Behavior and Mode Failure of Specimens D and E

The failure modes in the compression testes were quite different between specimens of type D and specimens of type E. In the compression test for specimens of type D a fiber kinking in the longitudinal fibers occurred which can be described as kink bands. From the kink bands a transverse shear failure in the specimens occurred. A kink band in the specimen can be seen in the red circle in figure 6.8. All transverse shear failures happened at the grip at the top or at the bottom. According to typical failure modes in ASTM D3410 (see Appendix E) the specimens failed in TAT or TAB modes (Transverse shear At grip/tab Top or Bottom).

In the compression test for specimens of type E in-plane shear in the fiber orientation occurred, which was 45°. The in-plane shear can be described as zigzag shear, as can be seen in the red circle in figure 6-9. All in-plane shear failures happened at the middle of the gage. According to typical failure modes in ASTM D3410 (see Appendix E) the specimens failed in MGM modes (Multi-mode Gage Middle).

Figures 6-7 to 6-10 show the broken specimens after the static compression test, and graphically how they failed. The figures show the specimens from the front and side views.

Figure 6-7 Broken specimens, type D $[(0°/90°)_3]_S$, after the compression tests, front view.

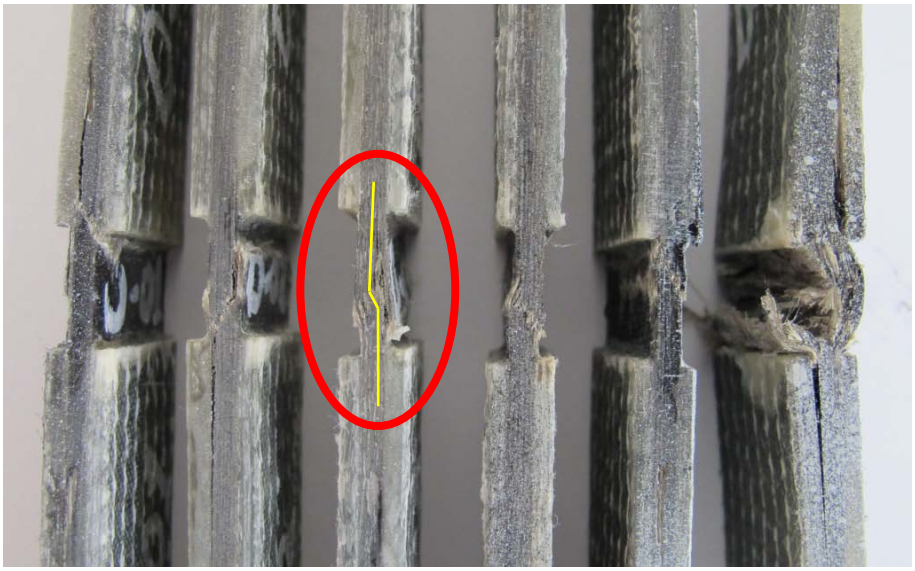

Figure 6-8 Broken specimens, type D $[(0°/90°)_3]_S$, after the compression tests, side view. Within the red circle is a schematic of kink-band geometry.

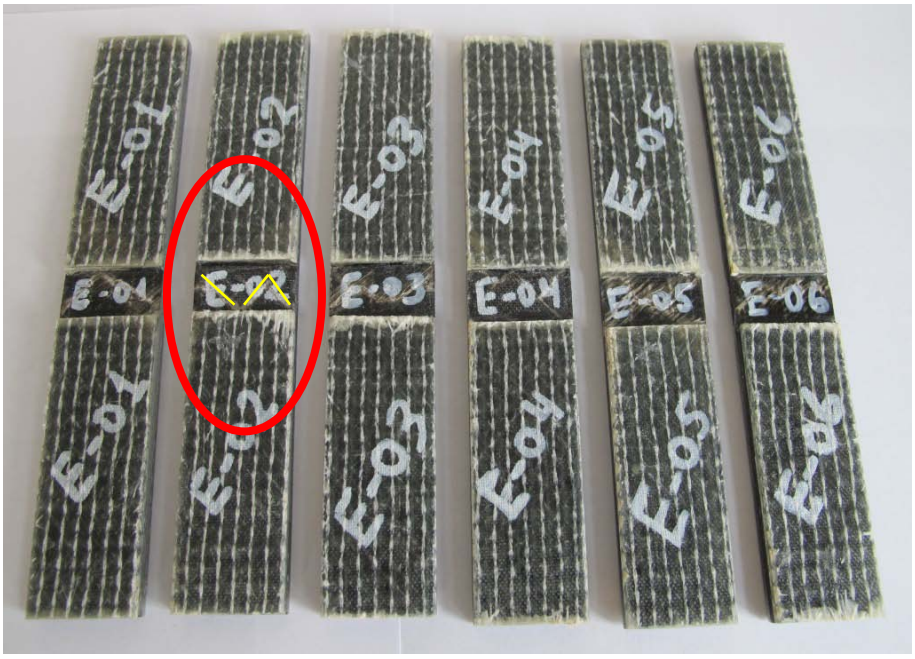

Figure 6-9 Broken specimens, type E $[(\pm 45°)_3]_S$, after the compression tests, front view. Within the red circle is a schematic of in-plane shear failure geometry.

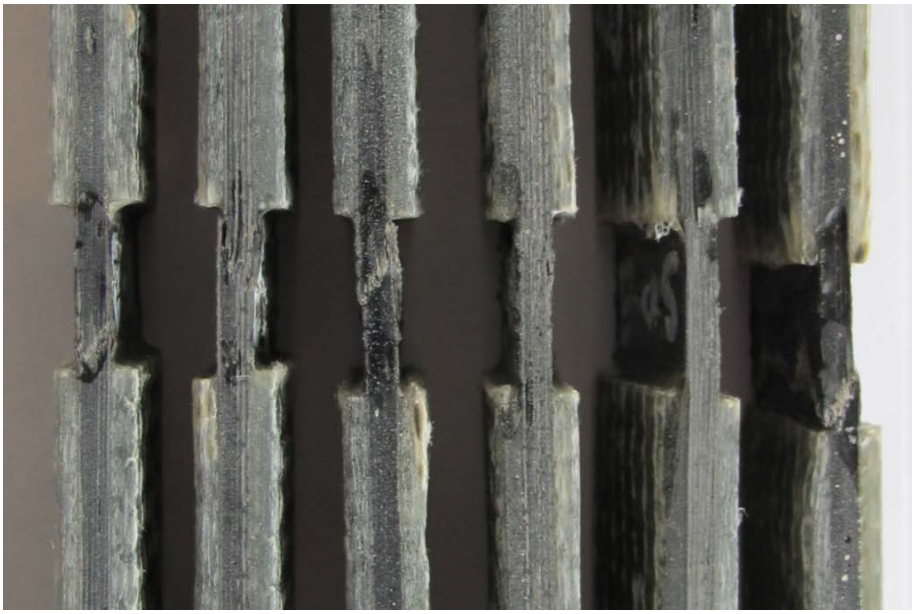

Figure 6-10 Broken specimens, type E $[(\pm 45°)_3]_S$, after the compression tests, side view.

6.4.2 Test Results of Specimens D and E

The calculation procedures for the results in compression tests were exactly the same as the results for the tensile tests. All information about the calculation procedures for the compression tests can be found in section 6.3.2. The results for the specimen D-05 were based on figures 6-11 and 6-12. The gage length for the all specimens in types D and E measured: $l_g = 13.2 \pm 0.15\ mm$.

Table 6-5 Compression testing results of specimens type D $[(0°/90°)_3]_S$.

Specimens Type D	Maximum load bef. failure P^{max} [kN]	Ultimate compressive strength F^{tu} [MPa]	Deformation at break max_disp. [mm]	Ultimate compressive strain ε^{max} [%]	Poisson's ratio ν -	Compression Young's modulus E-modul [GPa]
D-01	14.34	212.6	1.71	-	-	-
D-02	13.89	201.0	1.97	-	-	-
D-03	16.41	236.5	1.85	-	-	-
D-04	11.74	168.3	1.50	-	-	-
D-05	12.56	181.0	1.56	0.47	0.187	38.70
D-06	error	error	error	error	error	error
Avg.	13.79	199.9	1.72	-	-	-
St.Dev.	1.80	26.7	0.20	-	-	-
c.v. (%)	13.03	13.4	11.42	-	-	-

Table 6-6 Compression testing results of specimens type E $[(\pm 45°)_3]_S$.

Specimens Type E	Maximum load bef. failure P^{max} [kN]	Ultimate compressive strength F^{tu} [MPa]	Deformation at break max_disp. [mm]	Ultimate compressive strain ε^{max} [%]	Poisson's ratio ν -	Compression Young's modulus E-modul [GPa]
E-01	6.16	89.1	1.14	-	-	-
E-02	6.47	92.9	1.32	-	-	-
E-03	6.60	94.8	1.34	-	-	-
E-04	6.16	88.8	1.02	-	-	-
E-05	6.10	87.9	1.19	-	-	-
E-06	6.94	99.6	1.49	-	-	-
Avg.	6.41	92.2	1.25	-	-	-
St.Dev.	0.33	4.5	0.17	-	-	-
c.v. (%)	5.11	4.9	13.50	-	-	-

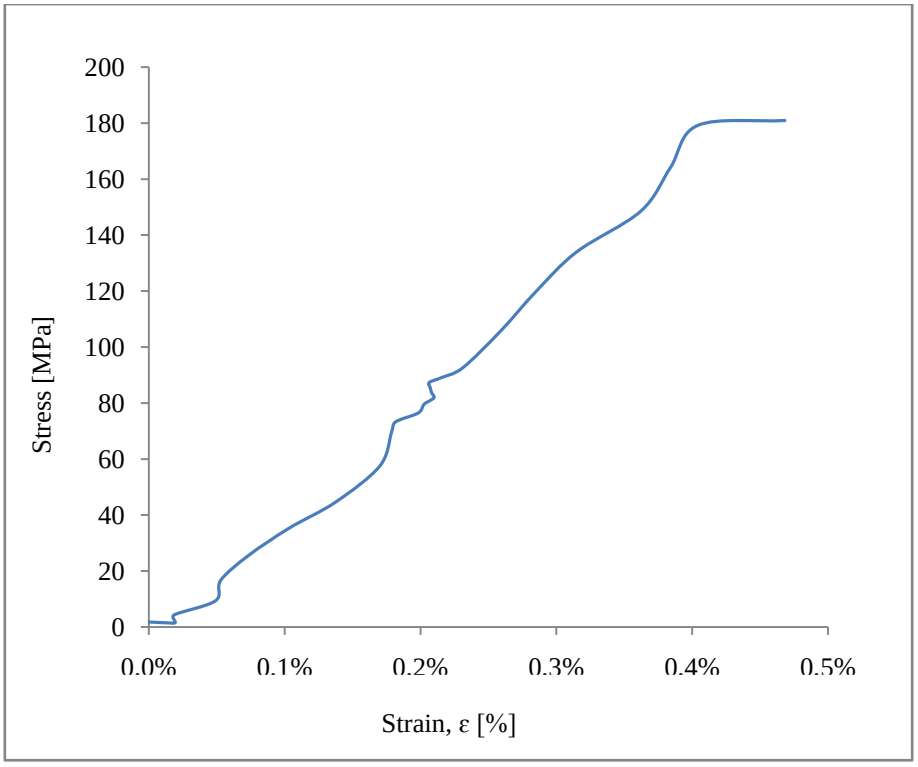

Figure 6-11 Compression stress-strain curve of specimen D-05 $[(0°/90°)_3]_S$.

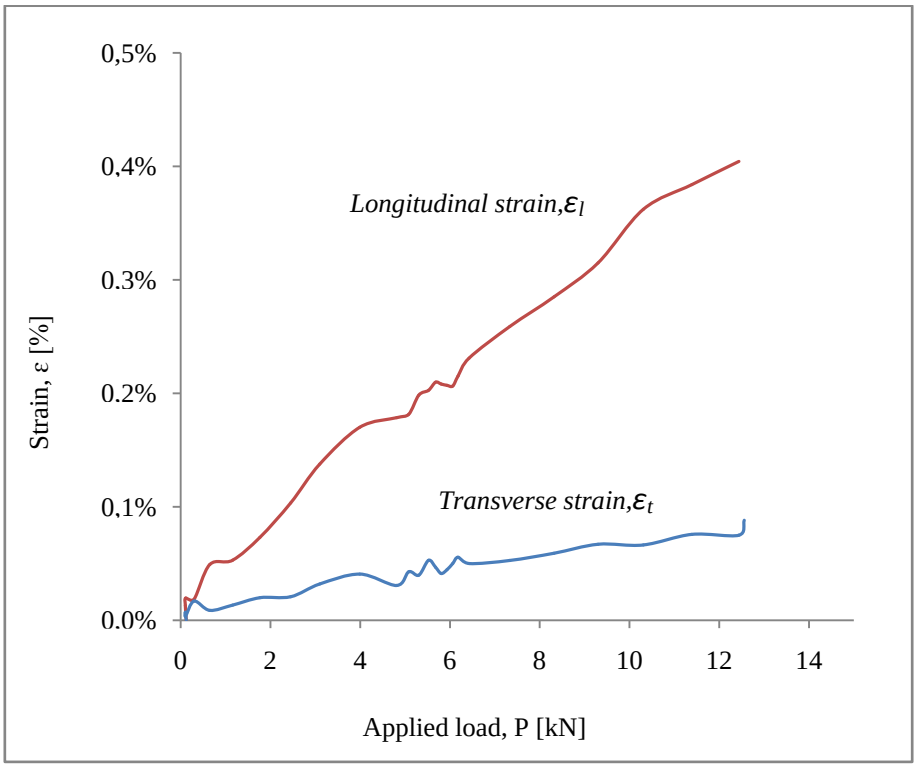

Figure 6-12 Compression strain-force curve of specimen D-05 $[(0°/90°)_3]_S$. The longitudinal strains are with steeper slopes and the transverse strains are with more gentle slopes.

6.5 In-Plane Shear Test ± 45° Results

Six specimens at type B were in-plane shear tested. All tests were with no errors and the specimens failed according to expectations. The basic results for the in-plane shear test can be found in Appendix D.

6.5.1 General Behavior and Mode Failure of Specimens B

All specimens in type B had the same failure mode. In the tests in-plane shear occurred parallel to the fiber orientation all around the gages. The shear failure in the specimens did not happen in certain places in the gages, as shown in figure 6-13. Figures 6-13 and 6-14 show graphically the broken specimens after the in-plane shear test and how the specimens failed. The figures show the specimens from the front and side views.

Figure 6-13 Broken specimens, type B $[(\pm 45°)_3]_S$, after the in-plane shear tests, front view.

Figure 6-14 Broken specimens, type B $[(\pm 45°)_3]_S$, after the in-plane shear tests, side view.

6.5.2 Test Results of Specimens B

All calculations were based on measured values from the in-plane shear tests. The applied load (P_i) was presented in Newton (N). The shear stress (τ_{12i}) was calculated by using the equation (6-3) and the shear strain (γ_{12i}) was calculated by using the equation (6-4). The longitudinal normal strain (ε_{xi}) and lateral normal strain (ε_{xi}) were obtained from the measured strain.

$$\tau_{12i} = \frac{P_i}{2A} \tag{6.3}$$

$$\gamma_{12i} = \varepsilon_{xi} - \varepsilon_{yi} \tag{6.4}$$

where: τ_{12i} = shear stress at *i*-th data point

P_i = load at *i*-th data point

A = cross-sectional area

γ_{12i} = shear strain at *i*-th data point

ε_{xi} = longitudinal normal strain at *i*-th data point

ε_{yi} = lateral normal strain at *i*-th data point

The shear stress-strain curves were performed as stress (τ_{12i}) versus strain (γ_{12i}) as illustrated in figure 6-15.The chord shear modulus of elasticity was calculated using strain reference points between 0.15% and 0.55%, which is according to ASTM D3518.

All the results for the specimens in type B in table 6-7 were based on figure 6-15.

Table 6-7 In-plane shear testing results of specimens type B $[(\pm 45°)_3]_S$.

Specimens Type B	Maximum load at or below 5% shear strain P^{max} [kN]	Maximum in-plane shear stress τ_{12}^{max} [MPa]	Maximum shear strain with τ_{12}^{max} γ_{12}^{max} [%]	Shear chord modulus of Elasticity G-modul [GPa]
B-01	5.18	37.5	3.41	2.42
B-02	5.36	38.7	2.45	3.17
B-03	5.03	36.8	1.47	2.93
B-04	5.04	36.7	2.52	2.36
B-05	5.06	36.4	2.46	2.85
B-06	5.27	38.0	2.51	2.76
Avg.	5.16	37.4	2.47	2.75
St.Dev.	0.13	0.9	0.62	0.31
c.v. (%)	2.6	2.4	24.9	11.3

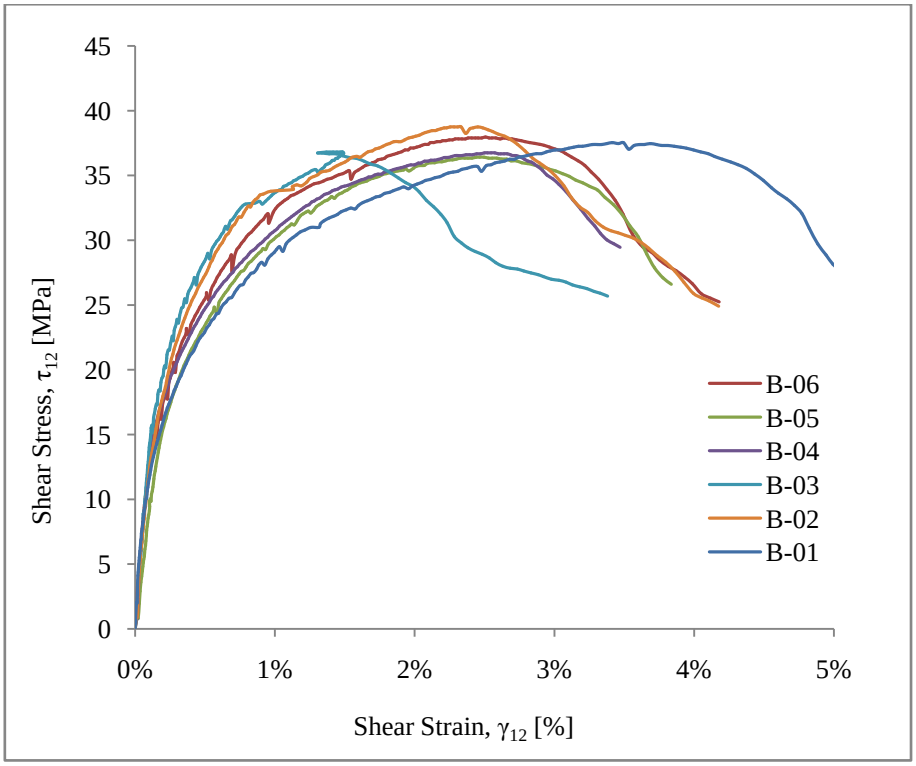

Figure 6-15 Shear stress-strain curves of specimens type B $[(\pm 45°)_3]_S$.

6.6 Pin Bearing Strength Test

Eighteen specimens were pin bearing strength tested, six from type G, six from type H and six from type I. All tests were with no errors and the specimens failed according to expectations. The basic results for the pin bearing test can be found in Appendix D.

6.6.1 General Behavior and Mode Failure of Specimens G, H and I

Types G, H and I had all the same failure mode with different damage mechanisms in the laminate when the pin bearing tests were performed. In the tests a shear-out failure occurred where the material in front of the pin was pushed out of the laminates.

The most damaged mechanisms in the laminate was in type G where the 90° fibers tended to separate from the polyester and pushed out without breaks. Figure 6-16 shows how the 90° continuous basalt fiber pushed out with effects of delamination.

Type H had the least damaged mechanisms in the laminate because there were no 90° fibers to make the delamination effects. There were only ±45° fibers which broke in front of the pin and pushed out of the laminates, as can be seen in figure 6-17.

Finally the damage in type I was somewhere between the damage in type G and in type H because the fiber orientations were a mix of 90° and ±45° in the laminates. Figure 6-18 shows the type I damage in the pin bearing test. Figures 6-19 and 6-20 show the differences between the damage mechanisms and how the fiber orientation can have a major impact on the delamination effects in types G, H and I.

According to common failure modes in ASTM D5961 (see Appendix E) the specimens failed in S1I modes (Shearout First Hole Inapplicable).

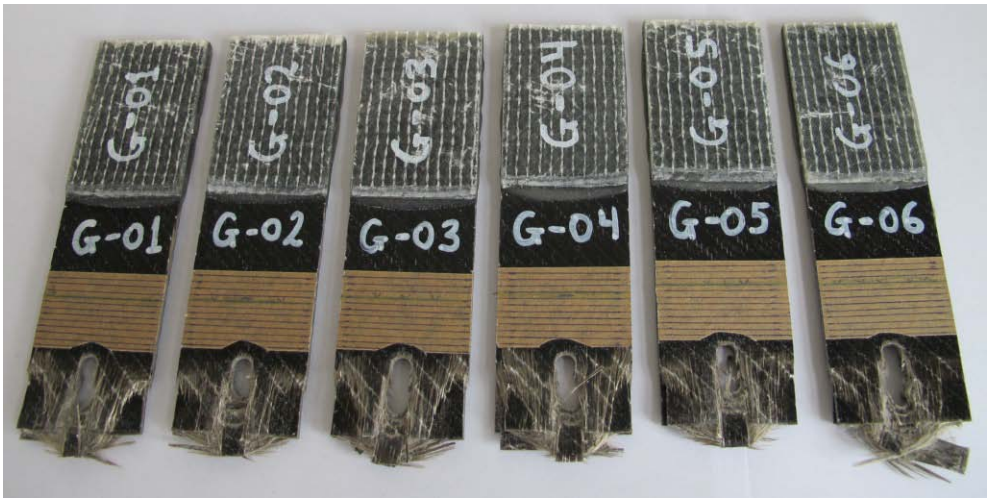

Figure 6-16 The damage mechanisms in the laminates, type G $[(0°/90°)_3]_S$, after the pin bearing strength tests, front view.

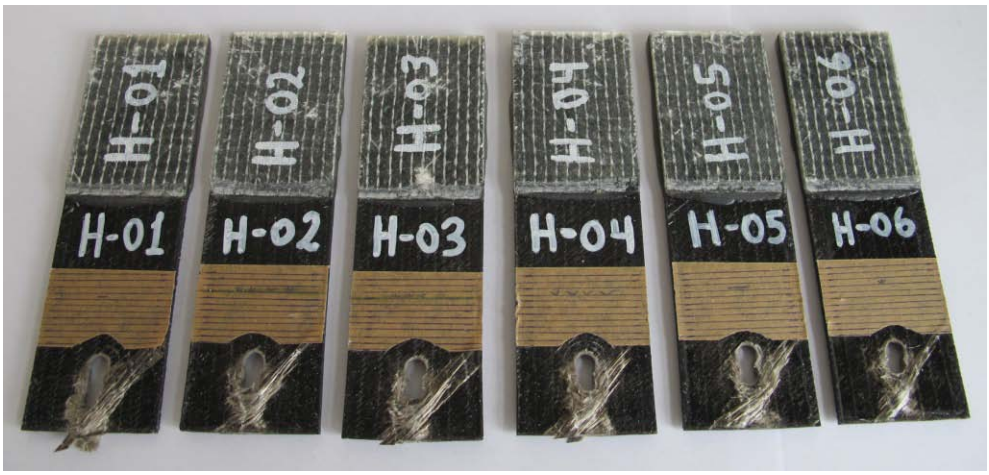

Figure 6-17 The damage mechanisms in the laminates, type H $[(\pm45°)_3]_S$, after the pin bearing strength tests, front view.

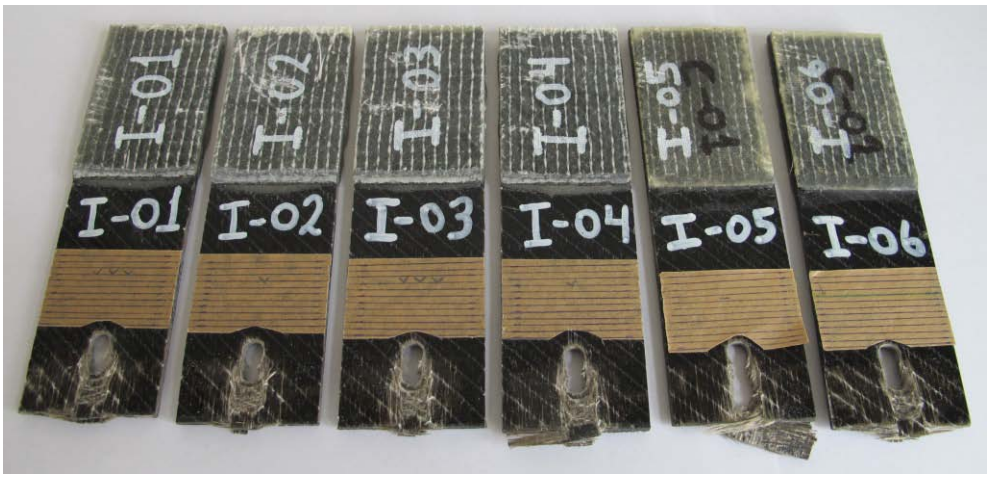

Figure 6-18 The damage mechanisms in the laminates, type I $[(0°/90°/\pm45°/0°/90°)]_S$, after the pin bearing strength tests, front view.

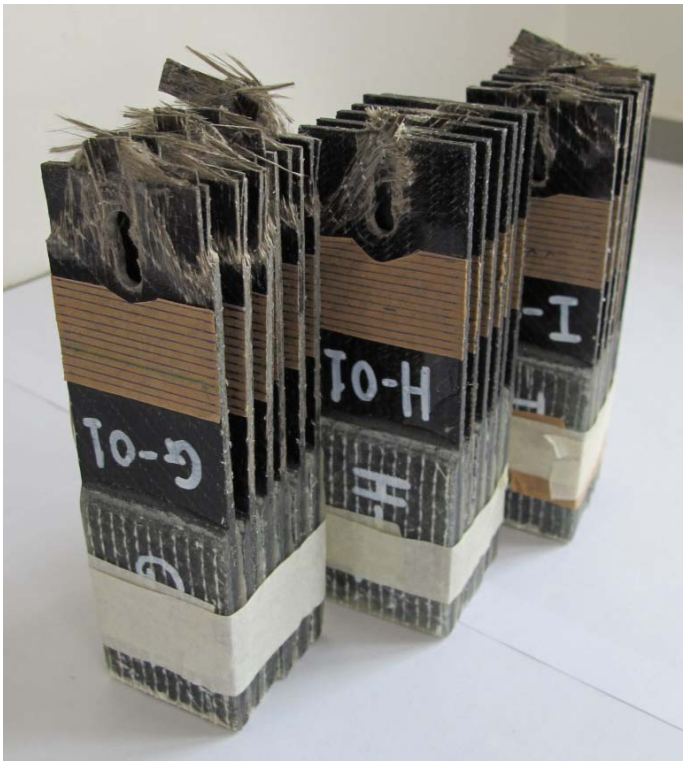

Figure 6-19 Three different damage mechanisms in the laminates, types G, H and I, after the pin bearing strength tests, side view.

Figure 6-20 Three different damage mechanisms in the laminates, types G, H and I, after the pin bearing strength tests, top view.

6.6.2 Test Results of Specimens G, H and I

All calculations were based on measured values from the pin bearing strength tests. The applied load (P_i) was presented in Newton (N). The pin bearing stress (σ_i^{br}) was calculated by using the equation (6-5) and the pin bearing strain (ε_i^{br}) was calculated by using the equation (6-6). The bolt hole elongations (δ_i) were obtained from the measured hole deformation.

$$\sigma_i^{br} = \frac{P_i}{Dh} \tag{6.5}$$

$$\varepsilon_i^{br} = \frac{\delta_i}{D} \tag{6.6}$$

where: σ_i^{br} = bearing stress at *i*-th data point

P_i = load at *i*-th data point

D = specimen hole diameter

h = specimen thickness

ε_i^{br} = bearing strain at *i*-th data point

δ_i = hole elongation at *i*-th data point

The bearing stress-strain curves were performed as stress (σ_i^{br}) versus strain (ε_i^{br}), as illustrated in figure 6-21 to 6-23. The stress-strain behavior of the different laminates (types G, H and I) was similar until the bearing strain reached 10%, where the first damage occurred in the first specimens. Tables 6-8 to 6-10 report the first damage mechanisms in the laminate and are denoted as yield bearing strength (F^{bry}) and strain (ε^{bry}).

The width to diameter ratio for all the eighteen specimens was: $w/D = 6.8$

The diameter to thickness ratio for all the eighteen specimens was: $D/h = 2.2$

The edge distance ratio for all the eighteen specimens was: $e/D = 3.3$

where: w = specimen width

e = distance, parallel to load, from hole center to end of specimen.

All the results for the specimens in type G in table 6-8 were based on figure 6-21. In the same way the results for the specimens in type H in table 6-9 were based on figure 6-22 and the specimens in type I in table 6-10 were based on figure 6-23.

Table 6-8 Pin bearing testing results of specimens type G $[(0°/90°)_3]_S$.

Specimens Type G	Maximum load prior to failure P^{max} [kN]	Ultimate bearing strength F^{bru} [MPa]	Ultimate bearing strain ε^{bru} [%]	Yield bearing strength $F^{bry}*$ [MPa]	Yield bearing strain $\varepsilon^{bry}*$ [%]
G-01	7.32	466.3	170.73	208.2	10.71
G-02	6.20	396.5	158.98	280.5	22.55
G-03	7.48	472.9	156.15	243.3	7.28
G-04	6.45	400.8	127.13	233.0	8.05
G-05	5.64	353.0	139.14	229.6	26.12
G-06	5.70	354.8	126.18	226.5	19.41
Avg.	6.46	407.4	146.38	236.9	15.69
St.Dev.	0.79	52.3	18.32	24.2	8.05
c.v. (%)	12.2	12.8	12.5	10.2	51.3

*First damage mechanism in the laminate

Table 6-9 Pin bearing testing results of specimens type H $[(\pm 45°)_3]_S$.

Specimens Type H	Maximum load prior to failure P^{max} [kN]	Ultimate bearing strength F^{bru} [MPa]	Ultimate bearing strain ε^{bru} [%]	Yield bearing strength $F^{bry}*$ [MPa]	Yield bearing strain $\varepsilon^{bry}*$ [%]
H-01	5.19	319.5	29.95	319.5	29.95
H-02	5.20	321.3	57.45	318.8	19.21
H-03	4.96	310.6	27.61	310.6	27.61
H-04	4.57	282.6	60.70	272.3	15.62
H-05	5.12	319.9	71.05	315.7	30.32
H-06	4.62	293.0	59.54	273.8	22.66
Avg.	4.94	307.8	51.05	301.8	24.23
St.Dev.	0.28	16.3	17.89	22.5	6.05
c.v. (%)	5.7	5.3	35.1	7.5	25.0

*First damage mechanism in the laminate

Table 6-10 Pin bearing testing results of specimens type I $[(0°/90°/\pm45°/0°/90°)]_S$.

Specimens Type I	Maximum load prior to failure P^{max} [kN]	Ultimate bearing strength F^{bru} [MPa]	Ultimate bearing strain ε^{bru} [%]	Yield bearing strength F^{bry*} [MPa]	Yield bearing strain ε^{bry*} [%]
I-01	5.37	338.2	53.70	291.2	21.67
I-02	4.88	307.9	52.39	301.1	16.00
I-03	4.95	310.0	48.39	274.4	24.48
I-04	5.15	325.2	69.37	279.3	15.45
I-05	5.02	308.4	64.35	266.8	18.31
I-06	5.29	321.0	53.26	283.5	19.67
Avg.	5.11	318.5	56.91	282.7	19.26
St.Dev.	0.19	12.0	8.09	12.2	3.44
c.v. (%)	3.8	3.8	14.2	4.3	17.9

*First damage mechanism in the laminate

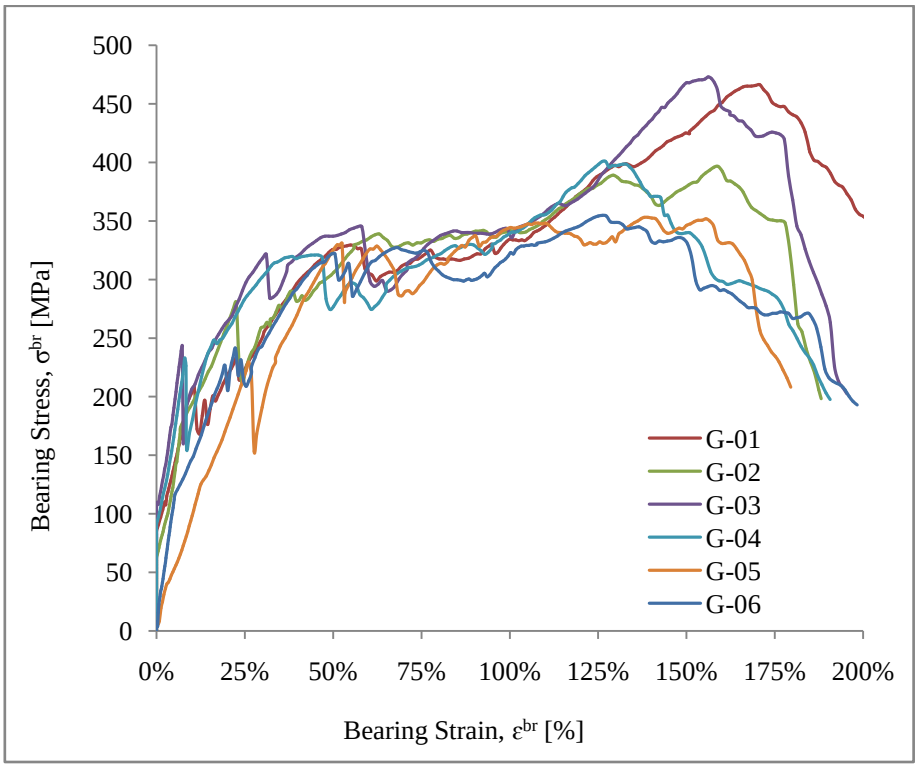

Figure 6-21 Bearing stress-strain curves of specimens type G $[(0°/90°)_3]_S$.

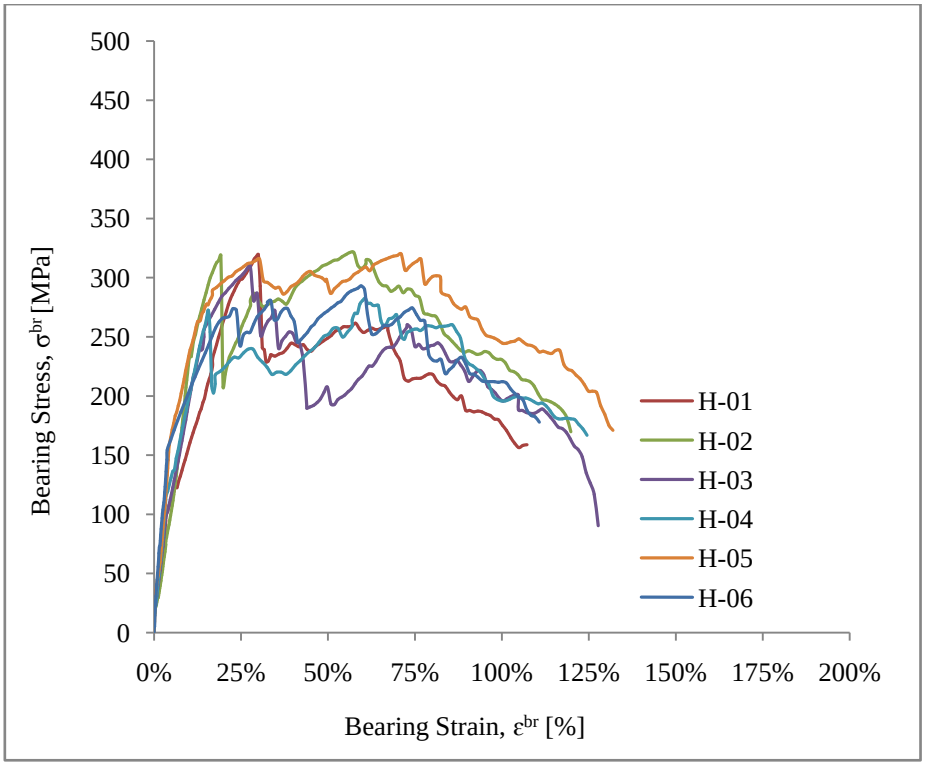

Figure 6-22 Bearing stress-strain curves of specimens type H $[(\pm 45°)_3]_S$.

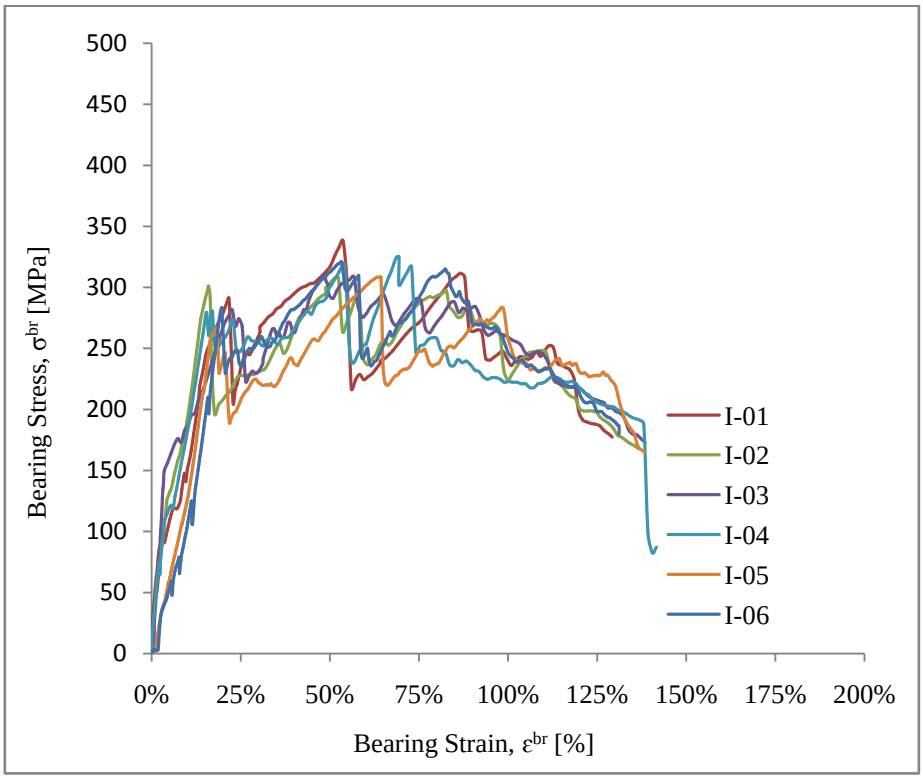

Figure 6-23 Bearing stress-strain curves of specimens type I $[(0°/90°/\pm 45°/0°/90°)]_S$.

6.7 Tube Test Results

Two Tubes were tested, one was environmental tested and the other was load tested. The basic results for the load test can be found in Appendix D.

6.7.1 Weathering Test Results of Tube no.1

The tube was meant to be in the environmental testing for several years. When this thesis was submitted, August 10, 2012, the tube was in perfect order. Another conclusion would be unacceptable because it can take years to get any visible results. The results of this part of the experiment will then be published later on.

6.7.2 Load Test Results of Tube no.2

The graph in figure 6-24 shows the force acting on the tube as a function of displacement. The graph shows four cycle loads, back and forth, without stopping between rounds. The force which was acting on the tube was given in Newton kilos [kN] and displacement in millimeters [mm].

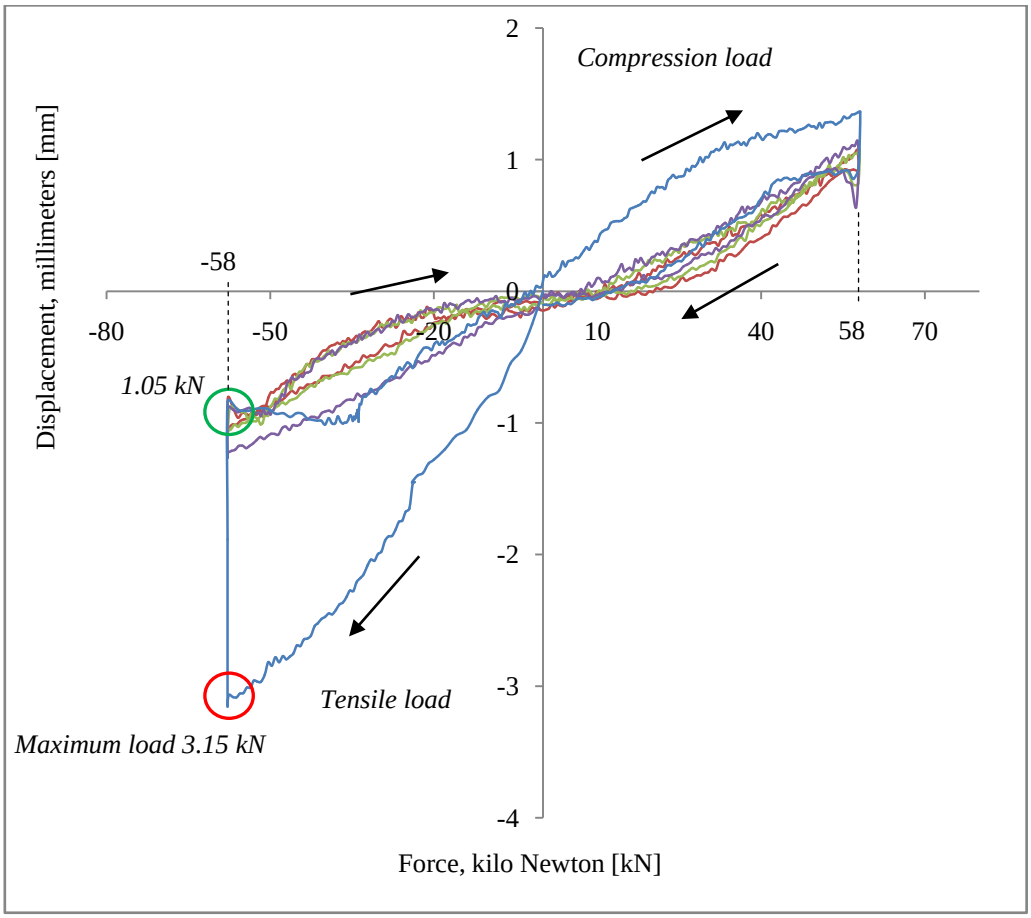

Figure 6-24 The graph from the load test of the tube, four rounds of a swing load. The UTM transferred data to a computer which drew a graph showing load versus displacement.

The graph in figure 6-24 shows that the greatest force acting on the tube was 3.15 kN (shown in the red circle) when the tube moved about 58 mm at the top to the left in the first cycle. Following this high force on the tube, the force fell down suddenly to 1.05 kN (shown in the green circle in figure 6-24). This force was the greatest force which occurred in the load test. Closer inspection of the tube after the load test showed that the glue in the iron pipe (fastener) between the tube and the UTM failed. When the glue failed, the moment was reduced and the tube began to rotate slightly in the fastener.

6.8 Summary

- The composite density, the weight and volume ratio for the basalt fiber and the polyester resin were reported.
- The results of the tensile tests were reported (specimens types A and C).
- The results of the compression tests were reported (specimens types D and E).
- The results of the in-plane shear tests were reported (specimens type B).
- The results of the pin bearing tests were reported (specimens type G, H and I).
- The result of the tube in the load test was reported.

Discussion

7.1 General

This section presents a general discussion of the results and their interpretation.

7.2 Conclusion of Research

7.2.1 Constituent Content Determination Conclusion

The ratio between the fiber and resin has a major impact on strength and stiffness in a composite material (Yuhazri, M. & Sihombing, H., n.d.). The most important factor in the ratio between the fiber and resin is the volume fraction of reinforcing fibers. As pointed out in section 2.3.1, the volume fraction of reinforcing fibers is used to calculate the composite properties. Manufacturing processes such as Vacuum Infusion generally give a higher volume fraction of reinforcing fibers than the Hand Lay-up process using composite materials (Tsai, S.W., 1979, p. 251). The fiber volume fraction for Vacuum Infusion is generally 50% or higher and for Hand Lay-up it is normally less than 50%.

The forty-eight specimens, which were cut out of the two thin plates and made by the Vacuum Infusion process, had 50.68 ± 0.45% a basalt fiber volume which is an acceptable value. The tubes were made with the Hand Lay-up process and the basalt fiber volume fraction was about 38%, which is also an acceptable value.

7.2.2 Tensile Test Conclusion of Specimens A and C

In the tensile test delamination occurred in all specimens where the basalt fibers tended to separate from the polyester resin. Because of that, the adhesion between the polyester resin and basalt fiber was the weakest factor in the composite material. A resin with good adhesion with fiber can give more strength and stiffness in the laminate; for example an epoxy resin gives better composite strength and stiffness than a vinylester resin (Colombo et al., 2012). With this in mind, the resin can reduce the strength and stiffness in a composite material.

The ultimate tensile strength for type A became 19.6% stronger than type C. The tensile Young's modulus became 25.8% higher in type A than in type C. This conclusion should fit the theory (see section 2.3) because type A had more layers with fiber orientation in a 0° direction. The ultimate tensile strain was around 2.8% for both type A and type C. That is a little bit lower than ultimate tensile strain in dry

continuous basalt fibers, which is 3.2% (Bruijn, M., 2007). The Poisson's ratio was much lower in type A than in type C. In type A there were more layers with a fiber orientation of 90° than in type C. The fiber orientation in the 90° direction pressed against the strain formation in the transverse direction and that may explain the differences between the Poisson's ratios.

7.2.3 Compression Test Conclusion of Specimens D and E

The matrix properties can mainly determine the material response in a compression test (Colombo et al., 2012). When type D failed in the compression tests, the polyester resin crushed and because of that a kinking in the basalt fiber occurred. In type E in-plane shear in the fiber orientation occurred and that happened because of the shear cracking in the polyester resin and adhesion between the fibers and the resin. In both types, D and E, the polyester resin was the weakest factor in the composite material. To get good mechanical properties of a composite material in a compression test, the resin has to be strong and have good adhesion with the fiber.

The ultimate compressive strength for type D became 116.8% stronger than type E. This conclusion indicates that the fiber orientation can have a big influence on strength in a compression test, as happens in a tensile test.

7.2.3 In-Plane Shear Test ± 45° Conclusion of Specimens B

In all specimens (type B) in-plane shear occurs in the fiber orientation and that happened because of the shear cracking in the polyester resin. It also happened because of the adhesion between the fibers and the resin. To get good mechanical properties of a composite material in an in-plane shear test, the resin must have good shear strength and good adhesion with the fiber.

The maximum in-plane shear stress was 37.5 MPa and at the same time the strain was 2.47%. According to the manufacturer Reichhold (Appendix B), the tensile elongation in polyester resin is 2.1%. The maximum in-plane shear stress should be around the strain 2.1% on the shear stress-strain curves.

7.2.3 Pin Bearing Strength Test Conclusion of Specimens G, H and I

All the specimens in the pin bearing test had the same failure mode with different damage mechanisms in the laminate. The mode is called shear-out failure where the material in front of the pin is pushed out of the laminates. The diameter to thickness ratio *D/h* was acceptable because the bearing pin did not fail in the test. The width to diameter ratio *w/D* was also acceptable because the tension failure mode (see Appendix E) did not occur in the specimens. The edge distance ratio *e/D* was not

acceptable because the shear-out failure occurred in all the specimens in the pin bearing test. To avoid the shear-out failure the edge distance *e* must be larger than it was. If the adhesion between the fibers and the resin in types G and I were stronger the edge distance *e* could be unchanged. If the *e/D* and *w/D* ratios were sufficiently large, the result would be the bearing failure mode (Annex E), as was expected in this research. The first damage mechanisms in the laminate, in all specimens, were close to 20% yield bearing strain. The yield bearing strength at the same point was similar for types H and type I or close to 290 MPa. But type G was little bit lower or 237 MPa. The ultimate bearing strength for type G became 32.4% stronger than in type H and type I.

7.3 Calculated According to CLT and the Failure theories

The specimen type C was calculated using Classical Laminate Theory (CLT) and the Failure Theories to estimate when the first layer failed in the laminate. All calculation methods for these theories can be found in section 2.3. The MATLAB code, based on the theories, was used in all calculations and the code can be found in Appendix F. A part of the MATLAB code was taken from the thesis "*DETERMINATION OF RESIDUAL STRESS AND THERMAL BEHAVIOR FOR COMPOSITE LAMINATES*" (Schulz, W.A., 2005) and adjusted to this study. The other part of the MATLAB code was written by the author of this thesis.

The lamination sequences were $[(0°/90°/\pm45°/0°/90°)]_S$ and the thickness of each layer was 0.225 mm. All material properties for the basalt fiber and polyester resin were obtained from tables 3-1 and 3-2. The ultimate strength for one layer was estimated from the experimental results in chapter 6. All 90° layers (layers no. 2, 6, 7 and 11) failed at the same time when the applied load was around 9.0 kN in the x direction. The 9.0 kN would be the ultimate tensile strength in the laminate for the x direction. Table 7-1 shows the failure values from maximum stress, maximum strain, Tsai Hill and Tsai Wu for the critical layers.

Table 7-1 The results from the failure theories, greater than one means failed.

Failure	Number of layers in the laminate							
Theory	2	3	4	6	7	9	10	11
Maximum stress	0.976	0.655	0.655	0.976	0.976	0.655	0.655	0.976
Maximum strain	1.008	0.655	0.655	1.008	1.008	0.655	0.655	1.008
Tsai Hill	0.994	0.680	0.680	0.994	0.994	0.680	0.680	0.994
Tsai Wu	1.064	0.596	0.596	1.064	1.064	0.596	0.596	1.064

Figures 7-1 to 7-9 illustrate the stress and strain in all layers in the global and local coordinate system. The y-axis describes the layers and the x-axis describes either the stress or strain in the layers.

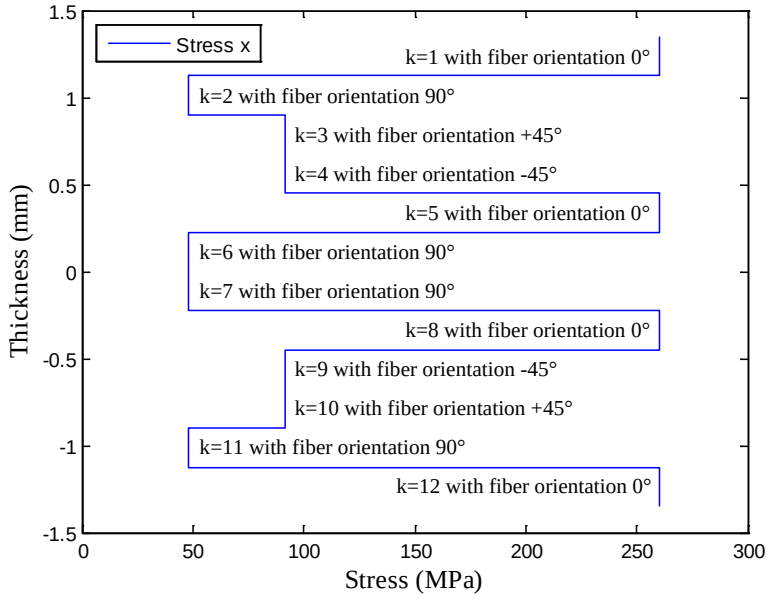

Figure 7-1 The stress in each layer in the global coordinated system in the x direction.

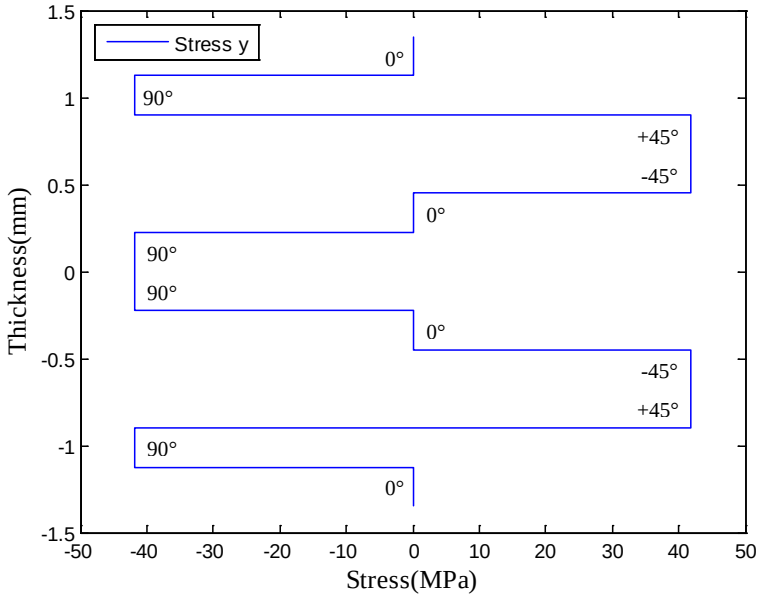

Figure 7-2 The stress in each layer in the global coordinated system in the y direction.

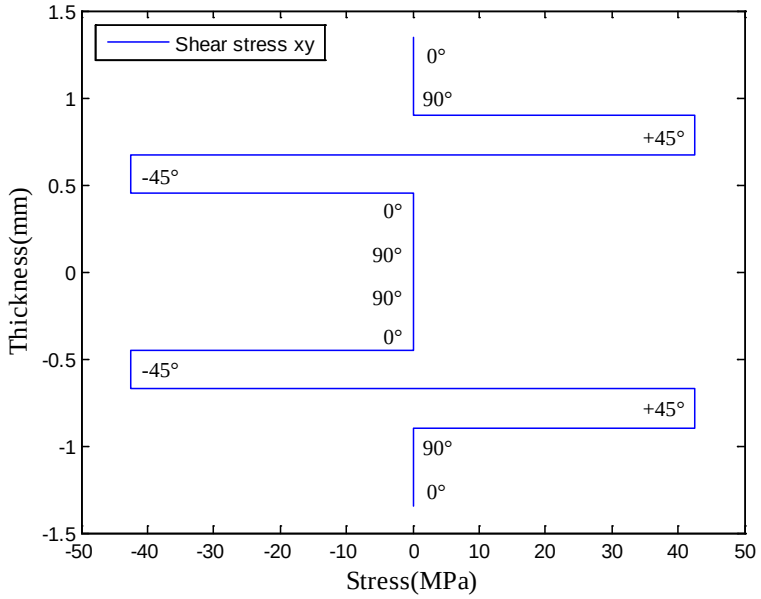

Figure 7-3 The shear stress in each layer in the global coordinated system in the x-y plane.

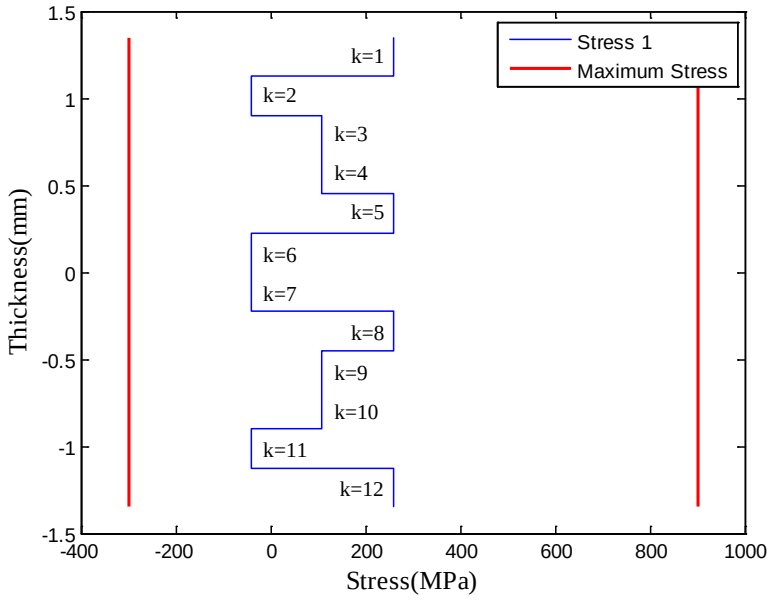

Figure 7-4 The stress in each layer in the local coordinated system in 1 direction (longitudinal) is described by the blue line. The maximum stresses in 1 direction are the red lines. Here there is no failure crisis in any layers.

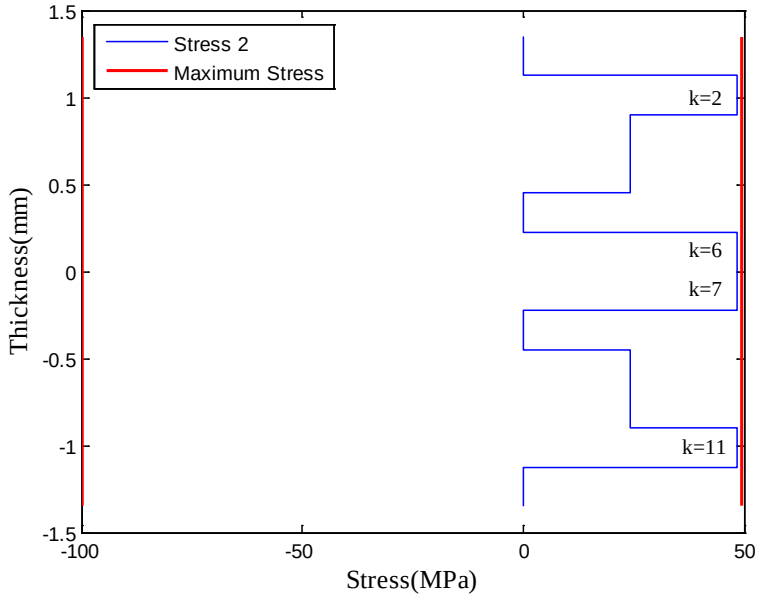

Figure 7-5 The stress in each layer in the local coordinated system in 2 direction (transverse) is described by the blue line. The maximum stresses in 2 direction are the red lines. The layers 2, 6, 7 and 11 are about to fail according to the maximum stress failure theory.

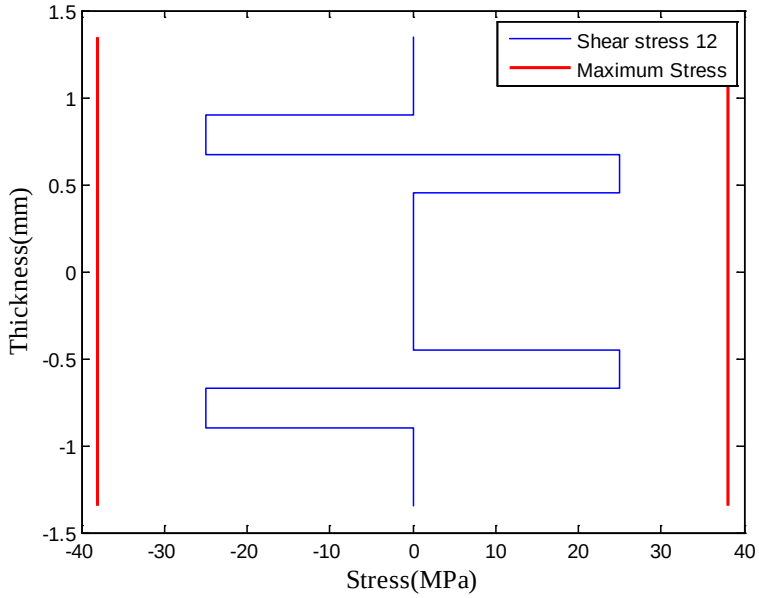

Figure 7-6 The shear stress in each layer in the local coordinated system in 1-2 plane is described by the blue line. The maximum shear stress in 1-2 plane are the red lines. Here there is no failure crisis.

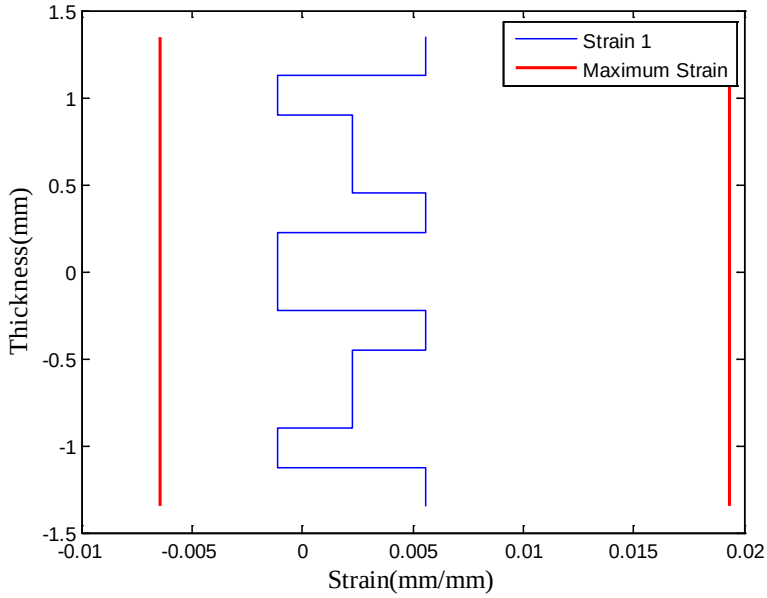

Figure 7-7 The strain in each layer in the local coordinated system in 1 direction (longitudinal) is described by the blue line. The maximum strains in 1 direction are the red lines. Here there is no failure crisis in any layers.

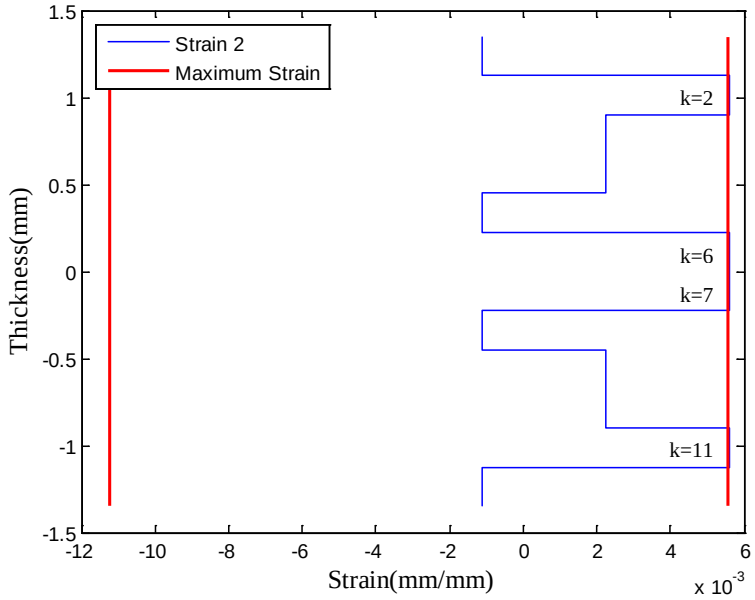

Figure 7-8 The strain in each layer in the local coordinated system in 2 direction (transverse) is described by the blue line. The maximum strains in 2 direction are the red lines. The layers 2, 6, 7 and 11 have failed according to the maximum strain failure theory.

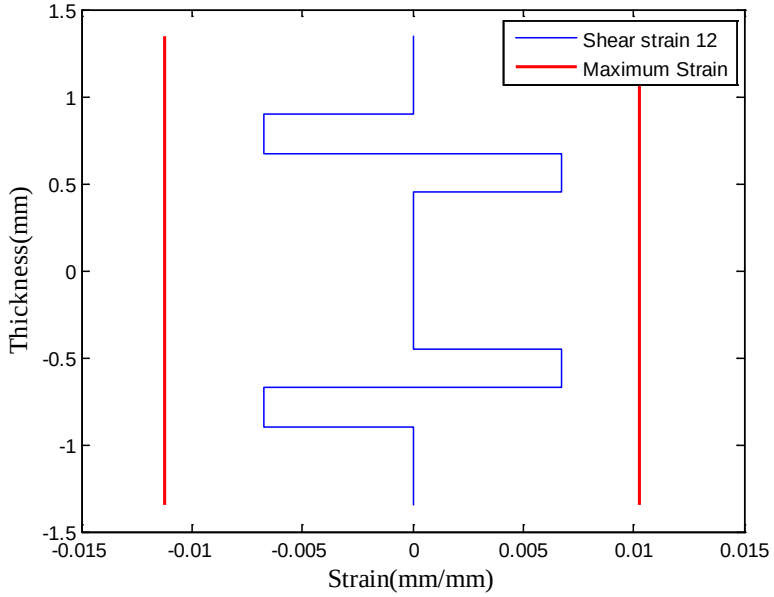

Figure 7-9 The shear strain in each layer in the local coordinated system in 1-2 plane is described by the blue line. The maximum shear strains in 1-2 plane are the red lines. Here there is no failure crisis in any layers.

7.4 Comparison with Other Composite materials

One way to estimate a quality of materials properties is to make comparisons with other materials. The biaxial stitched basalt fabric BAS BI 600, in polyester resin, was compared with other types of weave fabrics in epoxy resin. The composite properties for the stitched basalt fabric were obtained from types A, D and B in the experiment results.

The first two fabrics, which were compared to the stitched basalt fabric, were made of continuous basalt fiber. The composite properties were obtained from a report from Iran (Talebi Mazraehshahi & Zamani, 2010).The third fabric was made of continuous E-glass fiber by Hexcel (ASTM International, 2002, pp. 428–437). The last fabric was made of continuous carbon filaments made from PAM precursor (ASTM International, 2002, pp. 276–285). The composite properties for the fabrics, E-glass (E7781/EA9396) and carbon (T300 3k/EA9396), were obtained from *The Composite Materials Handbook-MIL17* (ASTM International, 2002).

The tensile test method ASTM D3039 and the in-plane shear test method ASTM D3518 were used to find the composite properties in tensile and shear for all fabrics. The compression tests methods ASTM D3410 and DIN EN 2850 were used to find the composite properties in compression for all fabrics.

The comparison of composite properties of these different fabrics can be found in table 7-2. The results in table 7-2 show that the composite density of basalt and E-glass fabrics were similar, but 24.3% higher than the carbon fabric. The sum of ultimate tensile strength of both directions (longitudinal and transverse direction) was similar for all basalt fabrics. The stitched basalt fabric (which was examined in this project) became 19.3% stronger than the E-glass fabric, but was 27.1% weaker than carbon fabric. The ultimate tensile strain in the stitched basalt fabric became 25 to 160% higher than in the other fabrics. For that reason the tensile Young's modulus of elasticity was lowest in the stitched basalt fabric in comparison to the other fabrics. The stitched basalt fabric was reinforced in polyester resin and the other fabrics were reinforced in epoxy resin. The epoxy resin is generally stronger then polyester resin. That can be the main reason for how low the ultimate compression strength and shear Young's modulus of elasticity was in the stitched basalt fabric.

Table 7-2 Comparison of composite properties of different fabrics.

Material properties	[1*]Basalt A, D and B Fabric	[2*]Basalt (fine) Fabric	[3*]Basalt (coarse) fabric	[4*]E-glass fabric	[5*]Carbon fabric
E_1^t(GPa)	19.82	22.40	25.30	24.96	57.78
E_2^t(GPa)	19.82	23.0	16.0	25.3	58.67
E_1^c(GPa)	[6*]38.70	-	-	25.37	57.71
E_2^c(GPa)	[6*]38.70	-	-	25.23	54.19
F_1^{tu}(MPa)	436.3	437.4	578.8	357.1	555.7
F_2^{tu}(MPa)	436.3	429.8	251.9	374.4	641.2
F_1^{cu} (MPa)	199.9	244.3	175.1	342	481.9
F_2^{cu}(MPa)	199.9	-	-	281.3	419.9
F_{12}^{su}(MPa)	37.5	55.1	65.7	79.29	88.25
G_{12}^s(GPa)	2.75	[6*]3.15	[6*]3.31	5.23	4.371
ν_{12}^t	0.054	-	[6*]0.1576	0.115	0.0587
ν_{21}^t	0.054	-	[6*]0.0775	0.127	0.0509
ε_1^{tu}(%)	2.74	2.2	2.4	1.77	0.783
ε_2^{tu} (%)	2.74	2.0	2.2	1.82	1.05
ε_1^{cu} (%)	[6*]0.47	-	-	1.47	0.894
ε_2^{cu} (%)	[6*]0.47	-	-	1.19	0.826
t (mm)	0.45	0.175	0.28	0.22	0.38
density(g/cm^3)	1.84	1.87	1.88	1.89-1.93	1.48

[1*] Basalt stitched fabric / Polyester resin / Vacuum Infusion / Fiber volume 50.7%
[2*] Basalt (fine) weave fabric / Epoxy resin / Vacuum Bag cure / Fiber volume 48-49%
[3*] Basalt (coarse) weave fabric / Epoxy resin / Vacuum Bag cure / Fiber volume 50-51%
[4*] E-glass weave fabric / Epoxy resin / Vacuum Bag cure / Fiber volume 52-56%
[5*] Carbon weave fabric / Epoxy resin / Vacuum Bag cure / Fiber volume 54-57%
[6*] Only one test

7.5 Conclusion of the Tube Research

7.5.1 Load Test Comparison of Tube no.2

The measured results of the load tests were compared with the calculated design value for a four-meter high lamppost. The design value, used to compare with the measured results, was obtained on the website Ferro Zinc in Iceland (Ferro Zink, 2007). Table 7-3 shows the comparison of the measured values of the tube and design values for a four-meter high lamppost. Table 7-3 also shows that the tube satisfied the design requirements for a four-meter high lamppost.

Table 7-3 Comparison between measured values and design values.

Measured and design	Moment [kNm]	Displacement [mm]
[1*] Tube, 1200 mm long, measured values	3.78	58
[2*] Design values for lamppost, calculated values	2.42	72

[1*] The maximum displacement on the tube was 58 mm when the force was F = 3.15 kN.

[1*] The maximum moment in the tube was M = 3.78 kNm (h*F) and it was next to the fastener.

[2*] A permissible displacement is 72 mm for a 1200 mm high lamppost (0,06*h) and will be the design value for the tube (h = high of the tube).

[2*] A permissible moment is 2.42 kNm next to the ground for a four-meter high lamppost and will be the design value for the tube.

7.5.2 Load Test Conclusion of Tube no.2

When the comparison between the measured values for the tube and design values for a four-meter high lamppost are examined it can be seen that the tube satisfied the design values for a four-meter high lamppost. It should be noted, however, that only one load test was carried out, which would be considered too few tests to assure people that the tube would perform satisfactorily. As mentioned above, the fastener between the tube and testing machine failed and at the same time the force was considerably reduced. Closer inspection of the tube revealed that the tube was undamaged, and it was thought that the tube would withstand much more load than it actually received from the UTM. From this study the conclusion can be accepted that a four-meter high pole made of polyester resin with basalt fiber reinforcement with four or more layers of basalt fabric would be feasible. The pole could most likely meet the same design standards as a regular four-meter high lamppost has to fulfill.

7.6 Summary

- Vacuum Infusion processes gave a 50.68 ±0.45 % basalt fiber volume and Hand Lay-up processes gave a 38% basalt fiber volume.
- In the tensile test specimens A became 19.6% stronger than specimens C.
- In the compression test specimens D became 116.8% stronger than specimens E.
- In the in-plane shear test the shear strength was low because of the polyester resin and adhesion between the fibers and the resin.
- In the pin bearing test the first damage mechanisms in the laminate were close to 20% bearing strain.
- In calculations according to Classical Laminate Theory the first layers failed at 9.0 kN in specimens C.
- In the comparison, the stitched basalt fabric (which was examined in this project) became 19.3% stronger than the E-glass fabric.
- The basalt tube could most likely satisfy the design values for a four-meter high lamppost.

Summary

8.1 General

The results of the experiments in this thesis indicate that continuous basalt fibers, as reinforcement material in polymer matrix, can be used as a composite material for structural design. The static uniaxial test showed that basalt fiber was stronger than E-glass fiber. As pointed out in chapter 2, glass fibers are the most used fiber in the world in all kinds of structures and basalt fiber could possibly be used instead of these types of fibers. In addition, the basalt tube was strong enough to be used as a regular four-meter high lamppost. To ensure that basalt fiber could be used as a feasible composite and reinforcement material in a matrix more and different types of testing are required. But this study has shown that this composite material could be usable in structures design and that further testing is justified.

8.2 Further Research

This study was concentrated on static testing to get basic results for the feasibility of using continuous basalt fibers in polyester resin. To get more information about the material properties for basalt fiber as a reinforcement material in matrix various other tests could be performed. Here are a few of the experimental studies that could be carried out:

- Carry out a dynamic load test. Because in reality the applied loads are usually dynamical, for example because of wind load and earthquake load.
- Carry out a more static load test, for example a flexural test and a delamination test. It is very important to investigate delamination in the material because it continued to in the present experiment.
- Investigate the adhesion between the basalt fiber and other resin. The adhesion between the basalt fiber and polyester resin was one of the weakest factors in the experiment.
- Carry out a fatigue test. This is very important for structures that are under variable continuous loads.

References

ASTM D3039 / D3039M - 00 : Standard test method for tensile properties of polymer matrix composite materials. (2000). West Conshohocken, PA: ASTM International.

ASTM D3171 - 99 : Standard test method for constituent of composite materials. (2000). West Conshohocken, PA: ASTM International.

ASTM D3410 / D3410M - 03 : Standard test method for compressive properties of polymer matrix composite materials with unsupported gage section by shear loading. (2003). West Conshohocken, PA: ASTM International.

ASTM D3518 / D3518M - 94 : Standard test method for in plane shear response of polymer matrix composite materials by tensile test of a ±45° laminate. (1994). West Conshohocken, PA: ASTM International.

ASTM D5961 / D5961M - 01 : Standard test method for bearing response of polymer matrix composite laminates. (2001). West Conshohocken, PA: ASTM International.

ASTM D695 - 02 : Standard test method for compressive properties of rigid plastics. (2002). West Conshohocken, PA: ASTM International.

ASTM E111 - 97 : Standard test method for young's modulus, tangent modulus, and chord modulus. (1997). West Conshohocken, PA: ASTM International.

ASTM E132 - 04 : Standard test method for Poisson's ratio at room temperature. (2004). West Conshohocken, PA: ASTM International.

ASTM International. (2002). *The composite materials handbook-MIL 17: Polymer matrix composites: materials properties*. West Conshohocken, PA: ASTM International.

ASTM International. (2012). About ASTM International - ASTM overview. Retrieved May 8, 2012, from http://www.astm.org/ABOUT/overview.html

Árnason, P. (2007). *Plast 3*. Reykjavík: Nýsköpunarmiðstöð Íslands.

Boeing. (n.d.). Commercial airplanes - 787 Dreamliner. *Boeing 787*. Retrieved May 31, 2012, from http://www.boeing.com/commercial/787family/background.html

Bruijn, M. (2007). *Evaluation of basalt continuous filament fibres in composite material*. Belgium: Universiteit Leuven. Retrieved from http://www.basaltex.com/files/cms1/Report-Evaluation-of-Basalt-Continuous-Filament-Fibres-in-composite-material_June%202007.pdf

Chang, Z. L., Zou, G. P., Chen, S., & Chen, L. (2011). The study of AE and ESSPI technique on the CBF composite. *Key Engineering Materials*, *488-489*, 436–439. doi:10.4028/www.scientific.net/KEM.488-489.436

Chapter 4 failure theories. (n.d.). Retrieved May 4, 2012, from http://www.docstoc.com/docs/101939810/Chapter-4-Failure-Theories

Colombo, C., Vergani, L., & Burman, M. (2012). Static and fatigue characterisation of new basalt fibre reinforced composites. *Composite Structures*, *94*(3), 1165–1174. doi:10.1016/j.compstruct.2011.10.007

Europe's first plastic bridge is open. (2010). Retrieved May 31, 2012, from http://www.plasticseurope.co.uk/information-centre-8484/news/archives/europes-first-plastic-bridge-is-open.aspx

Ferro Zink. (2007). Ljósastaur 4x60. Retrieved June 8, 2012, from http://www.ferro.is/ferrozink/upload/files/acrobat/framleidsluvorur/102-staur_4x60_ch.pdf

Greene, E. (n.d.). Marine composites. Retrieved May 1, 2012, from http://www.marinecomposites.com/PDF_Files/H_Micromechanics.pdf

Hyer, M. (2008). *Stress analysis of fiber-reinforced composite materials* (Updated.). Lancaster, PA: Destech Pubns Inc.

Jones, R. M. (1998). *Mechanics of composite materials* (2 Sub.). Blacksburg, VA: CRC Press.

Kamenny Vek. (2009). Advanced basalt fiber. *Basfiber*. Retrieved May 9, 2012, from http://www.basfiber.com/

Kant, T. (2010). Composite mechanics in the last 50 years. Retrieved May 6, 2012, from http://www.ircc.iitb.ac.in/IRCC-Webpage/PDF/TarunKant2010.pdf

Manjunatha, B. S., & Kant, T. (1992). A comparison of 9 and 16 node quadrilateral elements based on higher-order laminate theories for estimation of transverse stresses. *Journal of Reinforced Plastics and Composites*, *11*(9), 968–1002. doi:10.1177/073168449201100902

McGeorge, D., & Höyning, B. (n.d.). NATO-RTO. Retrieved May 31, 2012, from http://research.dnv.com/euclid_rtp3.21/PW_Tools/PWE/Input/NATO-RTO-DagMcGeorgeBjornHoyning.pdf

Meunier, M., & Knibbs, S. (2007). *Design tools for fibre reinforced polymer structures*. National Composites Network.

Parnas, R., & Shaw, M. (2007). *Basalt fiber reinforced polymer composites* (No. 03-7). New England, MA: Transportation Consortium.

Reissner, E., & Stavsky, Y. (1961). Bending and stretching of certain types of heterogeneous aeolotropic elastic plates. *Journal of Applied Mechanics*, *28*(3), 402. doi:10.1115/1.3641719

Ross, A. (2006). Basalt fibers: Alternative to glass? *Composites World*. Retrieved May 9, 2012, from http://www.compositesworld.com/articles/basalt-fibers-alternative-to-glass

Schulz, W.A. (2005). *Determination of residual stress and thermal behavior for composite laminates* (Master thesis). University of Florida, Florida. Retrieved from http://ufdcimages.uflib.ufl.edu/UF/E0/01/04/06/00001/schulz_w.pdf

Shakespeare composite structures. (n.d.). Retrieved May 31, 2012, from http://www.skp-cs.com/default.asp

SP Systems. (n.d.). *Guide to composites*. Retrieved from http://www.bolton.ac.uk/codate/spguidetocomposites.pdf

Staab, G. H. (1999). *Laminar composites*. Woburn, MA: Butterworth-Heinemann.

Talebi Mazraehshahi, H., & Zamani, H. (2010). Investigation on mechanical properties of basalt composite fabrics (experiment study). *EPJ Web of Conferences, 6*, 20008. doi:10.1051/epjconf/20100620008

Tsai, S.W. (Ed.). (1979). *Composite materials: Testing and design (fifth conference): Stp 674*. ASTM International.

Van de Velde, K., Kiekens, P., & Van Langenhove, L. (n.d.). *Basalt fibres as reinforcement-for composites*. Belgium: Ghent University.

Yuhazri, M., & Sihombing, H. (n.d.). A comparison process between vacuum infusion and hand lay-up method toward kenaf/polyester composites. *International Journal of Basic & Applied Sciences, 10*(3), 63–66.

Appendix A – Technical Data of basalt fabrics

BASALTEX™
The thread of stone

ISO 9001 A Division of FLOCART nv

Technical Data Sheet
Fabric Type BAS BI 600

Multiaxial fabric for composite applications, is entirely made of 100% BCF (basalt continuous filament) roving.
The silane sizing is selected, which has components to ensure elasticity of the yarn during textile processes. The sizing allows good compatibility with epoxy, vinyl ester and polyester resin systems.

Property	Standard/Method	Unit	Value	Tolerance
Base material				
Density of unsized filament matl		kg/dm³	2.67	± 5%
Moisture content of basaltic rock		%	0.1	± 0.05
Melting point		°C	1350	± 100
Fabric				
Specific surface weight	ISO 3374:2000	g/m²	605	± 8%
Weave type			biaxial	
Weight per layer (Yarn type): - +45° - -45° - stitching		 g/m² g/m² g/m²	 298.5 298.5 8	
Width	ISO 5025:1997	mm	1270	± 3%
Thickness	ISO 4603:1993	mm	0.50	
Sizing type			silane	
Breaking load: - +45° - -45°	ISO 4606:1995 – Type II	 N/25mm N/25mm	 >5025 >5025	
Moisture content (fabric)	ISO 3344:1997	%	<0.3	
LOI, also sizing content	ISO 1887:1995*	%	0.4 – 0.6	
Combustibility	NF P92-503:1995	M0	Pass	
UV stability	ISO 105-B02		6	
Colour fastness	ISO 1005-BX12		6	

* after drying according ISO 3344:1997

Packaging
Fabric length is approximately 50 lm per roll. Other length on request. Identification label. Standard packing.

Product Stability:
BASALTEX™ Products have not been designed for full external exposure conditions and cannot be guaranteed for use in such situations. However, these BASALTEX™ products have considerable tolerance to damp conditions and occasional water immersion. After drying out, the product will give the same level of performance as the original sample.

Stability over time:
Said products not being subjected to excessive heat, wear and abrasion, all evidence obtained to date indicates that their performance should not significantly change over a significant period of time.
It is the responsibility of the developer of the end-product, finished device or system to test its performance in the end-application.

Rev 03.11 BASALTEX Division, FLOCART nv • Zuidstraat, 18 • B-8560 Wevelgem • BELGIUM
PHONE +32(0)56 43 00 95 • FAX +32 (0)56 42 42 34 – info.basaltex@flocart.com

BASALTEX™
The thread of stone

ISO 9001 A Division of FLOCART nv

Technical Data Sheet
Fabric Type BAS UNI 600

Unidirectional fabric for composite applications, is entirely made of 100% BCF (basalt continuous filament) roving.
The silane sizing is selected, which has components to ensure elasticity of the yarn during textile processes. The sizing allows good compatibility with epoxy, vinyl ester and polyester resin systems.

Property	Standard/Method	Unit	Value	Tolerance
Base material				
Density of unsized filament matl		kg/dm³	2.67	± 5%
Moisture content of basaltic rock		%	0.1	± 0.05
Melting point		°C	1350	± 100
Fabric				
Specific surface weight	ISO 3374:2000	g/m²	657	± 8%
Weave type			UD	
Weight per layer : - 0° - 90° - stitching		 g/m² g/m² g/m²	 600 50 7	
Width**	ISO 5025:1997	mm	1270	± 3%
Thickness	ISO 4603:1993	mm	0.65	
Sizing type			silane	
Moisture content (fabric)	ISO 3344:1997	%	<0.3	
LOI, also sizing content	ISO 1887:1995*	%	0.4 – 0.6	
Combustibility	NF P92-503:1995	M0	Pass	
UV stability	ISO 105-B02		6	
Colour fastness	ISO 1005-BX12		6	

* after drying according ISO 3344:1997

Packaging
Fabric length is approximately 50 lm per roll. Other length on request. Identification label. Standard packing.

Product Stability:
BASALTEX™ Products have not been designed for full external exposure conditions and cannot be guaranteed for use in such situations. However, these BASALTEX™ products have considerable tolerance to damp conditions and occasional water immersion. After drying out, the product will give the same level of performance as the original sample.

Stability over time:
Said products not being subjected to excessive heat, wear and abrasion, all evidence obtained to date indicates that their performance should not significantly change over a significant period of time.
It is the responsibility of the developer of the end-product, finished device or system to test its performance in the end-application.

Rev 03.11 BASALTEX Division, FLOCART nv • Zuidstraat, 18 • B-8560 Wevelgem • BELGIUM
PHONE +32(0)56 42 00 95 • FAX +32 (0)56 42 42 34 – info.basaltex@flocart.com

Appendix B – Technical Data of polyester resins

REICHHOLD

PRODUCT BULLETIN

November 2005

POLYLITE® 440-M850

Standard orthophthalic polyester resin

DESCRIPTION

POLYLITE® 440-M850 is a medium reactive orthophthalic polyester resin.
POLYLITE® 440-M850 is thixotropic and has a built-in accelerator system giving medium gel time, rapid curing combined with relatively low exothermic temperature and short demolding time.

POLYLITE® 440-M850 contains special additives which improve the working environment during and after application due to substantially reduced styrene evaporation. The resin contains wax which gives the cured laminate a tack-free surface.

APPLICATION

- POLYLITE® 440-M850 is a hand layup/sprayup resin.
- POLYLITE® 440-M850 is designed for marine, industrial and transport application.

Recommended laminate thickness applied wet-on-wet: 2-8 mm.

FEATURES	BENEFITS
• Excellent application properties	• Short application time • Good fiber wetting • Higher fiber content
• Medium reactivity	• Good curing • Short demoulding time
• Approvals	• Det norske Veritas, DNV, grade 2 Lloyd's Register of Shipping Bureau Veritas Germanischer Lloyd Russian Maritime register

919-990-7500 • 800-448-3482 • P.O. Box 13582, Research Triangle Park, NC 27709 USA • 2400 Ellis Road, Durham, NC 27703 USA • www.reichhold.com
Reichhold, P.O.Box 2061, N-3202 Sandefjord, Norway, Tel. +47 33 44 86 00, Fax + 47 33 44 86 01

TYPICAL PROPERTIES

PHYSICAL DATA IN LIQUID STATE AT 23°C

Properties	Unit	Value	Test method
Viscosity - Brookfield Model LVF, Spindle 2 at 12 rpm - Cone & Plate	 mPa·s(cP) mPa·s(cP)	 1100-1300 170-200	 ASTM D 2196-86 ISO 2884-1999
Specific gravity / Density	g/cm³	1,10	ISO 2811-2001
Acid number (max.)	mgKOH/g	24	ISO 2114-1996
Styrene content	% weight	43 ± 2	B070
Flash point	°C	32	ASTM D 3278-95
Gel time: 1% NORPOL PEROXIDE 1 (MEKP)	minutes	35-45	G020
Storage stability from date of manufacture	months	6	G180

TYPICAL NON-REINFORCED CASTING PROPERTIES

Fully post cured.

Properties	Unit	Value	Test method
Tensile strength	MPa	50	ISO 527-1993
Tensile modulus	MPa	4600	ISO 5271993
Tensile elongation	%	1.6	ISO 527-1993
Flexural strength	MPa	90	ISO 178-2001
Flexural modulus	MPa	4000	ISO 178-2001
Impact strength P4J	mJ/mm²	5.0-6.0	ISO 179-2001
Volume shrinkage	%	5.5-6.5	ISO 3521-1976
Heat distortion temp.	°C	62	ISO 75-1993

STORAGE

To ensure maximum stability and maintain optimum resin properties, resins should be stored in closed containers at temperatures below 24°C/75°F and away from heat ignition sources and sunlight. Resin should be warmed to at least 18°C/65°F prior to use in order to assure proper curing and handling. All storage areas and containers should conform to local fire and building codes. Copper or copper containing alloys should be avoided as containers. Store separate from oxidizing materials, peroxides and metal salts. Keep containers closed when not in use. Inventory levels should be kept to a reasonable minimum with first-in, first-out stock rotation.

Additional information on handling and storing unsaturated polyesters is available in Reichhold's application bulletin "Bulk Storage and Handling of Unsaturated Polyester Resins." For information on other Reichhold resins or initiators, contact your sales representative or authorized Reichhold distributor.

SAFETY

READ AND UNDERSTAND THE MATERIAL SAFETY DATA SHEET BEFORE WORKING WITH THIS PRODUCT

Obtain a copy of the material safety data sheet on this product prior to use. Material safety data sheets are available from your Reichhold sales representative. Such information should be requested from suppliers of all products and understood prior to working with their materials.

DIRECTLY MIXING ANY ORGANIC PEROXIDE WITH A METAL SOAP, AMINE, OR OTHER POLYMERIZATION ACCELERATOR OR PROMOTER WILL RESULT IN VIOLENT DECOMPOSITION

REICHHOLD

PRODUCT BULLETIN

December 2007

POLYLITE® 506-647

DCPD based Infusion Resin

(Ex. PD-3247)

DESCRIPTION

POLYLITE® 506-647 is a medium reactive, low styrene based DCPD polyester resin.
POLYLITE® 506-647 is accelerated and non-thixotropic.

APPLICATION

- POLYLITE® 506-647 is designed for all general purpose composite products and is designed for vacuum infusion processes.
- Cured with standard MEK Peroxide a wet-in-wet laminate thickness of 3-9 mm is recommended. NORPOL PEROXIDE 18 gives longer gel times, lower exotherm and wet-in-wet laminate thickness > 9 mm is possible.
- The resin impregnates the glass fibre rapidly, has long gel times and gives good curing rate.

FEATURES	BENEFITS
• Low styrene content, <35%	• Reduced shrinkage • Improved surface aspects • Reduced styrene emission
• Good fibre wetting properties	• Easy lamination and air release
• Excellent curing characteristics	• Improved state of cure when demoulding, giving improved surface aspects. Relatively short cycle times (3-9 mm wet-in-wet laminates with 1% standard MEK Peroxide). Cured with 1.4% NORPOL PEROXIDE 18, the wet-in-wet thickness span can be increased > 9 mm with glass content ≥ 35%, giving improved state of cure when demoulding, and relatively short cycle times.
• Approvals	• Det norske Veritas, DNV, grade 2 • Lloyd's Register of Shipping

919-990-7500 • 800-448-3482 • P.O. Box 13582, Research Triangle Park, NC 27709 USA • 2400 Ellis Road, Durham, NC 27703 USA • www.reichhold.com
Reichhold, P.O.Box 2061, N-3202 Sandefjord, Norway, Tel. +47 33 44 86 00, Fax + 47 33 44 86 01

TYPICAL PROPERTIES

PHYSICAL DATA IN LIQUID STATE AT 23°C

Properties	Unit	Value	Test method
Viscosity - Cone & Plate	 mPa·s(cP)	 270-290	 ISO 2884-1999
Density	g/cm³	1.11 ± 0.02	ISO 2811-2001
Styrene content	% weight	33 ± 2	B070
Flash point	°C	32	ASTMD 3278-95
Gel time at 23°C: 1,0 % NORPOL PEROXIDE 1 Gel time at 19°C : 1,4 % NORPOL PEROXIDE 18	Minutes Minutes	125-145 155-175	G020 G020
Storage stability from date of manufacture	Months	4	G180

TYPICAL NON-REINFORCED CASTING PROPERTIES

Fully post cured (24 hrs at RT + 24 hrs at 60°C + 3 hrs at 90°C)

Properties	Unit	Value	Test method
Tensile strength	MPa	50	ISO 527-1993
Tensile modulus	MPa	3100	ISO 527-1993
Tensile elongation	%	2,1	ISO 527-1993
Flexural strength	MPa	90	ISO 178-2001
Flexural modulus	MPa	3300	ISO 178-2001
Heat distortion temp.	°C	75	ISO 75-1993

STORAGE

To ensure maximum stability and maintain optimum resin properties, resins should be stored in closed containers at temperatures below 24°C/75°F and away from heat ignition sources and sunlight. Resin should be warmed to at least 18°C/65°F prior to use in order to assure proper curing and handling. All storage areas and containers should conform to local fire and building codes. Copper or copper containing alloys should be avoided as containers. Store separate from oxidizing materials, peroxides and metal salts. Keep containers closed when not in use. Inventory levels should be kept to a reasonable minimum with first-in, first-out stock rotation.

Additional information on handling and storing unsaturated polyesters is available in Reichhold's application bulletin "Bulk Storage and Handling of Unsaturated Polyester Resins." For information on other Reichhold resins or initiators, contact your sales representative or authorized Reichhold distributor.

SAFETY

READ AND UNDERSTAND THE MATERIAL SAFETY DATA SHEET BEFORE WORKING WITH THIS PRODUCT

Obtain a copy of the material safety data sheet on this product prior to use. Material safety data sheets are available from your Reichhold sales representative. Such information should be requested from suppliers of all products and understood prior to working with their materials.

DIRECTLY MIXING ANY ORGANIC PEROXIDE WITH A METAL SOAP, AMINE, OR OTHER POLYMERIZATION ACCELERATOR OR PROMOTER WILL RESULT IN VIOLENT DECOMPOSITION

Appendix C–Measured Values

Specimens	Overall Length	Width	Thickness	Mass	Density	Fiber Content	Fiber Volume	Resin Content	Resin Volume	Total Volume
A-01	250,30 mm	25,75 mm	2,67 mm	31,9 g	1,854 g/cm3	73,34 %	50,92 %	26,66 %	44,92 %	95,84 %
A-02	250,20 mm	25,75 mm	2,69 mm	31,7 g	1,829 g/cm3	73,78 %	50,54 %	26,22 %	43,61 %	94,15 %
A-03	250,20 mm	25,70 mm	2,67 mm	31,8 g	1,852 g/cm3	73,40 %	50,92 %	26,60 %	44,39 %	95,31 %
A-04	250,50 mm	25,75 mm	2,70 mm	31,9 g	1,832 g/cm3	73,40 %	50,35 %	26,60 %	43,89 %	94,25 %
A-05	250,20 mm	25,65 mm	2,66 mm	31,6 g	1,851 g/cm3	73,72 %	51,11 %	26,28 %	43,82 %	94,93 %
A-06	250,40 mm	25,70 mm	2,65 mm	31,7 g	1,859 g/cm3	73,69 %	51,30 %	26,31 %	44,06 %	95,36 %
B-01	249,80 mm	25,65 mm	2,69 mm	31,7 g	1,839 g/cm3	73,37 %	50,54 %	26,63 %	44,12 %	94,66 %
B-02	250,00 mm	25,60 mm	2,70 mm	32,1 g	1,858 g/cm3	72,37 %	50,35 %	27,63 %	46,23 %	96,59 %
B-03	250,00 mm	25,60 mm	2,67 mm	31,5 g	1,843 g/cm3	73,75 %	50,92 %	26,25 %	43,59 %	94,51 %
B-04	250,00 mm	25,60 mm	2,68 mm	31,5 g	1,837 g/cm3	73,75 %	50,73 %	26,25 %	43,43 %	94,16 %
B-05	250,10 mm	25,65 mm	2,71 mm	31,7 g	1,823 g/cm3	73,46 %	50,17 %	26,54 %	43,60 %	93,77 %
B-06	250,10 mm	25,60 mm	2,71 mm	32,0 g	1,844 g/cm3	72,63 %	50,17 %	27,37 %	45,48 %	95,65 %
C-01	250,30 mm	25,65 mm	2,64 mm	31,7 g	1,870 g/cm3	73,52 %	51,50 %	26,48 %	44,62 %	96,12 %
C-02	250,40 mm	25,70 mm	2,63 mm	31,7 g	1,873 g/cm3	73,69 %	51,69 %	26,31 %	44,39 %	96,09 %
C-03	250,50 mm	25,60 mm	2,67 mm	31,6 g	1,846 g/cm3	73,67 %	50,92 %	26,33 %	43,78 %	94,70 %
C-04	250,30 mm	25,65 mm	2,64 mm	31,6 g	1,864 g/cm3	73,75 %	51,50 %	26,25 %	44,09 %	95,59 %
C-05	250,50 mm	25,60 mm	2,69 mm	31,5 g	1,826 g/cm3	73,90 %	50,54 %	26,10 %	42,94 %	93,48 %
C-06	250,70 mm	25,70 mm	2,67 mm	31,5 g	1,831 g/cm3	74,25 %	50,92 %	25,75 %	42,48 %	93,40 %
D-01	154,20 mm	25,65 mm	2,70 mm	19,7 g	1,845 g/cm3	72,88 %	50,35 %	27,12 %	45,07 %	95,42 %
D-02	154,50 mm	25,70 mm	2,67 mm	19,4 g	1,830 g/cm3	74,30 %	50,92 %	25,70 %	42,37 %	93,29 %
D-03	154,50 mm	25,70 mm	2,68 mm	19,6 g	1,842 g/cm3	73,54 %	50,73 %	26,46 %	43,91 %	94,64 %
D-04	153,60 mm	25,65 mm	2,71 mm	19,7 g	1,845 g/cm3	72,60 %	50,17 %	27,40 %	45,55 %	95,72 %
D-05	153,80 mm	25,80 mm	2,70 mm	19,6 g	1,829 g/cm3	73,49 %	50,35 %	26,51 %	43,69 %	94,05 %
D-06	153,60 mm	25,70 mm	2,70 mm	19,5 g	1,830 g/cm3	73,48 %	50,35 %	26,52 %	43,70 %	94,06 %

Specimens	Overall Length	Width	Thickness	Mass	Density	Fiber Content	Fiber Volume	Resin Content	Resin Volume	Total Volume
E-01	153,00 mm	25,60 mm	2,65 mm	19,2 g	1,850 g/cm3	74,05 %	51,30 %	25,95 %	43,24 %	94,55 %
E-02	153,40 mm	25,80 mm	2,70 mm	19,6 g	1,834 g/cm3	73,30 %	50,35 %	26,70 %	44,12 %	94,48 %
E-03	153,00 mm	25,80 mm	2,65 mm	19,3 g	1,845 g/cm3	74,24 %	51,30 %	25,76 %	42,81 %	94,12 %
E-04	153,20 mm	25,75 mm	2,70 mm	19,5 g	1,831 g/cm3	73,44 %	50,35 %	26,56 %	43,81 %	94,17 %
E-05	153,10 mm	25,70 mm	2,73 mm	19,7 g	1,834 g/cm3	72,50 %	49,80 %	27,50 %	45,43 %	95,23 %
E-06	153,10 mm	25,80 mm	2,70 mm	19,7 g	1,847 g/cm3	72,78 %	50,35 %	27,22 %	45,29 %	95,64 %
G-01	135,60 mm	40,90 mm	2,66 mm	27,4 g	1,857 g/cm3	73,47 %	51,11 %	26,53 %	44,38 %	95,49 %
G-02	135,50 mm	40,90 mm	2,65 mm	27,3 g	1,859 g/cm3	73,69 %	51,30 %	26,31 %	44,06 %	95,37 %
G-03	135,45 mm	40,85 mm	2,67 mm	27,4 g	1,855 g/cm3	73,30 %	50,92 %	26,70 %	44,61 %	95,53 %
G-04	135,45 mm	40,90 mm	2,68 mm	27,4 g	1,845 g/cm3	73,39 %	50,73 %	26,61 %	44,24 %	94,97 %
G-05	135,45 mm	40,90 mm	2,69 mm	27,4 g	1,839 g/cm3	73,39 %	50,54 %	26,61 %	44,07 %	94,61 %
G-06	135,40 mm	40,90 mm	2,70 mm	27,3 g	1,826 g/cm3	73,64 %	50,35 %	26,36 %	43,37 %	93,72 %
H-01	134,50 mm	40,85 mm	2,73 mm	27,1 g	1,807 g/cm3	73,60 %	49,80 %	26,40 %	42,98 %	92,78 %
H-02	134,60 mm	40,80 mm	2,72 mm	27,0 g	1,808 g/cm3	73,83 %	49,98 %	26,17 %	42,61 %	92,60 %
H-03	134,50 mm	40,45 mm	2,70 mm	26,9 g	1,831 g/cm3	73,42 %	50,35 %	26,58 %	43,86 %	94,21 %
H-04	134,50 mm	40,75 mm	2,71 mm	27,2 g	1,831 g/cm3	73,15 %	50,17 %	26,85 %	44,30 %	94,47 %
H-05	134,60 mm	40,70 mm	2,69 mm	27,1 g	1,839 g/cm3	73,38 %	50,54 %	26,62 %	44,10 %	94,64 %
H-06	134,50 mm	40,60 mm	2,65 mm	27,0 g	1,866 g/cm3	73,42 %	51,30 %	26,58 %	44,69 %	95,99 %
I-01	135,20 mm	40,75 mm	2,68 mm	27,2 g	1,842 g/cm3	73,53 %	50,73 %	26,47 %	43,94 %	94,67 %
I-02	135,20 mm	40,65 mm	2,67 mm	27,2 g	1,854 g/cm3	73,35 %	50,92 %	26,65 %	44,51 %	95,43 %
I-03	135,20 mm	40,60 mm	2,69 mm	27,1 g	1,835 g/cm3	73,53 %	50,54 %	26,47 %	43,77 %	94,31 %
I-04	135,35 mm	40,75 mm	2,68 mm	27,1 g	1,833 g/cm3	73,88 %	50,73 %	26,12 %	43,14 %	93,87 %
I-05	135,50 mm	40,90 mm	2,67 mm	27,3 g	1,845 g/cm3	73,69 %	50,92 %	26,31 %	43,73 %	94,65 %
I-06	135,50 mm	40,85 mm	2,70 mm	27,3 g	1,827 g/cm3	73,60 %	50,35 %	26,40 %	43,45 %	93,80 %

A-specimens	Composite density (g/cm3)	Fiber content (wt %)	Fiber volume (vol %)	Resin content (wt %)	Resin volume (vol %)	Volume total (vol %)
average	1,846	73,56	50,86	26,44	44,12	94,97
standard deviation	0,012	0,19	0,35	0,19	0,47	0,67
coefficient of variation (%)	0,68	0,26	0,70	0,73	1,07	0,70

B-specimens	Composite density (g/cm3)	Fiber content (wt %)	Fiber volume (vol %)	Resin content (wt %)	Resin volume (vol %)	Volume total (vol %)
average	1,841	73,22	50,48	26,78	44,41	94,89
standard deviation	0,011	0,59	0,31	0,59	1,17	1,04
coefficient of variation (%)	0,61	0,80	0,61	2,19	2,63	1,10

C-specimens	Composite density (g/cm3)	Fiber content (wt %)	Fiber volume (vol %)	Resin content (wt %)	Resin volume (vol %)	Volume total (vol %)
average	1,852	73,80	51,18	26,20	43,72	94,90
standard deviation	0,020	0,25	0,45	0,25	0,84	1,24
coefficient of variation (%)	1,10	0,34	0,88	0,97	1,93	1,31

D-specimens	Composite density (g/cm3)	Fiber content (wt %)	Fiber volume (vol %)	Resin content (wt %)	Resin volume (vol %)	Volume total (vol %)
average	1,837	73,38	50,48	26,62	44,05	94,53
standard deviation	0,008	0,59	0,28	0,59	1,13	0,92
coefficient of variation (%)	0,43	0,81	0,56	2,22	2,56	0,97

E-specimens	Composite density (g/cm3)	Fiber content (wt %)	Fiber volume (vol %)	Resin content (wt %)	Resin volume (vol %)	Volume total (vol %)
average	1,840	73,39	50,58	26,61	44,12	94,70
standard deviation	0,008	0,68	0,60	0,68	1,07	0,61
coefficient of variation (%)	0,44	0,93	1,19	2,57	2,41	0,65

G-specimens	Composite density (g/cm3)	Fiber content (wt %)	Fiber volume (vol %)	Resin content (wt %)	Resin volume (vol %)	Volume total (vol %)
average	1,847	73,48	50,83	26,52	44,12	94,95
standard deviation	0,013	0,15	0,36	0,15	0,42	0,70
coefficient of variation (%)	0,70	0,21	0,70	0,57	0,96	0,73

H-specimens	Composite density (g/cm3)	Fiber content (wt %)	Fiber volume (vol %)	Resin content (wt %)	Resin volume (vol %)	Volume total (vol %)
average	1,830	73,46	50,36	26,54	43,76	94,11
standard deviation	0,022	0,23	0,53	0,23	0,80	1,27
coefficient of variation (%)	1,20	0,31	1,06	0,87	1,83	1,35

I-specimens	Composite density (g/cm3)	Fiber content (wt %)	Fiber volume (vol %)	Resin content (wt %)	Resin volume (vol %)	Volume total (vol %)
average	1,839	73,59	50,70	26,41	43,76	94,46
standard deviation	0,010	0,18	0,22	0,18	0,46	0,60
coefficient of variation (%)	0,52	0,24	0,44	0,68	1,06	0,64

Tubes	Overall Length	Width	Thickness	Mass	Density	Fiber Content	Fiber Volume	Resin Content	Resin Volume	Total Volume
T-01	1270,00 mm	346,00 mm	3,20 mm	2300,0 g	1,636 g/cm3	60,87 %	37,29 %	39,13 %	58,19 %	95,48 %
T-02	1270,00 mm	346,00 mm	3,00 mm	2230,0 g	1,692 g/cm4	62,78 %	39,78 %	37,22 %	57,24 %	97,01 %

Appendix D – Original Graphs

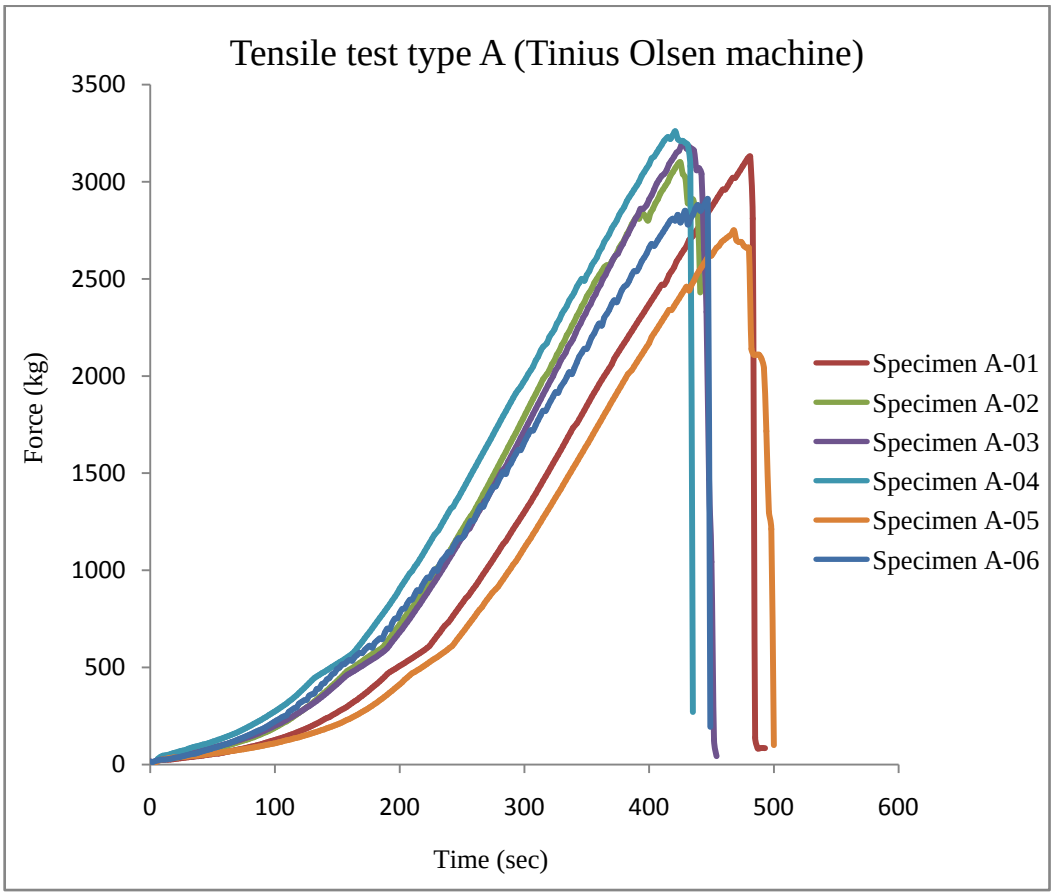

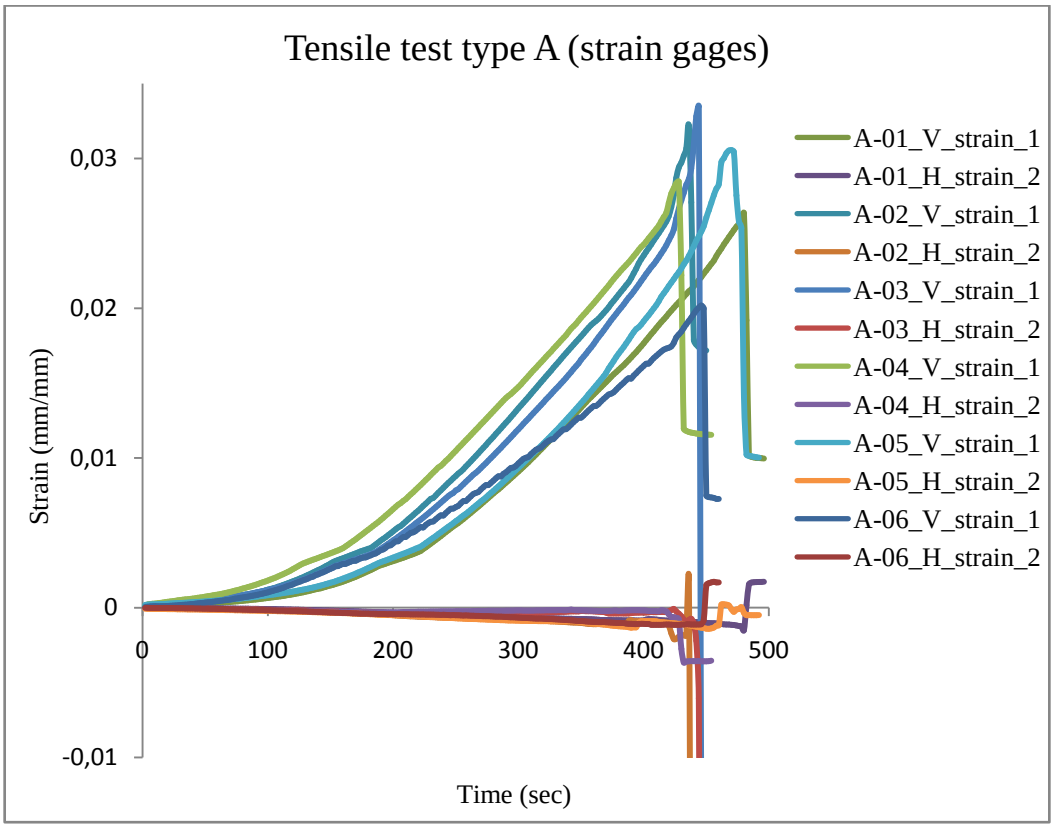

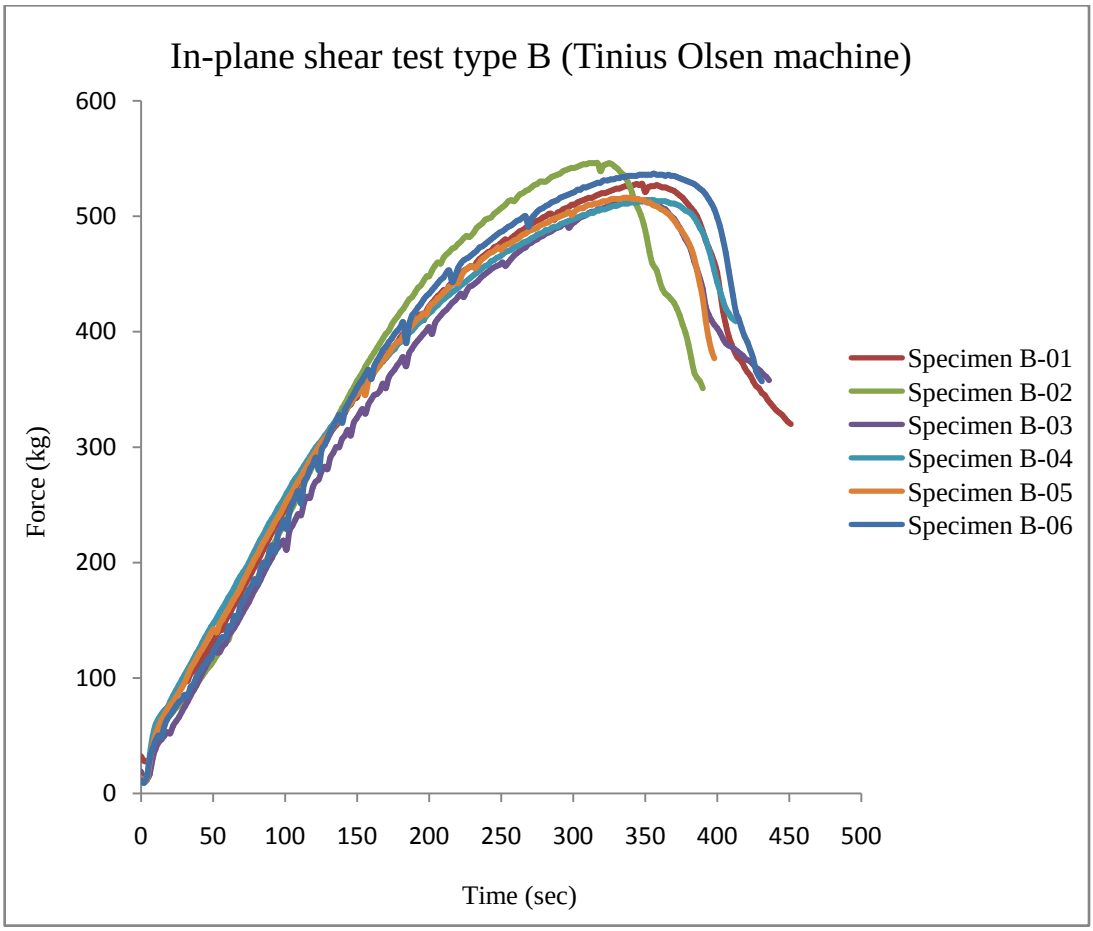
In-plane shear test type B (Tinius Olsen machine)
Force (kg)
600
500
400
300
200
100
0
0
50
100
150
200
250
300
350
400
450
500
Time (sec)
Specimen B-01
Specimen B-02
Specimen B-03
Specimen B-04
Specimen B-05
Specimen B-06

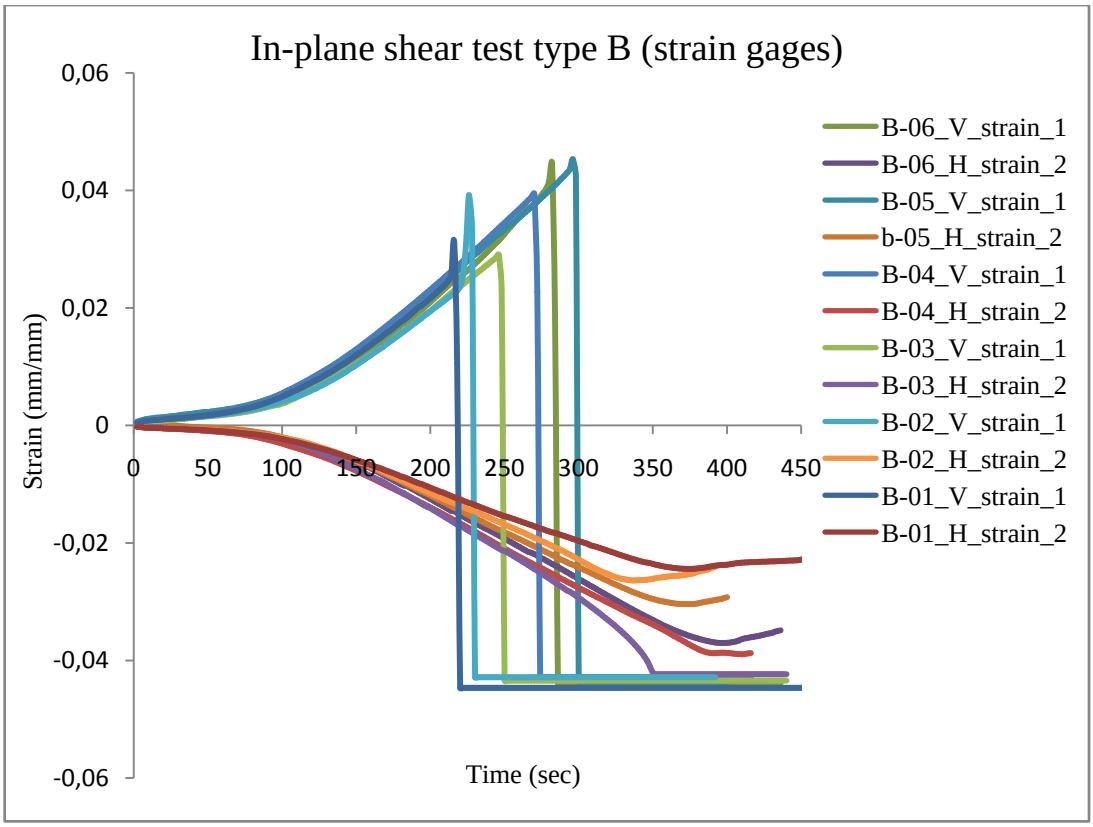
In-plane shear test type B (strain gages)
Strain (mm/mm)
0,06
0,04
0,02
0
-0,02
-0,04
-0,06
0
50
100
150
200
250
300
350
400
450
Time (sec)
B-06_V_strain_1
B-06_H_strain_2
B-05_V_strain_1
b-05_H_strain_2
B-04_V_strain_1
B-04_H_strain_2
B-03_V_strain_1
B-03_H_strain_2
B-02_V_strain_1
B-02_H_strain_2
B-01_V_strain_1
B-01_H_strain_2

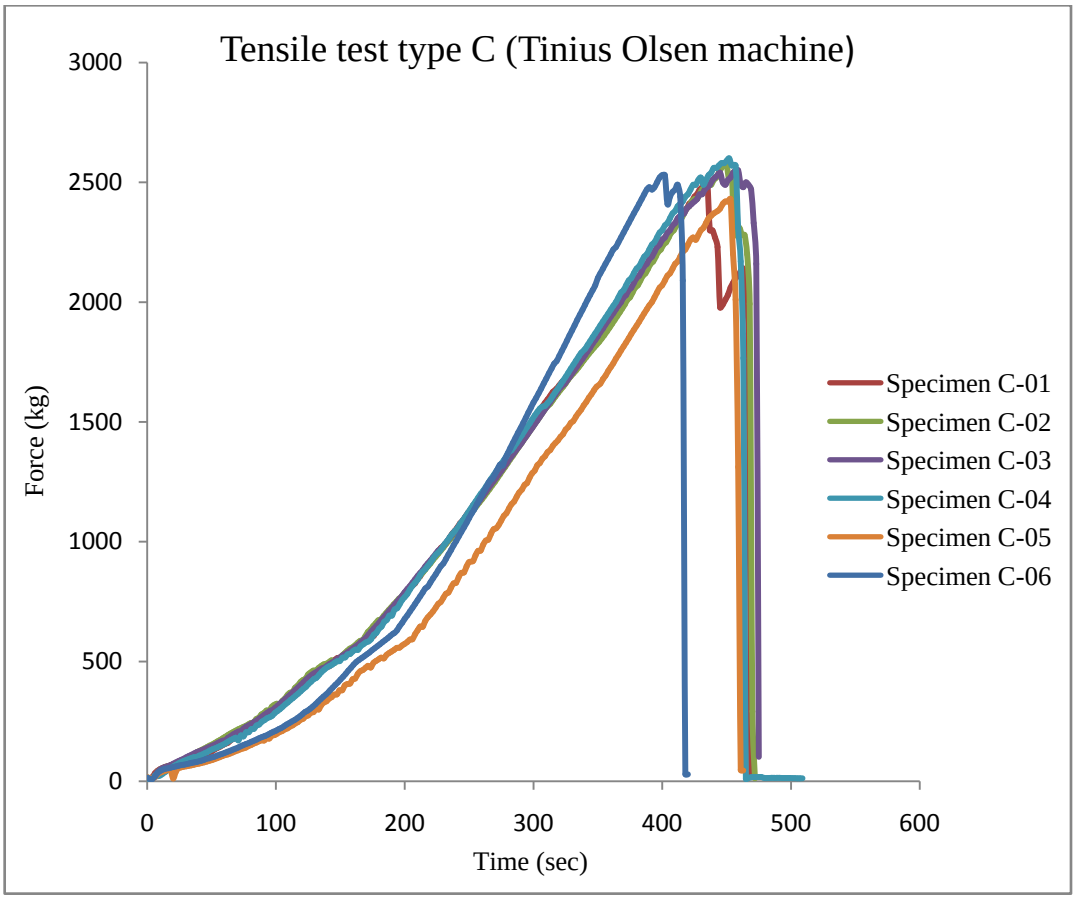
Tensile test type C (Tinius Olsen machine)
Force (kg)
3000
2500
2000
1500
1000
500
0
0
100
200
300
400
500
600
Time (sec)
Specimen C-01
Specimen C-02
Specimen C-03
Specimen C-04
Specimen C-05
Specimen C-06

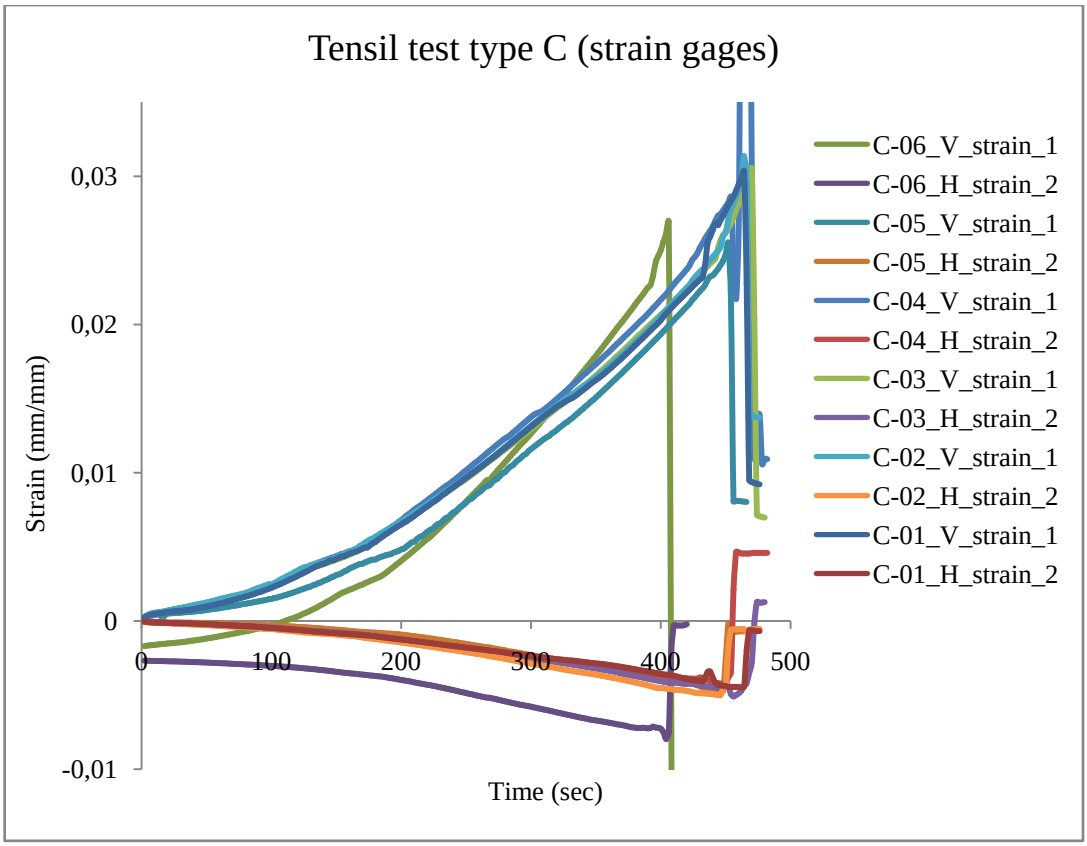
Tensil test type C (strain gages)
Strain (mm/mm)
0,03
0,02
0,01
0
-0,01
0
100
200
300
400
500
Time (sec)
C-06_V_strain_1
C-06_H_strain_2
C-05_V_strain_1
C-05_H_strain_2
C-04_V_strain_1
C-04_H_strain_2
C-03_V_strain_1
C-03_H_strain_2
C-02_V_strain_1
C-02_H_strain_2
C-01_V_strain_1
C-01_H_strain_2

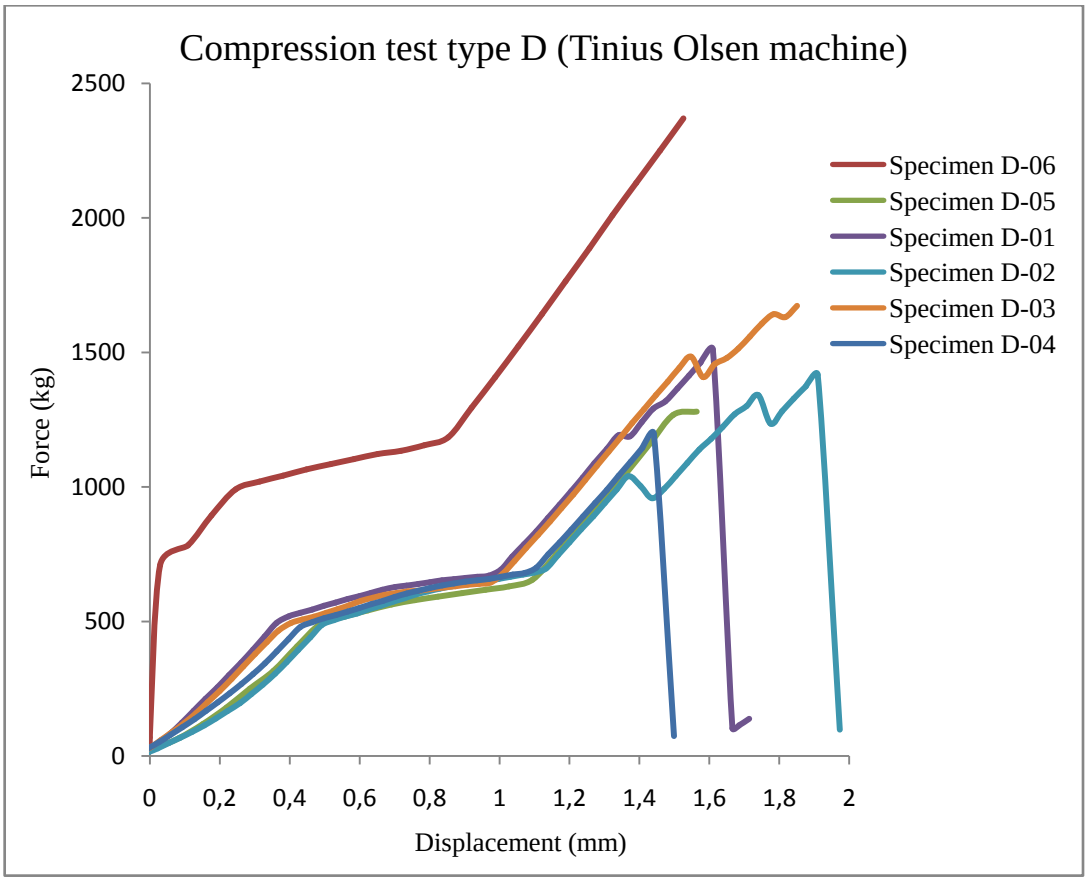
Compression test type D (Tinius Olsen machine)
Force (kg)
2500
2000
1500
1000
500
0
0
0,2
0,4
0,6
0,8
1
1,2
1,4
1,6
1,8
2
Displacement (mm)
Specimen D-06
Specimen D-05
Specimen D-01
Specimen D-02
Specimen D-03
Specimen D-04

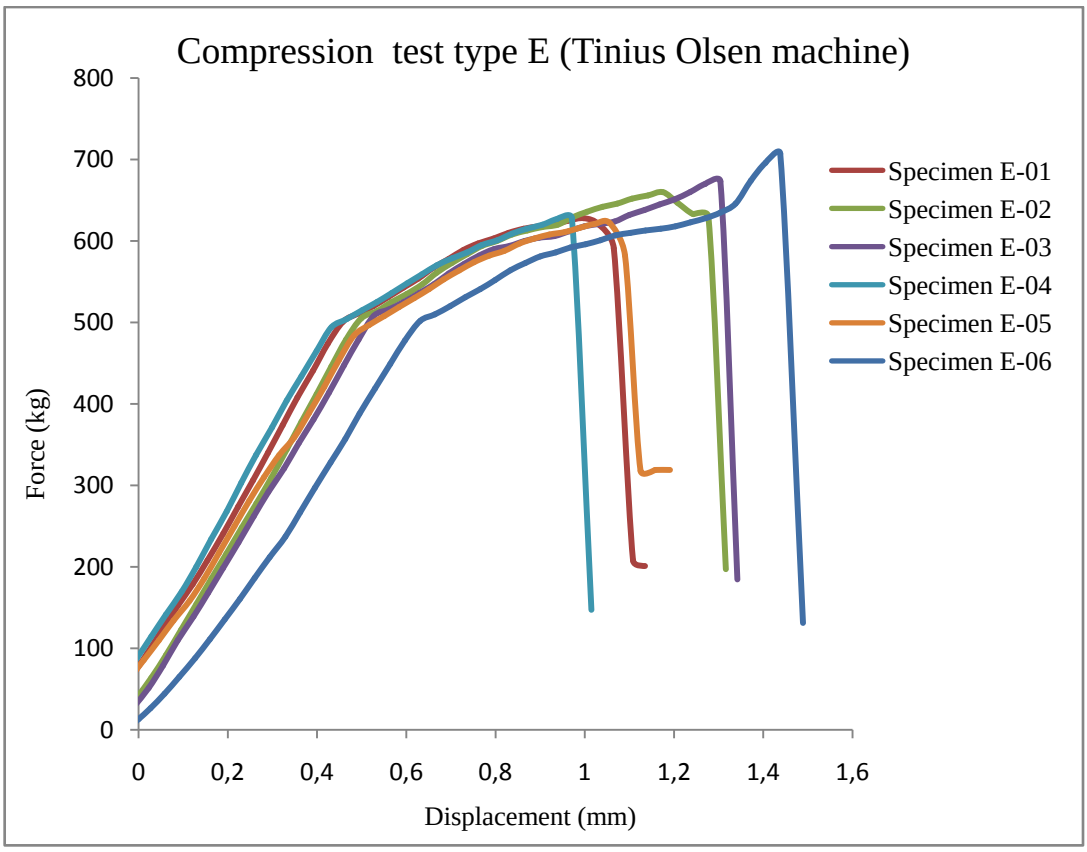
Compression test type E (Tinius Olsen machine)
Force (kg)
800
700
600
500
400
300
200
100
0
0
0,2
0,4
0,6
0,8
1
1,2
1,4
1,6
Displacement (mm)
Specimen E-01
Specimen E-02
Specimen E-03
Specimen E-04
Specimen E-05
Specimen E-06

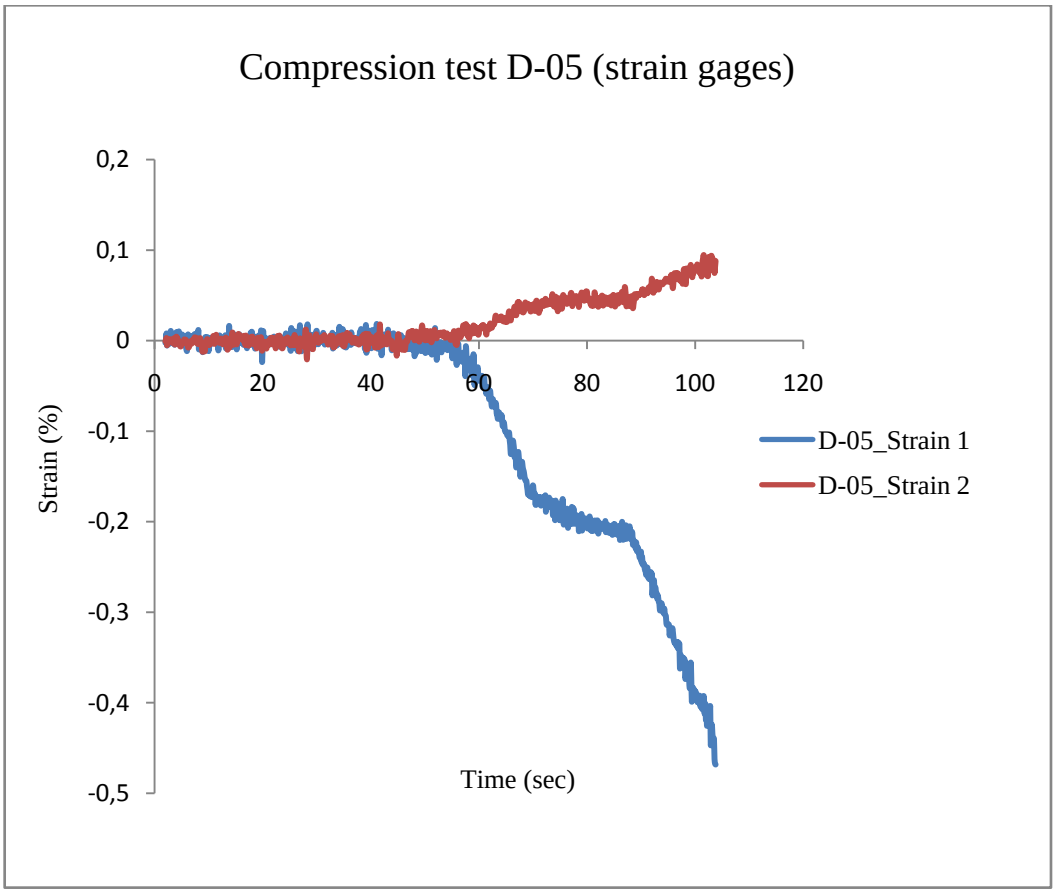
Compression test D-05 (strain gages)
0,2
0,1
0
-0,1
-0,2
-0,3
-0,4
-0,5
0
20
40
60
80
100
120
Strain (%)
Time (sec)
D-05_Strain 1
D-05_Strain 2

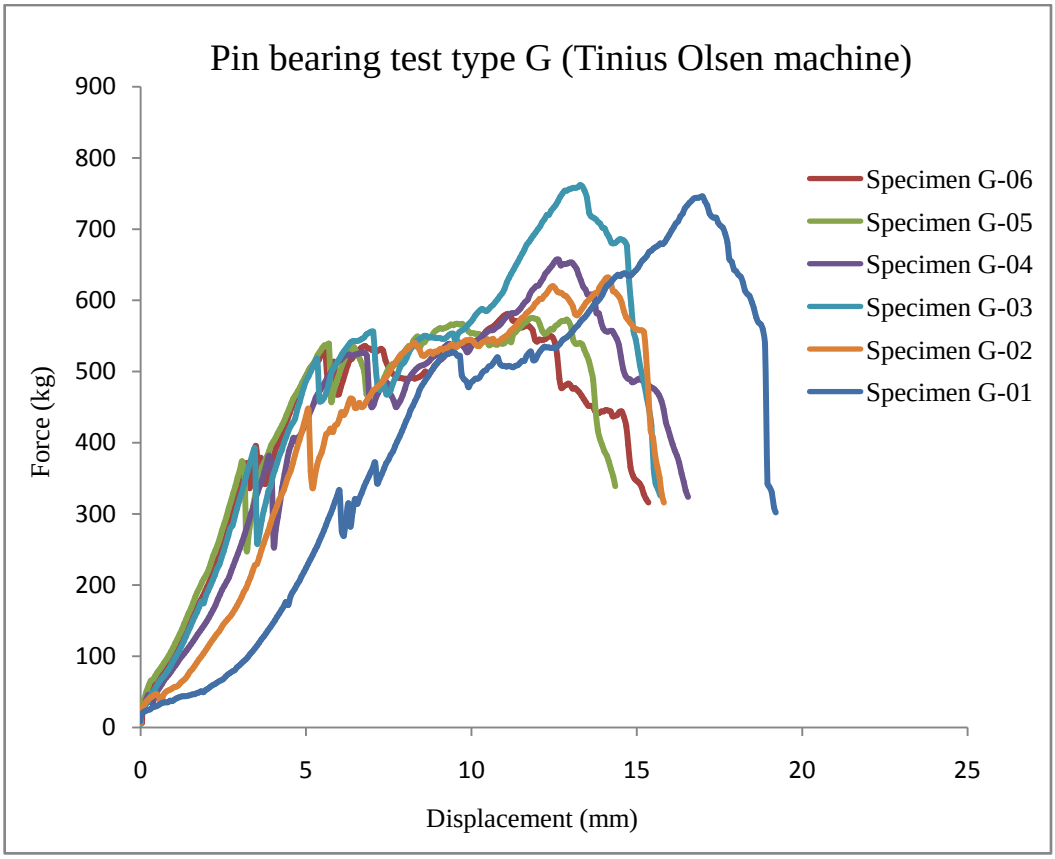
Pin bearing test type G (Tinius Olsen machine)
900
800
700
600
500
400
300
200
100
0
0
5
10
15
20
25
Force (kg)
Displacement (mm)
Specimen G-06
Specimen G-05
Specimen G-04
Specimen G-03
Specimen G-02
Specimen G-01

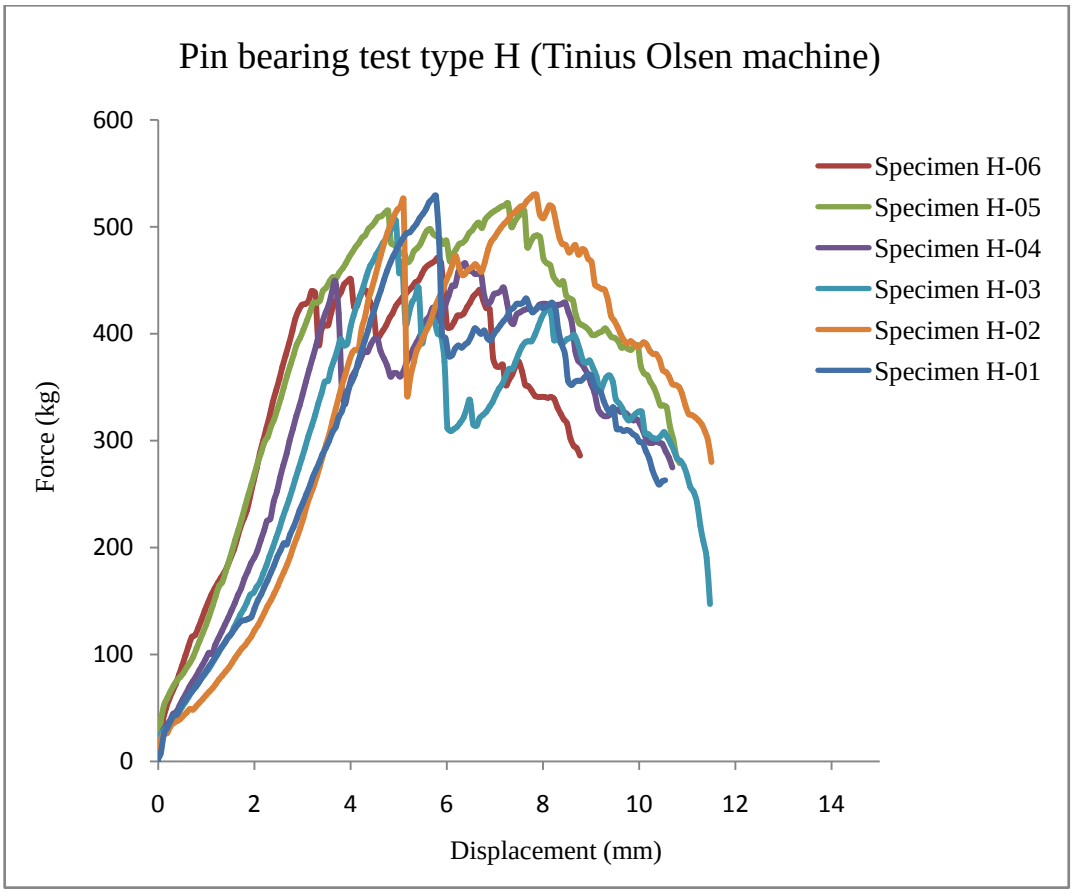
Pin bearing test type H (Tinius Olsen machine)
600
500
400
300
200
100
0
Force (kg)
0
2
4
6
8
10
12
14
Displacement (mm)
Specimen H-06
Specimen H-05
Specimen H-04
Specimen H-03
Specimen H-02
Specimen H-01

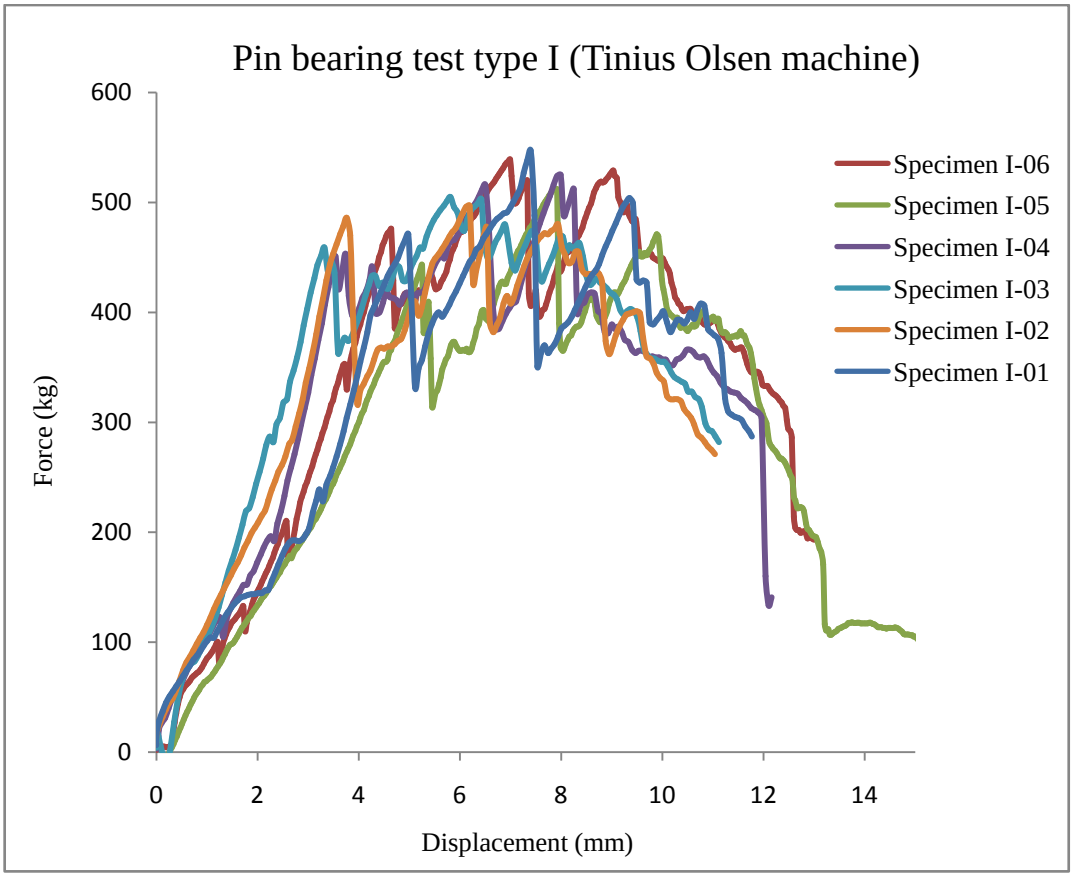
Pin bearing test type I (Tinius Olsen machine)
600
500
400
300
200
100
0
Force (kg)
0
2
4
6
8
10
12
14
Displacement (mm)
Specimen I-06
Specimen I-05
Specimen I-04
Specimen I-03
Specimen I-02
Specimen I-01

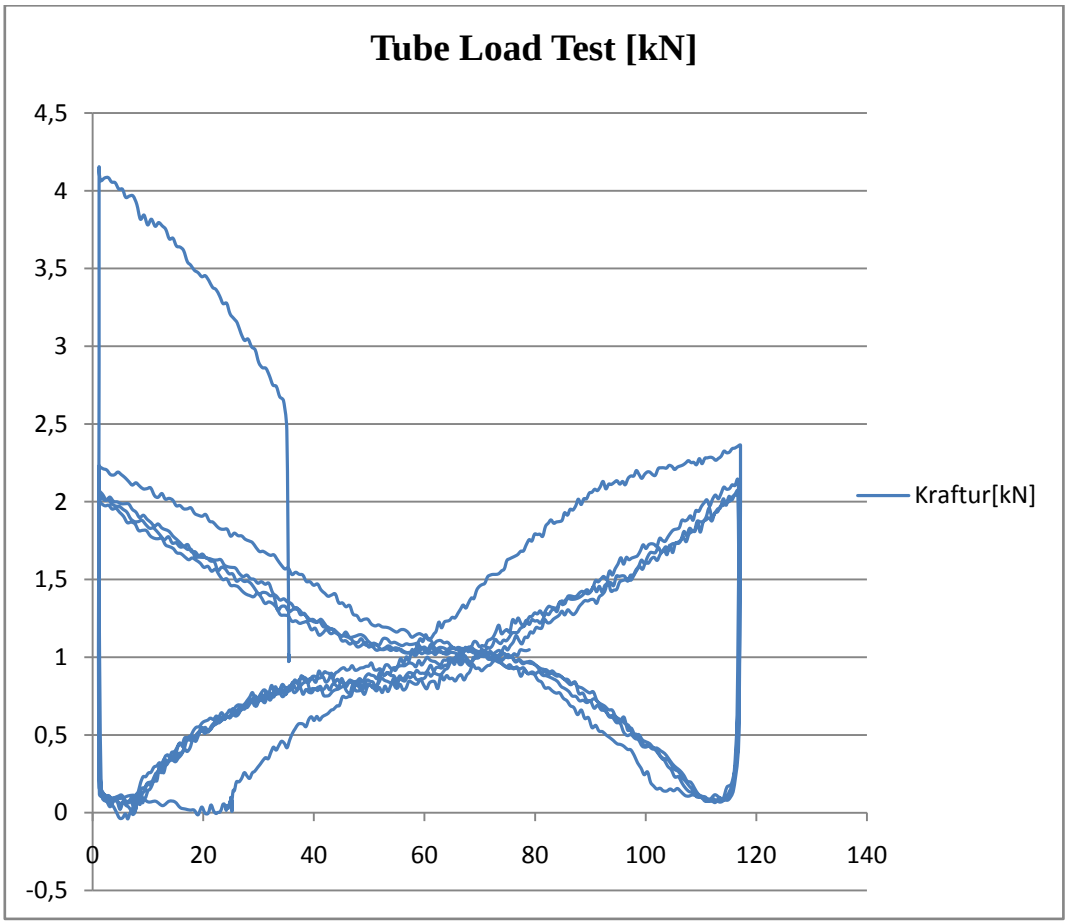
Tube Load Test [kN]
4,5
4
3,5
3
2,5
2
1,5
1
0,5
0
-0,5
0
20
40
60
80
100
120
140
Kraftur[kN]

Appendix E – Failure Models

ASTM D3039 (*ASTM D3039*, 2000, p. 10)

Tensile Test Failure Codes/Typical Models


LIT


GAT


LAT


DGM


LGM


SGM


AGM(1)


AGM(2)


XGM

First Character

Failure Type	Code
Angled	A
edge Delamination	D
Grip/tab	G
Lateral	L
Multi-mode	M(xyz)
long. Splitting	S
eXplosive	X
Other	O

Second Character

Failure Area	Code
Inside grip/tab	I
At grip/tab	A
<1W from grip/tab	W
Gage	G
Multiple areas	M
Various	V
Unknown	U

Third Character

Failure Location	Code
Bottom	B
Top	T
Left	L
Right	R
Middle	M
Various	V
Unknown	U

ASTM D3410 (*ASTM D3410*, 2003, p. 13)

Compression Test Specimen Three-Part Failure Identification Codes and Overall Specimen Failure Schematics.

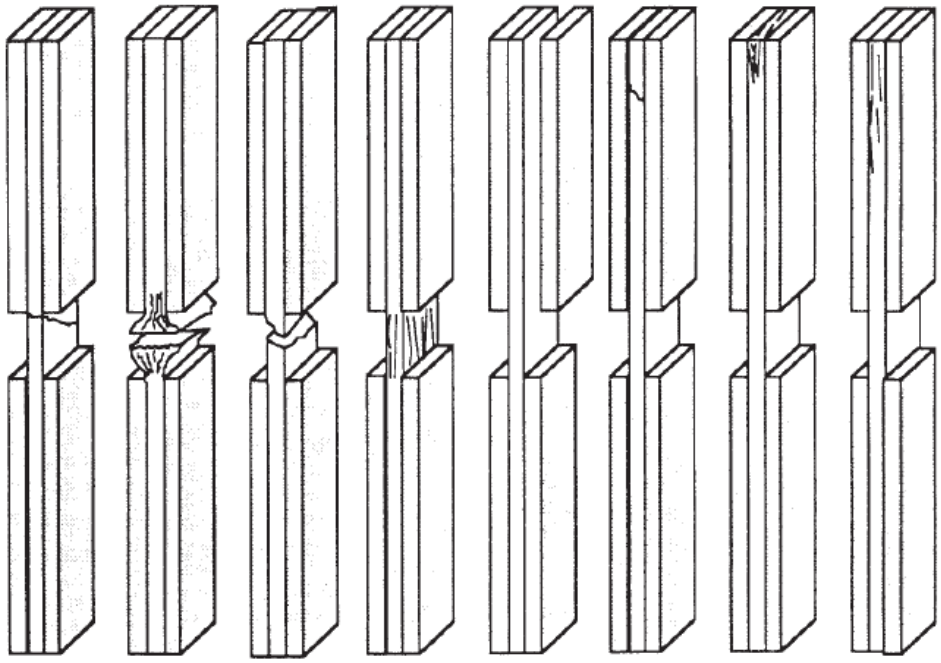

TAT BGM HAT SGV DTT HIT CIT DIT

Acceptable Failure Modes and Areas **Unaceptable Failure Modes and Areas**

First Character

Failure Mode	Code
Angled	A
Brooming	B
end-Crushing	C
Delamination	D
Euler buckling	E
tHrough-thickness	H
Kink bands	K
Lateral	L
Multi-mode	M(xyz)
long.-Splitting	S
Transverse shear	T
eXplosive	X
Other	O

Second Character

Failure Area	Code
Inside grip/tab	I
At grip/tab	A
Gage	G
Multiple Areas	M
Tab adhesive	T
Various	V
Unknown	U

Third Character

Failure Location	Code
Bottom	B
Top	T
Left	L
Right	R
Middle	M
Various	V
Unknown	U

ASTM D5961(*ASTM D5961*, 2001, p. 23)

Bearing Test Failure Codes With Illustrations of Common Modes.

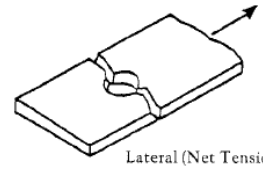

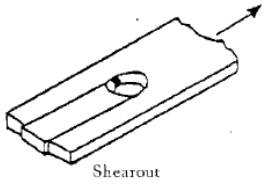

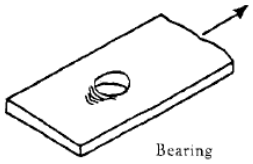

B1I

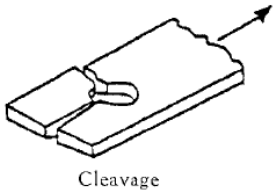

C1I

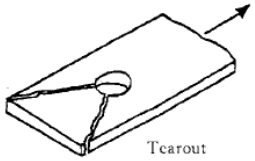

T1I

First Part

Failure Type	Code
Bearing	B
Cleavage	C
Fastener or pin	F
Lateral (net tension)	L
Multi-mode	M(xyz)
Shearout	S
Tearout	T
Other	O

Second Part

Failure Area	Code
First Hole	1
Second Hole	2
Both Holes	B
Fastener or pin	F
Unknown	U

Third Part

Failure Location	Code
Bolt Head Side	B
Nut Side	N
Inapplicable	I
Unknown	U

Appendix F – MATLAB code

```
clear all; close all; clc

prompt={'1. Ef  Modulus of Fibre  (N/mm^2)'...
    ,'2. Em  Modulus of Matrix  (N/mm^2)'...
    ,'3. Gf  Shear Modulus of Fibre  (N/mm^2)'...
    ,'4. Gm  Shear Modulus of Matrix  (N/mm^2)'...
    ,'5. vf  Poisson of fibre','6 vm  Poisson of Matrix'...
    ,'7. V  Volume fraction','8. Df  Density of fibre  (g/cm^3)'...
    ,'9. Dm  Density of Matrix  (g/cm^3)'...
    ,'10. t  Thickness of plate  (mm)'};

def={'86500','3100','36041','1291','0.2','0.2','0.52',...
'2.67','1.11','0.225'};  % 0.225 or 0.45

TITLE='Define Composite Properties';
line=1;
ANSWER=inputdlg(prompt,TITLE,line,def);
convertc=char(ANSWER);
prec=str2num(convertc);

Ef=prec(1);              %%%%Elastic Modulus of Fiber (N/mm^2)
Em=prec(2);              %%%%Elastic Modulus of Matrix (N/mm^2)
Gf=prec(3);              %%%%Shear Modulus of Fiber (N/mm^2)
Gm=prec(4);              %%%%Shear Modulus of Matrix (N/mm^2)
vf=prec(5);              %%%%Poisson's Ratio of Fiber
vm=prec(6);              %%%%Poisson's Ratio of Matrix
V=prec(7);               %%%%Volume Fiber Fraction
Df=prec(8);              %%%%Density of Fiber (g/cm^3)
Dm=prec(9);              %%%%Density Ratio of Matrix (g/cm^3)
tplys=prec(10);          %%%%Thickness of plate (mm)

prompt={'Enter the fiber orientation of the plys'};

% def={'[0 90 0 90 0 90 90 0 90 0 90 0]'};                % A-specimens
def={'[0 90 45 -45 0 90 90 0 -45 45 90 0]'};              % B-specimens
% def={'[45 -45 45 -45 45 -45 -45 45 -45 45 -45 45]'};    % C-specimens

%def={'[0 0 0 0 0 0]'};                                   % A-specimens
%def={'[0 45 0 0 45 0]'};                                 % B-specimens
%def={'[45 -45 45 45 -45 45]'};                           % C-specimens

TITLE='Define Composite Properties';
num_line=1;
ANSWER=inputdlg(prompt,TITLE,num_line,def);
convertc=char(ANSWER);
prec=str2num(convertc);
TT=prec;
plys=length(TT);
theta=prec;

format shortg
%%%%%%%%%Calculation of Macromechanical Properties%%%%%%%%
E11=Ef*V+Em*(1-V)
E22=Em*(Ef+Em+(Ef-Em)*V)/(Ef+Em-(Ef-Em)*V)
%%%%%%%% %E22=Em/(1-sqrt(V)*(1-(Em/Ef)))
%%%%%%%% %E22=1/((V/Ef)+((1-V)/Em))
%%%%%%%% %E22=(Ef*Em)/(Em*V+Ef*(1-V))
v12=vf*V+vm*(1-V)
v23=vf*V+vm*(1-V)*(1+vm-v12*Em/E11)/(1-vm^2+vm*v12*Em/E11)
G12=Gm*(Gf+Gm+(Gf-Gm)*V)/(Gf+Gm-(Gf-Gm)*V)
%%%%%%% %G12=(Gf*Gm)/(Gm*V+Gf*(1-V))
G23=E22/(2*(1+v23))
Den=Df*V+Dm*(1-V)
```

```
E1=E11;
E2=E22;
%%%%% %E2=1;
%%%%%%%%%%%%%%%%%%%%%%%%%%%%%%%%%%%%%%%%%%%%%%%%%%%%%%%%%%%%%%%%%%%%%%%

%%%%%%%%%%%%%%%%%%%%%%%%%%%%%%%%%%%%%%%%%%%%%%%%%%%%%%%%%%%%%%%%%%%%%%%
% E1=19817;
% E2=19817;
% v12=0.054;
% G12=2750;
%%%%%%%%%%%%%%%%%%%%%%%%%%%%%%%%%%%%%%%%%%%%%%%%%%%%%%%%%%%%%%%%%%%%%%%

%%
t(1:plys)=tplys;
for i = 1:plys
[Q,S,Qbar(:,:,i),Sbar(:,:,i),T(:,:,i)]=qands(E1,E2,G12,v12,theta(i));
end
[ABD,z,z0] = abd(t,Qbar,plys);

%%
% e0_K=[ex ey exy Kx Ky Kxy]'

% e0_K=[0.03 -0.005 0 0 0 0];
% N_M=(ABD*e0_K')'

%%

%N_M=[35000/25 0 0 0 0 0];           % A-specimens
%N_M=[5000/25 0 0 0 0 0];            % B-specimens
N_M=[9000/25 0 0 0 0 0];            % C-specimens

e0_K = inv(ABD)*N_M';

e0(:,1) = e0_K(1:3);
K(:,1) = e0_K(4:6);

%%

%************************
% GENERATES ALL Ex, Ey,exy
%************************
xstrain(1,1)=e0(1)+z0*K(1);
ystrain(1,1)=e0(2)+z0*K(2);
xystrain(1,1)=e0(3)+z0*K(3);
for i = 2:plys+1
xstrain(i,1)=e0(1)+z(i-1)*K(1);
ystrain(i,1)=e0(2)+z(i-1)*K(2);
xystrain(i,1)=e0(3)+z(i-1)*K(3);
if abs(xystrain) < 1e-9
xystrain(i,1)=0;
end
end
for i = 1:plys+1
e(:,i)=[xstrain(i,1);ystrain(i,1);xystrain(i,1)];
end

%************************************
% GENERATES ALL Global & Ply stresses
%************************************
for i = 1:plys
globalstresses(1:3,i)=Qbar(:,:,i)*e(:,i);
globalstresses(4:6,i)=Qbar(:,:,i)*e(:,(i+1));
plystresses(1:3,i)=T(:,:,i)*globalstresses(1:3,i);
plystresses(4:6,i)=T(:,:,i)*globalstresses(4:6,i);
end
```

```
%% Material strengths
sigma_1C = -300;   % Compression failure stress in the 1 direction (N/mm^2)
sigma_1T = 900;    % Tensile failure stress in the 1 direction (N/mm^2)
sigma_2C = -100;   % Compression failure stress in the 2 direction (N/mm^2)
sigma_2T = 49.5;   % Tensile failure stress in the 2 direction (N/mm^2)
tau_F12 = 38;      % Shear failure stress in the 1-2 plan (N/mm^2)
plystresses;

%% Maximum Stress Theory-----------------------------------------------------
StressFailure=zeros(3,plys);
for i = 1:plys
if plystresses(1,i) >= 0;
StressFailure(1,i)=plystresses(1,i)/sigma_1T;
else
StressFailure(1,i)=plystresses(1,i)/sigma_1C;
end
if plystresses(2,i) >= 0;
StressFailure(2,i)=plystresses(2,i)/sigma_2T;
else
StressFailure(2,i)=plystresses(2,i)/sigma_2C;
end
StressFailure(3,i)=abs(plystresses(3,i))/tau_F12;
end
StressFailure;

for i = 1:plys
StressFailureMax(:,i)=max(abs(StressFailure(:,i)));
end
StressFailureMax;

%% Maximum Strain Theory-----------------------------------------------------
% strain_local=zeros(3,plys);
strain_local(1,:)=(plystresses(1,:))./E1-(v12.*plystresses(2,:))./E1;
strain_local(2,:)=(plystresses(2,:))./E2-(v12.*plystresses(1,:))./E1;
strain_local(3,:)=(plystresses(3,:))./G12;


epsilon_1C = sigma_1C/E1;
epsilon_1T = sigma_1T/E1;
epsilon_2C = sigma_2C/E2;
epsilon_2T = sigma_2T/E2;
gamma_F12 = tau_F12/G12;

StrainFailure=zeros(3,plys);
for i = 1:plys
if strain_local(1,i) >= 0;
StrainFailure(1,i)=strain_local(1,i)./epsilon_1T;
else
StrainFailure(1,i)=strain_local(1,i)./epsilon_1C;
end
if strain_local(2,i) >= 0;
StrainFailure(2,i)=strain_local(2,i)./epsilon_2T;
else
StrainFailure(2,i)=strain_local(2,i)./epsilon_2C;
end
StrainFailure(3,i)=abs(strain_local(3,i))./gamma_F12;
end
StrainFailure;

for i = 1:plys
StrainFailureMax(:,i)=max(abs(StrainFailure(:,i)));
end
StrainFailureMax;
```

```
%% Tsai-Hill (Maximum Work) Theory (if sigma_1C = sigma_1T)
for i = 1:plys

if plystresses(1,i) >= 0;

if plystresses(2,i) >= 0;
Tsai_Hill(1,i) = (plystresses(1,i)^2/sigma_1T^2)+(plystresses(2,i)...
    ^2/sigma_2T^2)-((plystresses(1,i)*plystresses(2,i))/sigma_1T^2)+...
    (plystresses(3,i)^2/tau_F12^2);
else
Tsai_Hill(1,i) = (plystresses(1,i)^2/sigma_1T^2)+(plystresses(2,i)...
    ^2/sigma_2C^2)-((plystresses(1,i)*plystresses(2,i))/sigma_1T^2)+...
    (plystresses(3,i)^2/tau_F12^2);
end

else

if plystresses(2,i) >= 0;
Tsai_Hill(1,i) = (plystresses(1,i)^2/sigma_1C^2)+(plystresses(2,i)...
    ^2/sigma_2T^2)-((plystresses(1,i)*plystresses(2,i))/sigma_1C^2)+...
    (plystresses(3,i)^2/tau_F12^2);
else
Tsai_Hill(1,i) = (plystresses(1,i)^2/sigma_1C^2)+(plystresses(2,i)...
    ^2/sigma_2C^2)-((plystresses(1,i)*plystresses(2,i))/sigma_1C^2)+...
    (plystresses(3,i)^2/tau_F12^2);
end
end
end
Tsai_Hill;

%% Tsai-Wu Theory
f1=(1/sigma_1T)+(1/sigma_1C);
f11=-(1/(sigma_1T*sigma_1C));
f2=(1/sigma_2T)+(1/sigma_2C);
f22=-(1/(sigma_2T*sigma_2C));
f66=(1/tau_F12)^2;
%f12=-(1/2)*(1/(sigma_1T*sigma_1C*sigma_2T*sigma_2C))^0.5;
for i = 1:plys
Tsai_Wu(1,i)=f1*plystresses(1,i)+f2*plystresses(2,i)+...
    f11*plystresses(1,i)^2+f22*plystresses(2,i)^2+f66*plystresses(3,i)...
    ^2-(f11*f22)^2*plystresses(1,i)*plystresses(2,i);
end
Tsai_Wu;
```

```
%CALCULATES Q,Qbar, S, Sbar MATRICIES
%
function [Q,S,Qbar,Sbar,T]=qands(E1,E2,G12,v12,theta)
theta = theta*pi/180;
c = cos(theta);
s = sin(theta);
R = [1 0 0;0 1 0;0 0 2]; %Rueter Transformation Matrix
T = [c^2 s^2 2*c*s;s^2 c^2 -2*c*s; -c*s c*s c^2-s^2];%Transformation Matrix
%****************
%Formulation of S
%****************
S11 = 1/E1;
S22 = 1/E2;
S66 = 1/G12;
S12 = -v12/E1;
S21 = S12;
S = [S11,S12,0;S21,S22,0;0,0,S66];
%****************
%Formulation of Q
%****************
Q = S^-1;
%***************************
%Formulation of Q-BAR & S-BAR
%***************************
Qbar = (T^-1)*Q*R*T*(R^-1);
Sbar = R*(T^-1)*(R^-1)*S*T;
%Sub Program: ABD Assemblage
```

```
% CALCULATES THE ABD MATRIX OF THE PANEL
function [ABD,z,z0]=abd(t,Qbar,plys);
z0 = -sum(t)/2;
z(1) = z0+t(1);
% cant use a zeroth row... so notation is offset by 1 number ..
% for technically z_1 to z_(n+1) (same # of points)
for j = 2:plys
z(j)=z(j-1)+t(j);
end
for i = 1:3
for j = 1:3
A(i,j) = Qbar(i,j,1)*(z(1)-z0);
B(i,j) = Qbar(i,j,1)*(z(1)^2-z0^2)/2;
D(i,j) = Qbar(i,j,1)*(z(1)^3-z0^3)/3;
for k = 2:plys
A(i,j) = A(i,j)+Qbar(i,j,k)*(z(k)-z(k-1));
B(i,j) = B(i,j)+Qbar(i,j,k)*(z(k)^2-z(k-1)^2)/2;
D(i,j) = D(i,j)+Qbar(i,j,k)*(z(k)^3-z(k-1)^3)/3;
end
end
end
ABD = [A,B;B,D];
```

```
% PLOTTING FUNCTION
%*********************************************
% Plots and displays all needed values
%*********************************************
function [thickness,strainthickness] = graphics(z,z0,plys,globalstresses,...
    plystresses,xstrain,ystrain,xystrain,sigma_1C,sigma_2C,sigma_1T,...
    sigma_2T,tau_F12,strain_local,epsilon_1C,epsilon_1T,epsilon_2C,...
    epsilon_2T,gamma_F12);
%*************************************************************************



% sorts all stress/strains so they can be plotted
%*************************************************************************
j=1;
for i = 1:2:(plys*2-1)
sigx(i)=globalstresses(1,j);
sigx(i+1)=globalstresses(4,j);
sigy(i)=globalstresses(2,j);
sigy(i+1)=globalstresses(5,j);
sigxy(i)=globalstresses(3,j);
sigxy(i+1)=globalstresses(6,j);
sig1(i)=plystresses(1,j);
sig1(i+1)=plystresses(4,j);
sig2(i)=plystresses(2,j);
sig2(i+1)=plystresses(5,j);
sig12(i)=plystresses(3,j);
sig12(i+1)=plystresses(6,j);
str1(i)=strain_local(1,j);
str1(i+1)=strain_local(1,j);
str2(i)=strain_local(2,j);
str2(i+1)=strain_local(2,j);
str12(i)=strain_local(3,j);
str12(i+1)=strain_local(3,j);
j=j+1;
end
%*************************************************************************



% Generates all thicknesses so that they can be plotted against the stresses/strains
%*************************************************************************
thickness(1)=z0;
strainthickness(1)=z0;
m=2;
for i = 1:plys
thickness(m)=z(i);
thickness(m+1)=z(i);
m=m+2;
end
[m,n]=size(thickness);
thickness=thickness(1:(n-1));
m=2;
for i = 1:plys
strainthickness(m)=z(i);
m=m+1;
end
strainthickness;
clc
format shortg

labelfor={'fontname','times new roman','fontsize',12};
figure(1);plot(sigx,thickness,'b-')
legend('Stress x',0);ylabel('Thickness (mm)',labelfor{:});xlabel('Stress
(MPa)',labelfor{:});
%title('Stress through the thickness in the (X,Y) global coordinate system')

figure(2);plot(sigy,thickness,'b-')
legend('Stress
y',0);ylabel('Thickness(mm)',labelfor{:});xlabel('Stress(MPa)',labelfor{:});
%title('Stress through the thickness in the (X,Y) global coordinate system')
```

```
figure(3);plot(sigxy,thickness,'b-')
legend('Shear stress
xy',0);ylabel('Thickness(mm)',labelfor{:});xlabel('Stress(MPa)',labelfor{:});
%title('Stress through the thickness in the (X,Y) global coordinate system')

figure(4);plot(sig1,thickness,'b-')
hold on; plot([sigma_1C sigma_1C],[thickness(1)
thickness(length(thickness))],'r','LineWidth',2);
plot([sigma_1T sigma_1T],[thickness(1)
thickness(length(thickness))],'r','LineWidth',2);
%axis([sigma_1C-10 sigma_1T+10 thickness(1) thickness(length(thickness))]);
legend('Stress 1','Maximum
Stress');ylabel('Thickness(mm)',labelfor{:});xlabel('Stress(MPa)',labelfor{:});
%title('Stress through the thickness in the (1,2) local coordinate system')

figure(5);plot(sig2,thickness,'b-');
hold on; plot([sigma_2C sigma_2C],[thickness(1)
thickness(length(thickness))],'r','LineWidth',2);
plot([sigma_2T sigma_2T],[thickness(1)
thickness(length(thickness))],'r','LineWidth',2);
%axis([sigma_2C-10 sigma_2T+10 thickness(1) thickness(length(thickness))]);
legend('Stress 2','Maximum
Stress');ylabel('Thickness(mm)',labelfor{:});xlabel('Stress(MPa)',labelfor{:});
%title('Stress through the thickness in the (1,2) local coordinate system')

figure(6);plot(sig12,thickness,'b-')
hold on; plot([tau_F12 tau_F12],[thickness(1)
thickness(length(thickness))],'r','LineWidth',2);
plot([-tau_F12 -tau_F12],[thickness(1)
thickness(length(thickness))],'r','LineWidth',2);
%axis([-tau_F12-10 tau_F12+10 thickness(1) thickness(length(thickness))]);
legend('Shear stress 12','Maximum
Stress');ylabel('Thickness(mm)',labelfor{:});xlabel('Stress(MPa)',labelfor{:});
%title('Stress through the thickness in the (L,T) local coordinate system')

figure(7);plot(xstrain,strainthickness,'b-')
axis([-0.01 0.04 -1.5 1.5])
legend('Strain x',0);ylabel('Thickness(mm)',labelfor{:});xlabel('Strain
(mm/mm)',labelfor{:});
%title('Strain through the thickness in the (X,Y) global coordinate system')

figure(8);plot(ystrain,strainthickness,'b-')
axis([-0.01 0.04 -1.5 1.5])
legend('Strain y',0);ylabel('Thickness(mm)',labelfor{:});xlabel('Strain
(mm/mm)',labelfor{:});
%title('Strain through the thickness in the (X,Y) global coordinate system')

figure(9);plot(xystrain,strainthickness,'b-')
axis([-0.01 0.04 -1.5 1.5])
legend('Shear strain xy',0);ylabel('Thickness(mm)',labelfor{:});xlabel('Strain
(mm/mm)',labelfor{:});
%title('Strain through the thickness in the (X,Y) global coordinate system')


figure(10);plot(str1,thickness,'b-')
hold on; plot([epsilon_1C epsilon_1C],[thickness(1)
thickness(length(thickness))],'r','LineWidth',2);
plot([epsilon_1T epsilon_1T],[thickness(1)
thickness(length(thickness))],'r','LineWidth',2);
%axis([sigma_1C-10 sigma_1T+10 thickness(1) thickness(length(thickness))]);
legend('Strain 1','Maximum
Strain');ylabel('Thickness(mm)',labelfor{:});xlabel('Strain(mm/mm)',labelfor{:});
%title('Strain through the thickness in the (L,T) local coordinate system')

figure(11);plot(str2,thickness,'b-')
hold on; plot([epsilon_2C epsilon_2C],[thickness(1)
thickness(length(thickness))],'r','LineWidth',2);
plot([epsilon_2T epsilon_2T],[thickness(1)
thickness(length(thickness))],'r','LineWidth',2);
%axis([sigma_1C-10 sigma_1T+10 thickness(1) thickness(length(thickness))]);
legend('Strain 2','Maximum
Strain');ylabel('Thickness(mm)',labelfor{:});xlabel('Strain(mm/mm)',labelfor{:});
%title('Strain through the thickness in the (L,T) local coordinate system')
```

```
figure(12);plot(str12,thickness,'b-')
hold on; plot([epsilon_2C epsilon_2C],[thickness(1)
thickness(length(thickness))],'r','LineWidth',2);
plot([gamma_F12 gamma_F12],[thickness(1)
thickness(length(thickness))],'r','LineWidth',2);
%axis([sigma_1C-10 sigma_1T+10 thickness(1) thickness(length(thickness))]);
legend('Shear strain 12','Maximum
Strain');ylabel('Thickness(mm)',labelfor{:});xlabel('Strain(mm/mm)',labelfor{:});
%title('Strain through the thickness in the (L,T) local coordinate system')
```

Appendix G – Videos of the experiments (DVD)